IMA Journal of Numerical Analysis (2019) **00**, 1–51
doi:10.1093/imanum/drz012

Numerical approximation of curve evolutions in Riemannian manifolds

John W. Barrett
Department of Mathematics, Imperial College, London SW7 2AZ, UK

Harald Garcke
Fakultät für Mathematik, Universität Regensburg, 93040 Regensburg, Germany

and

Robert Nürnberg*
Department of Mathematics, Imperial College, London SW7 2AZ, UK
*Corresponding author: robert.nurnberg@imperial.ac.uk

[Received on 17 September 2018; revised on 7 February 2019]

We introduce variational approximations for curve evolutions in two-dimensional Riemannian manifolds that are conformally flat, i.e. conformally equivalent to the Euclidean plane. Examples include the hyperbolic plane, the hyperbolic disc and the elliptic plane, as well as any conformal parameterization of a two-dimensional manifold in $\mathbb{R}^d$, $d \geqslant 3$. In these spaces we introduce stable numerical schemes for curvature flow and curve diffusion, and we also formulate schemes for elastic flow. Variants of the schemes can also be applied to geometric evolution equations for axisymmetric hypersurfaces in $\mathbb{R}^d$. Some of the schemes have very good properties with respect to the distribution of mesh points, which is demonstrated with the help of several numerical computations.

Keywords: Riemannian manifolds; curve evolution equations; curvature flow; curve diffusion; elastic flow; hyperbolic plane; hyperbolic disc; elliptic plane; geodesic curve evolutions; finite element approximation; equidistribution.

1. Introduction

The evolution of curves in a two-dimensional manifold driven by a velocity involving the (geodesic) curvature of the curve appears in many situations in geometry and in applications. Examples are curve straightening via the elastic energy or image processing on surfaces. The first mathematical results on such flows go back to the work of Gage & Hamilton (1986), who studied curvature flow in the Euclidean plane. Later, evolutions in more complex ambient spaces have been studied; see, e.g., Grayson (1989), Cabezas-Rivas & Miquel (2007) and Andrews & Chen (2017). In the Euclidean case it can be shown that closed curves shrink to a point in finite time and they become more and more round as they do so; see Gage & Hamilton (1986) and Grayson (1987). In the case of a general ambient space the solution behaviour is more complex. For example, some solutions exist for arbitrary times and others can become unbounded in finite or infinite time; see, e.g., Grayson (1989).

Curvature flow is a second-order flow. However, fourth-order flows are also of interest. Here we mention the elastic (Willmore) flow of curves and curve diffusion, both of which are highly nonlinear. Elastic flow is the L^2-gradient flow of the elastic energy, and in the hyperbolic plane and on the sphere it was recently studied by Dall'Acqua & Spener (2017, 2018) and Dall'Acqua *et al.* (2018), respectively. The curve diffusion flow, sometimes also called surface diffusion flow, is the H^{-1}-gradient

flow for the length of the curve, and like the elastic flow, it also features second derivatives of the curvature.

In this paper we also want to study situations in which a curve evolves in a two-dimensional manifold that is not necessarily embedded in $\mathbb{R}^3$. An important example is the hyperbolic plane $\mathbb{H}^2$, which due to Hilbert's classical theorem cannot be embedded into $\mathbb{R}^3$; see Hilbert (1901) and, e.g., Pressley (2010, §11.1). It will turn out that we can derive stable numerical schemes for curve evolutions in two-dimensional Riemannian manifolds that are conformally equivalent to the Euclidean plane. This means that charts exist such that in the parameter domain, the metric tensor is a possibly inhomogeneous scalar multiple of the classical Euclidean metric. This in particular implies that the chart is angle preserving; we refer to Kühnel (2015) for more details.

The numerical approximation of the evolution of curves in an Euclidean ambient space is very well developed, with many papers on parametric as well as level set methods. We refer to Deckelnick *et al.* (2005) for an overview. However, for more general ambient spaces only a few papers dealing with numerical methods exist. Some numerical work is devoted to the evolution of curves on two-dimensional hypersurfaces in $\mathbb{R}^3$. We refer to Mikula & Ševčovič (2006), Barrett *et al.* (2010) and Benninghoff & Garcke (2016) for methods using a parametric approach. Besides, a level set setting is also possible in order to numerically move curves that are constrained to lie on hypersurfaces; see Cheng *et al.* (2002) and Spira & Kimmel (2007).

The setting in this paper is as follows. Let $I = \mathbb{R}/\mathbb{Z}$ be the periodic interval $[0, 1]$ and let $\vec{x} : I \to \mathbb{R}^2$ be a parameterization of a closed curve $\Gamma \subset \mathbb{R}^2$. On assuming that

$$|\vec{x}_\rho| \geqslant c_0 > 0 \qquad \text{in } I\,,$$

we introduce the arclength s of the curve, i.e. $\partial_s = |\vec{x}_\rho|^{-1}\,\partial_\rho$, and set

$$\vec{\tau}(\rho) = \vec{x}_s(\rho) = \frac{\vec{x}_\rho(\rho)}{|\vec{x}_\rho(\rho)|} \quad \text{and} \quad \vec{\nu}(\rho) = -[\vec{\tau}(\rho)]^\perp \qquad \text{in } I\,, \tag{1.1}$$

where $\cdot^\perp$ denotes a clockwise rotation by $\frac{\pi}{2}$.

On an open set $H \subset \mathbb{R}^2$ we define a metric tensor as

$$[(\vec{v}, \vec{w})_g](\vec{z}) = g(\vec{z})\,\vec{v}\,.\,\vec{w} \quad \forall\, \vec{v}, \vec{w} \in \mathbb{R}^2 \qquad \text{for } \vec{z} \in H\,, \tag{1.2}$$

where $\vec{v}\,.\,\vec{w} = \vec{v}^{\mathrm{T}}\,\vec{w}$ is the standard Euclidean inner product, and where $g : H \to \mathbb{R}_{>0}$ is a smooth positive weight function. This is the setting one obtains for a two-dimensional Riemannian manifold that is conformally equivalent to the Euclidean plane. In local coordinates the metric is precisely given by (1.2); see, e.g., Jost (2005), Kühnel (2015) and Schippers (2007). Let us mention that a two-dimensional Riemannian manifold locally allows for a conformal chart; see, e.g., Taylor (2011, §5.10). Examples of such situations are the hyperbolic plane, the hyperbolic disc and the elliptic plane. Other examples are given by curves in two-dimensional manifolds in $\mathbb{R}^d$, $d \geqslant 3$ that can be conformally parameterized, such as spheres without pole(s), catenoids and torii. Coordinates $(x_1, x_2) \in H$ together with a metric g as in (1.2) are called isothermal coordinates, i.e. in all situations considered in this paper we assume that we have isothermal coordinates. We refer to Section 2 and Kühnel (2015, 3.29 in §3D) for more information.

For a time-dependent curve $\vec{x}$ the simplest curvature driven flow is given as

$$\mathcal{V}_g = \varkappa_g \qquad \text{in } I\,. \tag{1.3}$$

Here $\mathcal{V}_g = g^{\frac{1}{2}}(\vec{x})\,\vec{x}_t\,.\,\vec{\nu}$ is the normal velocity with respect to the metric (1.2), and

$$\varkappa_g = g^{-\frac{1}{2}}(\vec{x})\left[\varkappa - \tfrac{1}{2}\,\vec{\nu}\,.\,\nabla\,\ln g(\vec{x})\right] \qquad \text{in } I \tag{1.4}$$

is the curvature of the curve with respect to the metric g. The vector $\vec{\nu}$, defined in (1.1), is the classical Euclidean normal, and $\varkappa$ is the classical Euclidean curvature of the curve. It satisfies the property

$$\varkappa\,\vec{\nu} = \vec{\varkappa} = \vec{\tau}_s = \vec{x}_{ss} = \frac{1}{|\vec{x}_\rho|}\left[\frac{\vec{x}_\rho}{|\vec{x}_\rho|}\right]_\rho \qquad \text{in } I\,; \tag{1.5}$$

see Deckelnick *et al.* (2005). At this stage we would like to draw the reader's attention to the different usages of subscripts in this paper. The subscripts $\cdot_g$ in (1.3), and throughout the paper, denote quantities associated with the metric g. The subscripts $\cdot_t$ and $\cdot_\rho$, on the other hand, denote partial derivatives with respect to t and ρ, respectively. Finally, $\cdot_s$ and $\cdot_{s_g}$ will denote weighted partial derivatives, and are defined in (1.1) and in (2.13) below, respectively.

In the Euclidean case, i.e. in the case $g \equiv 1$, the right-hand side in the curvature flow (1.3) is equal to $\varkappa$, and in particular the parameterization $\vec{x}$ only appears via $\vec{x}_\rho$; cf. (1.4) and (1.5). This is crucial for stability proofs for numerical methods that have been introduced earlier; cf. Dziuk (1988), Barrett *et al.* (2007a) and Deckelnick *et al.* (2005). In the case of a general ambient space, additional nonlinearities involving the variable $\vec{x}$ itself appear in $\varkappa_g$, so that the variational structure of (1.5) is lost. This makes the design of stable schemes highly nontrivial. In fact, no such schemes appear in the literature so far. We will introduce stable fully discrete schemes with the help of a nonstandard convex–concave splitting. In particular, the splitting has to be chosen in terms of $g^{\frac{1}{2}}$. With the help of the splitting, we propose in Section 3 a semi-implicit scheme for which stability can be shown.

The outline of this paper is as follows. In Section 2 we derive the governing equations for curvature flow, curve diffusion and elastic flow, provide weak formulations and relate the introduced flows to geometric evolution equations for axisymmetric hypersurfaces. In Section 3 we introduce finite element approximations and show existence and uniqueness as well as stability results. Section 4 is devoted to several numerical results, which demonstrate convergence rates as well as qualitatively good mesh behaviour. In two appendices we derive exact solutions and derive the geodesic curve evolution equations for a conformal parameterization.

2. Mathematical formulations

It is the aim of this paper to introduce numerical schemes for the situation where a curve $\Gamma = \vec{x}(I)$ evolves in a two-dimensional Riemannian manifold that is conformally equivalent to the Euclidean

plane. Curvature flow is the L^2-gradient flow of the length functional and we first review how length is defined with respect to the metric g. The length induced by (1.2) is defined as

$$[|\vec{\nu}|_g](\vec{z}) = \left([(\vec{\nu},\vec{\nu})_g](\vec{z})\right)^{\frac{1}{2}} = g^{\frac{1}{2}}(\vec{z})\,|\vec{\nu}| \quad \forall\,\vec{\nu}\in\mathbb{R}^2, \qquad \text{for } \vec{z}\in H\,. \tag{2.1}$$

The distance between two points $\vec{z}_0, \vec{z}_1$ in H is defined as

$$\operatorname{dist}_g(\vec{z}_0,\vec{z}_1) = \inf\left\{\int_0^1 [|\vec{\gamma}_\rho(\rho)|_g](\vec{\gamma}(\rho))\,\mathrm{d}\rho : \vec{\gamma}\in C^1([0,1],H)\,,\ \vec{\gamma}(0)=\vec{z}_0\,,\ \vec{\gamma}(1)=\vec{z}_1\right\}. \tag{2.2}$$

It can be shown that $(H,\operatorname{dist}_g)$ is a metric space; see Jost (2005, §1.4).

On recalling (2.1), the total length of the closed curve $\Gamma\subset H$ is given by

$$L_g(\vec{x}) = \int_I [|\vec{x}_\rho|_g](\vec{x})\,\mathrm{d}\rho = \int_I g^{\frac{1}{2}}(\vec{x})\,|\vec{x}_\rho|\,\mathrm{d}\rho. \tag{2.3}$$

If $\Gamma=\vec{x}(I)$ encloses a domain $\Omega\subset H$, with $\partial\Omega=\Gamma$, we define the total enclosed area as

$$A_g(\vec{x}) = \int_\Omega g(\vec{z})\,\mathrm{d}\vec{z}\,. \tag{2.4}$$

For later use we observe that if $\Gamma=\vec{x}(I)=\partial\Omega$ is parameterized clockwise, then $\vec{\nu}\circ\vec{x}^{-1}$, recall (1.1), denotes the outer normal to Ω on $\partial\Omega=\Gamma$. An anticlockwise parameterization, on the other hand, yields that $\vec{\nu}\circ\vec{x}^{-1}$ is the inner normal.

In the context of the numerical approximation of geometric evolution equations for axisymmetric hypersurfaces in $\mathbb{R}^3$, in the recent papers Barrett *et al.* (2019a,b) the authors considered gradient flows, and their numerical approximation, of the energy

$$E_{\mathcal{S}}(\vec{x}) = 2\pi\int_I \vec{x}.\vec{e}_2|\vec{x}_\rho|\,\mathrm{d}\rho\,. \tag{2.5}$$

Here we note that as the authors in Barrett *et al.* (2019a,b) considered surfaces that are rotationally symmetric with respect to the x_2-axis, they in fact considered (2.5) with $\vec{e}_2$ replaced by $\vec{e}_1$.

We remark that if we take (1.2) with

$$g(\vec{z}) = (\vec{z}\,.\,\vec{e}_2)^{-2} \quad \text{and} \quad H=\mathbb{H}^2=\left\{\vec{z}\in\mathbb{R}^2 : \vec{z}\,.\,\vec{e}_2>0\right\}, \tag{2.6a}$$

then we obtain the Poincaré half-plane model, which serves as a model for the hyperbolic plane. Clearly,

$$g(\vec{z}) = 1 \quad \text{and} \quad H=\mathbb{R}^2 \tag{2.6b}$$

simplifies to the standard Euclidean situation. Moreover, we note that (2.3) collapses to (2.5) for the choice

$$g(\vec{z}) = 4\,\pi^2\,(\vec{z}\,.\,\vec{e}_2)^2 \quad \text{and} \quad H=\mathbb{H}^2\,. \tag{2.6c}$$

We also consider more general variants of (2.6a), namely

$$g(\vec{z}) = (\vec{z}\,.\,\vec{e}_2)^{-2\,\mu}\,,\ \mu \in \mathbb{R} \quad \text{and} \quad H = \mathbb{H}^2\,, \tag{2.7}$$

so that (2.6a) corresponds to $\mu = 1$, while formally (2.6b) corresponds to $\mu = 0$. As the latter choice leads to a constant metric, a suitable translation of the initial data in the $\vec{e}_2$ direction will ensure that any evolution for (2.6b) is confined to $\mathbb{H}^2$, and so (2.6b) and (2.7) with $\mu = 0$ are equivalent. In addition, (2.6c), up to the constant factor $4\,\pi^2$, corresponds to $\mu = -1$. For the evolution equations we consider in this paper, the constant factor $4\,\pi^2$ will only affect the timescale of the evolutions.

We remark that for $\mu \neq 1$ the metric space $\mathbb{H}^2$ with the metric (2.2) induced by (2.7) is not complete. To see this, we observe that the distance (2.2) between $a\,\vec{e}_2$ and $b\,\vec{e}_2$, for $a < b$, is bounded from above by

$$\int_a^b u^{-\mu}\,\mathrm{d}u = (1-\mu)^{-1}\big(b^{1-\mu} - a^{1-\mu}\big).$$

Hence, in the case $\mu > 1$, the distance converges to zero as $a, b \to \infty$, and so $(n\,\vec{e}_2)_{n\in\mathbb{N}}$ is a Cauchy sequence without a limit in $\mathbb{H}^2$. In the case $\mu < 1$ we can argue similarly for the Cauchy sequence $(n^{-1}\,\vec{e}_2)_{n\in\mathbb{N}}$, as its limit $\vec{0} \notin \mathbb{H}^2$. The Hopf–Rinow theorem, cf. Jost (2005), then implies that the metric space $\mathbb{H}^2$ with the metric induced by (2.7) for $\mu \neq 1$ is not geodesically complete. Of course, in the special case $\mu = 0$ we can choose $H = \mathbb{R}^2$ to obtain the complete Euclidean plane, (2.6b).

Further examples are given by the family of metrics

$$g(\vec{z}) = \frac{4}{(1-\alpha\,|\vec{z}|^2)^2} \quad \text{and } H = \begin{cases} \mathbb{D}_\alpha = \left\{\vec{z} \in \mathbb{R}^2 : |\vec{z}| < \alpha^{-\frac{1}{2}}\right\}, & \alpha > 0\,, \\ \mathbb{R}^2, & \alpha \leqslant 0\,; \end{cases} \tag{2.8}$$

see, e.g., Schippers (2007, Definition 4.4). We note that (2.8) with $\alpha = 1$ gives a model for the hyperbolic disc; see also Kraus & Roth (2013, Definition 2.7). The metric (2.8) with $\alpha = -1$, on the other hand, models the geometry of the elliptic plane. This is obtained by doing a stereographic projection of the sphere onto the plane, see (2.72a) below for more details.

We note that the sectional curvature of g, also called the Gaussian curvature of g, can be computed by

$$S_0(\vec{z}) = -\frac{\Delta\,\ln g(\vec{z})}{2g(\vec{z})}, \qquad \vec{z} \in H\,; \tag{2.9}$$

see, e.g., Kraus & Roth (2013, Definition 2.4). We observe that for (2.7) it holds that

$$S_0(\vec{z}) = -\mu\,(\vec{z}\,.\,\vec{e}_2)^{2\,(\mu-1)}, \qquad \vec{z} \in H\,, \tag{2.10}$$

while for (2.8) it holds that

$$S_0(\vec{z}) = -\alpha, \qquad \vec{z} \in H\,. \tag{2.11}$$

Of special interest are metrics with constant sectional curvature. For example, (2.6b) gives $S_0 = 0$, (2.6a), i.e. (2.7) with $\mu = 1$, gives $S_0 = -1$, while (2.8) gives $S_0 = -\alpha$.

From now on we consider a family of curves $\Gamma(t)$, parameterized by $\vec{x}(\cdot,t) : I \to H \subset \mathbb{R}^2$. It then holds that

$$\frac{\mathrm{d}}{\mathrm{d}t} L_g(\vec{x}(t)) = \int_I \left[\nabla\, g^{\frac{1}{2}}(\vec{x}) \,.\, \vec{x}_t + g^{\frac{1}{2}}(\vec{x})\, \frac{(\vec{x}_t)_\rho \,.\, \vec{x}_\rho}{|\vec{x}_\rho|^2} \right] |\vec{x}_\rho| \,\mathrm{d}\rho \,. \tag{2.12}$$

Let

$$\partial_{s_g} = |\partial_\rho \vec{x}|_g^{-1}\, \partial_\rho = g^{-\frac{1}{2}}(\vec{x})\, |\vec{x}_\rho|^{-1}\, \partial_\rho = g^{-\frac{1}{2}}(\vec{x})\, \partial_s \qquad \text{in } I \,. \tag{2.13}$$

We introduce

$$\vec{\nu}_g = g^{-\frac{1}{2}}(\vec{x})\, \vec{\nu} = -g^{-\frac{1}{2}}(\vec{x})\, \vec{x}_s^{\,\perp} = -\vec{x}_{s_g}^{\,\perp} \quad \text{and} \quad \vec{\tau}_g = \vec{x}_{s_g} \qquad \text{in } I \,, \tag{2.14}$$

so that $\vec{\tau}_g \,.\, \vec{\nu}_g = 0$ and $|\vec{\tau}_g|_g^2 = |\vec{\nu}_g|_g^2 = (\vec{\nu}_g, \vec{\nu}_g)_g = g(\vec{x})\, \vec{\nu}_g \,.\, \vec{\nu}_g = 1$, and let

$$\mathcal{V}_g = (\vec{x}_t, \vec{\nu}_g)_g = g^{\frac{1}{2}}(\vec{x})\, \vec{x}_t \,.\, \vec{\nu} = g^{\frac{1}{2}}(\vec{x})\, \mathcal{V} \qquad \text{in } I \,. \tag{2.15}$$

It follows from (1.5) that

$$\begin{aligned} \nabla\, g^{\frac{1}{2}}(\vec{x}) &= [\vec{\nu}\,(\vec{\nu}\,.\,\nabla) + \vec{\tau}\,(\vec{\tau}\,.\,\nabla)]\, g^{\frac{1}{2}}(\vec{x}) = \vec{\nu}\,(\vec{\nu}\,.\,\nabla)\, g^{\frac{1}{2}}(\vec{x}) + \vec{\tau}\, \frac{1}{|\vec{x}_\rho|} \left[g^{\frac{1}{2}}(\vec{x}) \right]_\rho \\ &= \vec{\nu}\,(\vec{\nu}\,.\,\nabla)\, g^{\frac{1}{2}}(\vec{x}) + \frac{1}{|\vec{x}_\rho|} \left[g^{\frac{1}{2}}(\vec{x})\, \frac{\vec{x}_\rho}{|\vec{x}_\rho|} \right]_\rho - g^{\frac{1}{2}}(\vec{x})\, \frac{1}{|\vec{x}_\rho|} \left[\frac{\vec{x}_\rho}{|\vec{x}_\rho|} \right]_\rho \\ &= \vec{\nu}\,(\vec{\nu}\,.\,\nabla)\, g^{\frac{1}{2}}(\vec{x}) + \frac{1}{|\vec{x}_\rho|} \left[g^{\frac{1}{2}}(\vec{x})\, \frac{\vec{x}_\rho}{|\vec{x}_\rho|} \right]_\rho - g^{\frac{1}{2}}(\vec{x})\, \varkappa\, \vec{\nu} \qquad \text{in } I \,. \end{aligned} \tag{2.16}$$

Combining (2.12), (2.16), (2.14), (2.15) and (2.1) yields

$$\begin{aligned} \frac{\mathrm{d}}{\mathrm{d}t} L_g(\vec{x}(t)) &= \int_I \left(\nabla\, g^{\frac{1}{2}}(\vec{x}) - \frac{1}{|\vec{x}_\rho|} \left[g^{\frac{1}{2}}(\vec{x})\, \frac{\vec{x}_\rho}{|\vec{x}_\rho|} \right]_\rho \right) .\, \vec{x}_t\, |\vec{x}_\rho| \,\mathrm{d}\rho = \int_I \left[\vec{\nu}\,.\,\nabla\, g^{\frac{1}{2}}(\vec{x}) - g^{\frac{1}{2}}(\vec{x})\, \varkappa \right] \vec{\nu}\,.\,\vec{x}_t\, |\vec{x}_\rho| \,\mathrm{d}\rho \\ &= \int_I \left[\vec{\nu}_g \,.\, \nabla\, g^{\frac{1}{2}}(\vec{x}) - \varkappa \right] \mathcal{V}_g\, |\vec{x}_\rho| \,\mathrm{d}\rho = -\int_I g^{-\frac{1}{2}}(\vec{x}) \left[\varkappa - \vec{\nu}_g \,.\, \nabla\, g^{\frac{1}{2}}(\vec{x}) \right] \mathcal{V}_g\, |\vec{x}_\rho|_g \,\mathrm{d}\rho \\ &= -\int_I \varkappa_g\, \mathcal{V}_g\, |\vec{x}_\rho|_g \,\mathrm{d}\rho \,, \end{aligned} \tag{2.17}$$

where, on recalling (2.14),

$$\varkappa_g = g^{-\frac{1}{2}}(\vec{x}) \left[\varkappa - \vec{\nu}_g \,.\, \nabla\, g^{\frac{1}{2}}(\vec{x}) \right] = g^{-\frac{1}{2}}(\vec{x}) \left[\varkappa - \tfrac{1}{2}\, \vec{\nu} \,.\, \nabla\, \ln g(\vec{x}) \right] \qquad \text{in } I \,. \tag{2.18}$$

Clearly, the curvature $\varkappa_g$ is the first variation of the length (2.3).

For the metric (2.7) we obtain

$$\varkappa_g = (\vec{x}\,.\,\vec{e}_2)^\mu \left[\varkappa + \mu\,\frac{\vec{\nu}\,.\,\vec{e}_2}{\vec{x}\,.\,\vec{e}_2}\right] \qquad \text{in } I\,, \tag{2.19}$$

while for (2.8) we have

$$\varkappa_g = \tfrac{1}{2}\,(1-\alpha\,|\vec{x}|^2)\left[\varkappa - 2\,\alpha\,\left(1-\alpha\,|\vec{x}|^2\right)^{-1}\vec{x}\,.\,\vec{\nu}\right] \qquad \text{in } I\,. \tag{2.20}$$

In addition, combining (2.18), (2.14) and (2.16) yields

$$g(\vec{x})\,\varkappa_g\,\vec{\nu} = \frac{1}{|\vec{x}_\rho|}\left[g^{\frac{1}{2}}(\vec{x})\,\frac{\vec{x}_\rho}{|\vec{x}_\rho|}\right]_\rho - \nabla\, g^{\frac{1}{2}}(\vec{x}) \qquad \text{in } I\,. \tag{2.21}$$

Weak formulations of (1.5) and (2.21) will play an important role in this paper, and so we state them here for later reference. The natural weak formulation of (1.5) is

$$\int_I \varkappa\,\vec{\nu}\,.\,\vec{\eta}\,|\vec{x}_\rho|\,\mathrm{d}\rho + \int_I \vec{x}_\rho\,.\,\vec{\eta}_\rho\,|\vec{x}_\rho|^{-1}\,\mathrm{d}\rho = 0 \quad \forall\,\vec{\eta}\in[H^1(I)]^2\,, \tag{2.22}$$

while a natural weak formulation of (2.21) is

$$\int_I g(\vec{x})\,\varkappa_g\,\vec{\nu}\,.\,\vec{\eta}\,|\vec{x}_\rho|\,\mathrm{d}\rho + \int_I \left[\nabla\, g^{\frac{1}{2}}(\vec{x})\,.\,\vec{\eta} + g^{\frac{1}{2}}(\vec{x})\,\frac{\vec{x}_\rho\,.\,\vec{\eta}_\rho}{|\vec{x}_\rho|^2}\right]|\vec{x}_\rho|\,\mathrm{d}\rho = 0 \quad \forall\,\vec{\eta}\in[H^1(I)]^2\,. \tag{2.23}$$

2.1 *Curvature flow*

It follows from (2.17) that

$$\mathcal{V}_g = \varkappa_g \qquad \text{in } I \tag{2.24}$$

is the natural L^2-gradient flow of L_g with respect to the metric induced by g, i.e.

$$\frac{\mathrm{d}}{\mathrm{d}t}\,L_g(\vec{x}(t)) + \int_I \varkappa_g^2\,|\vec{x}_\rho|_g\,\mathrm{d}\rho = 0\,. \tag{2.25}$$

On recalling (2.15) and (2.18), we can rewrite (2.24) equivalently as

$$g(\vec{x})\,\vec{x}_t\,.\,\vec{\nu} = \varkappa - \tfrac{1}{2}\,\vec{\nu}\,.\,\nabla\,\ln g(\vec{x}) \qquad \text{in } I\,. \tag{2.26}$$

We consider the following weak formulation of (2.26) and (1.5).
($\mathcal{A}$): Let $\vec{x}(0)\in[H^1(I)]^2$. For $t\in(0,T]$ find $\vec{x}(t)\in[H^1(I)]^2$ and $\varkappa(t)\in L^2(I)$ such that (2.22) holds and

$$\int_I g(\vec{x})\,\vec{x}_t\,.\,\vec{\nu}\,\chi\,|\vec{x}_\rho|\,\mathrm{d}\rho = \int_I \left(\varkappa - \tfrac{1}{2}\,\vec{\nu}\,.\,\nabla\,\ln g(\vec{x})\right)\chi\,|\vec{x}_\rho|\,\mathrm{d}\rho \quad \forall\,\chi\in L^2(I)\,. \tag{2.27}$$

An alternative strong formulation of curvature flow to (2.26) is given by

$$g(\vec{x})\,\vec{x}_t = \vec{\varkappa} - \tfrac{1}{2}\,[\vec{\nu}\,.\,\nabla\,\ln g(\vec{x})]\,\vec{\nu} \qquad \text{in } I\,, \tag{2.28}$$

where we recall (1.5). We observe that (2.28) fixes $\vec{x}_t$ to be totally in the normal direction, in contrast to (2.26). We consider the following weak formulation of (2.28) and (1.5), recall (2.22).
($\mathcal{B}$): Let $\vec{x}(0) \in [H^1(I)]^2$. For $t \in (0,T]$ find $\vec{x}(t) \in [H^1(I)]^2$ and $\vec{\varkappa}(t) \in [L^2(I)]^2$ such that

$$\int_I g(\vec{x})\,\vec{x}_t\,.\,\vec{\chi}\,|\vec{x}_\rho|\,\mathrm{d}\rho = \int_I \left(\vec{\varkappa}\,.\,\vec{\chi} - \tfrac{1}{2}\,[\vec{\nu}\,.\,\nabla\,\ln g(\vec{x})]\,\vec{\nu}\,.\,\vec{\chi}\right)|\vec{x}_\rho|\,\mathrm{d}\rho \quad \forall\ \vec{\chi} \in [L^2(I)]^2\,, \tag{2.29a}$$

$$\int_I \vec{\varkappa}\,.\,\vec{\eta}\,|\vec{x}_\rho|\,\mathrm{d}\rho + \int_I \vec{x}_\rho\,.\,\vec{\eta}_\rho\,|\vec{x}_\rho|^{-1}\,\mathrm{d}\rho = 0 \quad \forall\ \vec{\eta} \in [H^1(I)]^2\,. \tag{2.29b}$$

In order to develop stable approximations, we investigate alternative formulations based on (2.23). First we note that combining (2.26) and (2.18) yields

$$g(\vec{x})\,\vec{x}_t\,.\,\vec{\nu} = g^{\frac{1}{2}}(\vec{x})\,\varkappa_g \qquad \text{in } I\,. \tag{2.30}$$

We then consider the following weak formulation of (2.30) and (2.21).
($\mathcal{C}$): Let $\vec{x}(0) \in [H^1(I)]^2$. For $t \in (0,T]$ find $\vec{x}(t) \in [H^1(I)]^2$ and $\varkappa_g(t) \in L^2(I)$ such that (2.23) holds and

$$\int_I g(\vec{x})\,\vec{x}_t\,.\,\vec{\nu}\,\chi\,|\vec{x}_\rho|\,\mathrm{d}\rho = \int_I g^{\frac{1}{2}}(\vec{x})\,\varkappa_g\,\chi\,|\vec{x}_\rho|\,\mathrm{d}\rho \quad \forall\ \chi \in L^2(I)\,. \tag{2.31}$$

Clearly, choosing $\chi = \varkappa_g$ in (2.31) and $\vec{\eta} = \vec{x}_t$ in (2.23) yields (2.25), on noting (2.12) and (2.1).

On recalling (2.14), we introduce

$$\vec{\varkappa}_g = \varkappa_g\,\vec{\nu}_g = g^{-\frac{1}{2}}(\vec{x})\,\varkappa_g\,\vec{\nu} \qquad \text{in } I\,, \tag{2.32}$$

so that an alternative formulation of curvature flow to (2.24) is given by

$$\vec{x}_t = \mathcal{V}_g\,\vec{\nu}_g = \vec{\varkappa}_g \qquad \text{in } I\,, \tag{2.33}$$

where we have recalled (2.15) and (2.14). Similarly to (2.28), the flow (2.33) is again totally in the normal direction. On recalling (2.23), we consider the following weak formulation of (2.33) and (2.32).
($\mathcal{D}$): Let $\vec{x}(0) \in [H^1(I)]^2$. For $t \in (0,T]$ find $\vec{x}(t) \in [H^1(I)]^2$ and $\vec{\varkappa}_g(t) \in [L^2(I)]^2$ such that

$$\int_I g(\vec{x})\,\vec{x}_t\,.\,\vec{\chi}\,|\vec{x}_\rho|\,\mathrm{d}\rho = \int_I g(\vec{x})\,\vec{\varkappa}_g\,.\,\vec{\chi}\,|\vec{x}_\rho|\,\mathrm{d}\rho \quad \forall\ \vec{\chi} \in [L^2(I)]^2\,, \tag{2.34a}$$

$$\int_I g^{\frac{3}{2}}(\vec{x})\,\vec{\varkappa}_g\,.\,\vec{\eta}\,|\vec{x}_\rho|\,\mathrm{d}\rho + \int_I \left[\nabla\, g^{\frac{1}{2}}(\vec{x})\,.\,\vec{\eta} + g^{\frac{1}{2}}(\vec{x})\,\frac{\vec{x}_\rho\,.\,\vec{\eta}_\rho}{|\vec{x}_\rho|^2}\right]|\vec{x}_\rho|\,\mathrm{d}\rho = 0 \quad \forall\ \vec{\eta} \in [H^1(I)]^2\,. \tag{2.34b}$$

Choosing $\vec{\chi} = g^{\frac{1}{2}}(\vec{x})\,\vec{\varkappa}_g$ in (2.34a) and $\vec{\eta} = \vec{x}_t$ in (2.34b), on noting (2.12), yields

$$\frac{\mathrm{d}}{\mathrm{d}t} L_g(\vec{x}(t)) + \int_I g^{\frac{3}{2}}(\vec{x})\,|\vec{\varkappa}_g|^2\,|\vec{x}_\rho|\,\mathrm{d}\rho = 0\,, \tag{2.35}$$

which is equivalent to (2.25), on recalling (2.32) and (2.1).

We observe that the variable $\varkappa_g$ can be eliminated from $(\mathcal{C})$ by choosing $\chi = g^{\frac{1}{2}}(\vec{x})\,\vec{\nu}\,.\,\vec{\eta}$ in (2.31), and then combining (2.31) and (2.22) to yield

$$\int_I g^{\frac{3}{2}}(\vec{x})\,(\vec{x}_t\,.\,\vec{\nu})\,\vec{\eta}\,.\,\vec{\nu}\,|\vec{x}_\rho|\,\mathrm{d}\rho + \int_I \left[\nabla\, g^{\frac{1}{2}}(\vec{x})\,.\,\vec{\eta} + g^{\frac{1}{2}}(\vec{x})\,\frac{\vec{x}_\rho\,.\,\vec{\eta}_\rho}{|\vec{x}_\rho|^2}\right]|\vec{x}_\rho|\,\mathrm{d}\rho = 0 \quad \forall\,\vec{\eta} \in [H^1(I)]^2\,. \tag{2.36}$$

Similarly, $\vec{\varkappa}_g$ can be eliminated from $(\mathcal{D})$ by choosing $\vec{\chi} = g^{\frac{1}{2}}(\vec{x})\,\vec{\eta}$ in (2.34a) to yield

$$\int_I g^{\frac{3}{2}}(\vec{x})\,\vec{x}_t\,.\,\vec{\eta}\,|\vec{x}_\rho|\,\mathrm{d}\rho + \int_I \left[\nabla\, g^{\frac{1}{2}}(\vec{x})\,.\,\vec{\eta} + g^{\frac{1}{2}}(\vec{x})\,\frac{\vec{x}_\rho\,.\,\vec{\eta}_\rho}{|\vec{x}_\rho|^2}\right]|\vec{x}_\rho|\,\mathrm{d}\rho = 0 \quad \forall\,\vec{\eta} \in [H^1(I)]^2\,. \tag{2.37}$$

The reason why we have introduced four different weak formulations for curvature flow is that upon discretization they lead to very different numerical approximations with different properties. Let us discuss some of these aspects in more detail. First, as mentioned before, the parameterizations $\vec{x}$ in the formulations $(\mathcal{B})$ and $(\mathcal{D})$ change only in the normal direction, and the tangential part of $\vec{x}_t$ is set to zero. Hence, finite element approximations based on them will be in the spirit of Dziuk (1994) for Euclidean curvature flow. In contrast, the formulations $(\mathcal{A})$ and $(\mathcal{C})$ only specify the normal part of $\vec{x}_t$, with the tangential part being arbitrary. However, upon discretization the tangential velocity will be fixed, and in the case of the formulation $(\mathcal{A})$ will lead to an equidistribution property. Hence, the finite element approximation based on it will be in the spirit of Barrett *et al.* (2007a,b, 2011). The tangential motion induced by the discretization of $(\mathcal{C})$ is less well defined, but in practice it leads to good distributions of mesh points and it avoids the coalescence of vertices.

We also remark that the formulations $(\mathcal{A})$ and $(\mathcal{B})$ are written in terms of the Euclidean geometry of $\mathbb{R}^2$. As a consequence, it does not seem possible to prove a stability result for finite element approximations based on them, i.e. a discrete analogue of (2.25). This lack of a stability result is the main motivation behind the alternative formulations $(\mathcal{C})$ and $(\mathcal{D})$. We note that these formulations use the proper Riemannian geometry, and so they are written in terms of $\varkappa_g$ and $\vec{\varkappa}_g$, respectively. This means that discretizations based on these formulations admit a stability proof, and so discrete analogues of (2.25) and (2.35) can be derived. Lastly we mention that the discussed properties of the resulting finite element schemes are also summarized in Table 2, below.

2.2 *Curve diffusion*

We consider the flow

$$\mathcal{V}_g = -(\varkappa_g)_{s_g s_g} = -g^{-\frac{1}{2}}(\vec{x})\left[g^{-\frac{1}{2}}(\vec{x})[\varkappa_g]_s\right]_s = -\frac{1}{g^{\frac{1}{2}}(\vec{x})\,|\vec{x}_\rho|}\left[\frac{[\varkappa_g]_\rho}{g^{\frac{1}{2}}(\vec{x})\,|\vec{x}_\rho|}\right]_\rho \qquad \text{in } I\,, \tag{2.38}$$

where we have recalled (2.13). On noting (2.17), and similarly (2.25), it follows that (2.38) is the natural H^{-1}-gradient flow of L_g with respect to the metric induced by g, i.e.

$$\frac{\mathrm{d}}{\mathrm{d}t} L_g(\vec{x}(t)) + \int_I (\partial_{s_g} \varkappa_g)^2\, |\vec{x}_\rho|_g \,\mathrm{d}\rho = 0\,. \tag{2.39}$$

Moreover, if $\Gamma(t) = \vec{x}(I,t)$ encloses a domain $\Omega(t) \subset \mathbb{R}^2$, with $\vec{\nu} \circ \vec{x}^{-1}$ denoting the outer normal on $\partial\Omega(t) = \Gamma(t)$, on recalling (2.4), (2.1) and (2.15), it follows from a transport theorem, see, e.g., Deckelnick *et al.* (2005, (2.22)), that

$$\frac{\mathrm{d}}{\mathrm{d}t} A_g(\vec{x}(t)) = \frac{\mathrm{d}}{\mathrm{d}t} \int_{\Omega(t)} g(\vec{z})\,\mathrm{d}\vec{z} = \int_I g(\vec{x})\,\mathcal{V}\,|\vec{x}_\rho|\,\mathrm{d}\rho = \int_I \mathcal{V}_g\,|\vec{x}_\rho|_g\,\mathrm{d}\rho\,.$$

Hence, solutions to (2.38) satisfy, on noting (2.13),

$$\frac{\mathrm{d}}{\mathrm{d}t} A_g(\vec{x}(t)) = -\int_I (\varkappa_g)_{s_g s_g}\,|\vec{x}_\rho|_g\,\mathrm{d}\rho = -\int_I \left[(\varkappa_g)_{s_g}\right]_\rho \,\mathrm{d}\rho = 0\,, \tag{2.40}$$

and so the total enclosed area is preserved.

Our weak formulations are going be to based on the following equivalent formulation of (2.38):

$$g(\vec{x})\,\vec{x}_t\,.\,\vec{\nu} = -\frac{1}{|\vec{x}_\rho|}\left(\frac{[\varkappa_g]_\rho}{g^{\frac{1}{2}}(\vec{x})\,|\vec{x}_\rho|}\right)_\rho \qquad \text{in } I\,, \tag{2.41}$$

where we have recalled (2.15).

We consider the following weak formulation of (2.41) and (1.5), on recalling (2.18).

($\mathcal{E}$): Let $\vec{x}(0) \in [H^1(I)]^2$. For $t \in (0,T]$ find $\vec{x}(t) \in [H^1(I)]^2$ and $\varkappa(t) \in H^1(I)$ such that (2.22) holds and

$$\int_I g(\vec{x})\,\vec{x}_t\,.\,\vec{\nu}\,\chi\,|\vec{x}_\rho|\,\mathrm{d}\rho = \int_I g^{-\frac{1}{2}}(\vec{x})\,\left(g^{-\frac{1}{2}}(\vec{x})\left[\varkappa - \tfrac{1}{2}\,\vec{\nu}\,.\,\nabla\,\ln g(\vec{x})\right]\right)_\rho \chi_\rho\,|\vec{x}_\rho|^{-1}\,\mathrm{d}\rho \quad \forall\,\chi \in H^1(I)\,. \tag{2.42}$$

Similarly to ($\mathcal{C}$) for curvature flow, we also introduce the following alternative weak formulation of curve diffusion, which treats the curvature $\varkappa_g$ as an unknown, and so is based on (2.41) and (2.21).

($\mathcal{F}$): Let $\vec{x}(0) \in [H^1(I)]^2$. For $t \in (0,T]$ find $\vec{x}(t) \in [H^1(I)]^2$ and $\varkappa_g(t) \in H^1(I)$ such that (2.23) holds and

$$\int_I g(\vec{x})\, \vec{x}_t \cdot \vec{\nu}\, \chi\, |\vec{x}_\rho|\, \mathrm{d}\rho = \int_I g^{-\frac{1}{2}}(\vec{x})\, [\varkappa_g]_\rho\, \chi_\rho\, |\vec{x}_\rho|^{-1}\, \mathrm{d}\rho \quad \forall\, \chi \in H^1(I)\,. \tag{2.43}$$

Choosing $\chi = \varkappa_g$ in (2.43) and $\vec{\eta} = \vec{x}_t$ in (2.23) yields that (2.39) holds, on noting from (2.13) that

$$(\partial_{s_g} \varkappa_g)^2\, |\vec{x}_\rho|_g = g^{-1}(\vec{x})\, |\vec{x}_\rho|^{-2}\, (\partial_\rho \varkappa_g)^2\, g^{\frac{1}{2}}(\vec{x})\, |\vec{x}_\rho| = g^{-\frac{1}{2}}(\vec{x})\, (\partial_\rho \varkappa_g)^2\, |\vec{x}_\rho|^{-1} \qquad \text{in } I\,. \tag{2.44}$$

We remark that ($\mathcal{E}$) and ($\mathcal{F}$) loosely correspond to the formulations ($\mathcal{A}$) and ($\mathcal{C}$) for curvature flow, and so they inherit the corresponding properties discussed at the end of Section 2.1. For example, approximations based on ($\mathcal{E}$) will satisfy an equidistribution property, while those based on ($\mathcal{F}$) will satisfy a stability result. It does not seem to be easily possible to derive a formulation of curve diffusion, (2.38), in terms of $\vec{x}$ or $\vec{\varkappa}_g$, and so we do not consider analogues of ($\mathcal{B}$) and ($\mathcal{D}$) here. In any case, schemes based on such formulations would be expected to suffer from coalescence of vertices in practice, as is the case, for example for the scheme in Dziuk *et al.* (2002) for Euclidean curve diffusion.

The discussed properties of the finite element schemes based on ($\mathcal{E}$) and ($\mathcal{F}$) are summarized in Table 2, below.

2.3 *Elastic flow*

Elastic flow is the L^2-gradient flow of the elastic energy

$$W_g(\vec{x}) = \tfrac{1}{2} \int_I |\vec{\varkappa}_g|_g^2\, |\vec{x}_\rho|_g\, \mathrm{d}\rho$$

with respect to the metric induced by g, in analogy to (2.24) being the L^2-gradient flow of $L_g(\vec{x})$; recall (2.17). An important ingredient in deriving the L^2-gradient flow of $W_g(\vec{x})$ is the first variation of this energy or, equivalently, necessary conditions that smooth critical points of the energy need to satisfy. For a general two-dimensional oriented Riemannian manifold, the latter have been derived with the help of differential geometry concepts in Langer & Singer (1984, (1.2)).

We will derive elastic flow, for arbitrary Riemannian manifolds that are conformally equivalent to the Euclidean plane, with the help of variational methods. The obtained formulation, in terms of $\varkappa_g$, easily lends itself to a suitable numerical approximation with the help of the techniques developed in this paper. Moreover, our derivation of elastic flow will guide the introduction of alternative numerical approximations for which a stability result can be shown, and we consider this topic in Barrett *et al.* (2018).

We remark that for the special case of a Riemannian manifold with constant sectional curvature, such as the hyperbolic plane, recall (2.9) and (2.6a), a formulation of elastic flow in terms of $\vec{\varkappa}_g$ was recently derived in Dall'Acqua & Spener (2017, (5)); see also Remark 2.2 below. Our derivation, on the other hand, holds true for Riemannian manifolds that are conformally equivalent to the Euclidean plane, with possibly nonconstant sectional curvature. Moreover, our derivation has the advantage that it does not require advanced knowledge of Riemannian differential geometry.

We begin by writing $W_g(\vec{x})$ in terms of the Euclidean curvature of the curve $\vec{x}(I)$. On noting (2.32), (1.2), (2.18) and (2.1), it holds that

$$W_g(\vec{x}) = \tfrac{1}{2} \int_I |\vec{x}_g|_g^2 \, |\vec{x}_\rho|_g \,\mathrm{d}\rho = \tfrac{1}{2} \int_I \varkappa_g^2 \, |\vec{x}_\rho|_g \,\mathrm{d}\rho = \tfrac{1}{2} \int_I g^{-\frac{1}{2}}(\vec{x}) \left(\varkappa - \tfrac{1}{2}\,\vec{\nu} \,.\, \nabla \,\ln g(\vec{x})\right)^2 |\vec{x}_\rho| \,\mathrm{d}\rho \,. \tag{2.45}$$

In order to simplify some of the following formulas, we introduce the abbreviations

$$\mathfrak{z} = \vec{\nu}_g \,.\, \nabla\, g^{\frac{1}{2}}(\vec{x}) = \tfrac{1}{2}\,\vec{\nu} \,.\, \nabla \,\ln g(\vec{x}) \quad \text{and} \quad \widetilde{\varkappa}_g = g^{\frac{1}{2}}(\vec{x})\,\varkappa_g = \varkappa - \mathfrak{z} \qquad \text{in } I \,, \tag{2.46}$$

where we have recalled (2.18). Moreover, in the following we will often omit the dependence of g on $\vec{x}$, and we simply write g for $g(\vec{x})$ and so on. It follows from (2.45), (2.46), (1.5), (2.15) and (2.1) that

$$\begin{aligned}
\frac{\mathrm{d}}{\mathrm{d}t}\, W_g(\vec{x}(t)) &= \tfrac{1}{2}\, \frac{\mathrm{d}}{\mathrm{d}t} \int_I g^{-\frac{1}{2}}(\vec{x})\, \widetilde{\varkappa}_g^2 \, |\vec{x}_\rho| \,\mathrm{d}\rho \\
&= \tfrac{1}{2} \int_I (g^{-\frac{1}{2}})_t \, \widetilde{\varkappa}_g^2 \, |\vec{x}_\rho| \,\mathrm{d}\rho + \int_I g^{-\frac{1}{2}} \, (\widetilde{\varkappa}_g)_t \, \widetilde{\varkappa}_g \, |\vec{x}_\rho| \,\mathrm{d}\rho + \tfrac{1}{2} \int_I g^{-\frac{1}{2}} \, \widetilde{\varkappa}_g^2 \, \vec{x}_\rho \,.\, (\vec{x}_t)_\rho \, |\vec{x}_\rho|^{-1} \,\mathrm{d}\rho \\
&= \tfrac{1}{2} \int_I \left(\vec{x}_t \,.\, \nabla\, g^{-\frac{1}{2}}\right) \widetilde{\varkappa}_g^2 \, |\vec{x}_\rho| \,\mathrm{d}\rho + \int_I g^{-\frac{1}{2}} \, (\widetilde{\varkappa}_g)_t \, \widetilde{\varkappa}_g \, |\vec{x}_\rho| \,\mathrm{d}\rho - \tfrac{1}{2} \int_I \left(g^{-\frac{1}{2}} \, \widetilde{\varkappa}_g^2 \, \vec{x}_s\right)_s \,.\, \vec{x}_t \, |\vec{x}_\rho| \,\mathrm{d}\rho \\
&= \tfrac{1}{2} \int_I \left(\vec{x}_t \,.\, \nabla\, g^{-\frac{1}{2}}\right) \widetilde{\varkappa}_g^2 \, |\vec{x}_\rho| \,\mathrm{d}\rho + \int_I g^{-\frac{1}{2}} \, (\widetilde{\varkappa}_g)_t \, \widetilde{\varkappa}_g \, |\vec{x}_\rho| \,\mathrm{d}\rho \\
&\quad - \tfrac{1}{2} \int_I \left[\left(\vec{x}_s \,.\, \nabla\, g^{-\frac{1}{2}}\right) \widetilde{\varkappa}_g^2 \, \vec{x}_s + 2 g^{-\frac{1}{2}} \, \widetilde{\varkappa}_g \, (\widetilde{\varkappa}_g)_s \, \vec{x}_s + g^{-\frac{1}{2}} \, \widetilde{\varkappa}_g^2 \, \varkappa \, \vec{\nu}\right] \,.\, \vec{x}_t \, |\vec{x}_\rho| \,\mathrm{d}\rho \\
&= \tfrac{1}{2} \int_I \left(\vec{\nu} \,.\, \nabla\, g^{-\frac{1}{2}}\right) \widetilde{\varkappa}_g^2 \, \mathcal{V} \, |\vec{x}_\rho| \,\mathrm{d}\rho + \int_I g^{-\frac{1}{2}} \, \widetilde{\varkappa}_g \, [(\widetilde{\varkappa}_g)_t - \, (\widetilde{\varkappa}_g)_s \, \vec{x}_s \,.\, \vec{x}_t] \, |\vec{x}_\rho| \,\mathrm{d}\rho \\
&\quad - \tfrac{1}{2} \int_I g^{-\frac{1}{2}} \, \widetilde{\varkappa}_g^2 \, \varkappa \, \mathcal{V} \, |\vec{x}_\rho| \,\mathrm{d}\rho \\
&= \tfrac{1}{2} \int_I \left[\left(\vec{\nu} \,.\, \nabla\, g^{-\frac{1}{2}}\right) - g^{-\frac{1}{2}} \, \varkappa\right] \varkappa_g^2 \, \mathcal{V}_g \, |\vec{x}_\rho|_g \,\mathrm{d}\rho + \int_I \varkappa_g \, [(\widetilde{\varkappa}_g)_t - \, (\widetilde{\varkappa}_g)_s \, \vec{x}_s \,.\, \vec{x}_t] \, |\vec{x}_\rho| \,\mathrm{d}\rho \,.
\end{aligned} \tag{2.47}$$

We have from (2.46) that

$$\varkappa_g - g^{-\frac{1}{2}} \, \varkappa = -\tfrac{1}{2}\, g^{-\frac{1}{2}} \, \vec{\nu} \,.\, \nabla \,\ln g = \vec{\nu} \,.\, \nabla\, g^{-\frac{1}{2}} \qquad \text{in } I \,,$$

and so it follows from (2.47) that

$$\frac{\mathrm{d}}{\mathrm{d}t}\, W_g(\vec{x}(t)) = \tfrac{1}{2} \int_I \left[\varkappa_g - 2 g^{-\frac{1}{2}} \, \varkappa\right] \varkappa_g^2 \, \mathcal{V}_g \, |\vec{x}_\rho|_g \,\mathrm{d}\rho + \int_I \varkappa_g \, [(\widetilde{\varkappa}_g)_t - \, (\widetilde{\varkappa}_g)_s \, \vec{x}_s \,.\, \vec{x}_t] \, |\vec{x}_\rho| \,\mathrm{d}\rho = T_1 + T_2 \,. \tag{2.48}$$

We first deal with the term T_2. It follows from (1.1), (1.5) and (2.15) that the following identities hold in I:

$$\vec{\nu}_s = -\varkappa\,\vec{x}_s\,, \quad \vec{\nu}_{ss} = -\varkappa_s\,\vec{x}_s - \varkappa^2\,\vec{\nu}\,, \tag{2.49a}$$

$$\vec{\nu}_t = -((\vec{x}_s)_t\,.\,\vec{\nu})\,\vec{x}_s = -\left(\left(\vec{x}_\rho\,|\vec{x}_\rho|^{-1}\right)_t\,.\,\vec{\nu}\right)\,\vec{x}_s = -((\vec{x}_t)_s\,.\,\vec{\nu})\,\vec{x}_s\,, \tag{2.49b}$$

$$\vec{\nu}_t - (\vec{x}_s\,.\,\vec{x}_t)\,\vec{\nu}_s = -\mathcal{V}_s\,\vec{x}_s\,. \tag{2.49c}$$

Combining (2.49a) and (2.49b) yields, on recalling (2.13) and (2.15),

$$\begin{aligned}\varkappa_t &= -\vec{x}_s\,.\,(\vec{\nu}_s)_t = -\vec{x}_s\,.\,(\vec{\nu}_\rho\,|\vec{x}_\rho|^{-1})_t = -\vec{x}_s\,.\,(\vec{\nu}_t)_s + (\vec{x}_s\,.\,\vec{\nu}_s)\,\vec{x}_s\,.\,(\vec{x}_t)_s = -\vec{x}_s\,.\,(\vec{\nu}_t)_s + \vec{\nu}_s\,.\,(\vec{x}_t)_s\\ &= \vec{x}_s\,.\,\big[((\vec{x}_t)_s\,.\,\vec{\nu})\,\vec{x}_s\big]_s + \vec{\nu}_s\,.\,(\vec{x}_t)_s = ((\vec{x}_t)_s\,.\,\vec{\nu})_s + \vec{\nu}_s\,.\,(\vec{x}_t)_s = (\vec{x}_t\,.\,\vec{\nu})_{ss} - \vec{x}_t\,.\,\vec{\nu}_{ss}\\ &= (\vec{x}_t\,.\,\vec{\nu})_{ss} + \vec{x}_t\,.\,[\varkappa_s\,\vec{x}_s + \varkappa^2\,\vec{\nu}] = \mathcal{V}_{ss} + \varkappa^2\,\mathcal{V} + \varkappa_s\,\vec{x}_s\,.\,\vec{x}_t \qquad \text{in } I;\end{aligned} \tag{2.50}$$

compare also with Barrett *et al.* (2017, (A.3)). It follows from (2.46), (2.50) and (2.49c) that

$$\begin{aligned}(\widetilde{\varkappa}_g)_t - (\widetilde{\varkappa}_g)_s\,\vec{x}_s\,.\,\vec{x}_t &= \varkappa_t - \varkappa_s\,\vec{x}_s\,.\,\vec{x}_t - (\mathfrak{z}_t - \mathfrak{z}_s\,\vec{x}_s\,.\,\vec{x}_t) = \mathcal{V}_{ss} + \varkappa^2\,\mathcal{V} - (\mathfrak{z}_t - \mathfrak{z}_s\,\vec{x}_s\,.\,\vec{x}_t)\\ &= \mathcal{V}_{ss} + \varkappa^2\,\mathcal{V} - \tfrac{1}{2}\,(\vec{\nu}_t - (\vec{x}_s\,.\,\vec{x}_t)\,\vec{\nu}_s)\,.\,\nabla\,\ln g - \tfrac{1}{2}\,((\nabla\,\ln g)_t - (\vec{x}_s\,.\,\vec{x}_t)\,(\nabla\,\ln g)_s)\,.\,\vec{\nu}\\ &= \mathcal{V}_{ss} + \varkappa^2\,\mathcal{V} + \tfrac{1}{2}\,\mathcal{V}_s\,\vec{x}_s\,.\,\nabla\,\ln g - \tfrac{1}{2}\,((\nabla\,\ln g)_t - (\vec{x}_s\,.\,\vec{x}_t)\,(\nabla\,\ln g)_s)\,.\,\vec{\nu} \qquad \text{in } I\,.\end{aligned} \tag{2.51}$$

Combining (2.48) and (2.51) yields, on noting (2.15), (2.1), (1.5) and (2.46),

$$\begin{aligned}T_2 &= \int_I \varkappa_g\,[\mathcal{V}_{ss} + \varkappa^2\,\mathcal{V}]\,|\vec{x}_\rho|\,\mathrm{d}\rho + \tfrac{1}{2}\int_I \varkappa_g\,[\mathcal{V}_s\,\vec{x}_s\,.\,\nabla\,\ln g - ((\nabla\,\ln g)_t - (\vec{x}_s\,.\,\vec{x}_t)\,(\nabla\,\ln g)_s)\,.\,\vec{\nu}]\,|\vec{x}_\rho|\,\mathrm{d}\rho\\ &= \int_I [(\varkappa_g)_{ss} + \varkappa^2\,\varkappa_g]\,\mathcal{V}\,|\vec{x}_\rho|\,\mathrm{d}\rho - \tfrac{1}{2}\int_I [(\varkappa_g)_s\,\vec{x}_s\,.\,\nabla\,\ln g + \varkappa_g\,\vec{x}_{ss}\,.\,\nabla\,\ln g + \varkappa_g\,\vec{x}_s\,.\,(\nabla\,\ln g)_s]\,\mathcal{V}\,|\vec{x}_\rho|\,\mathrm{d}\rho\\ &\quad - \tfrac{1}{2}\int_I \varkappa_g\,[((\nabla\,\ln g)_t - (\vec{x}_s\,.\,\vec{x}_t)\,(\nabla\,\ln g)_s)\,.\,\vec{\nu}]\,|\vec{x}_\rho|\,\mathrm{d}\rho\\ &= \int_I g^{-1}\,[(\varkappa_g)_{ss} + \varkappa^2\,\varkappa_g]\,\mathcal{V}_g\,|\vec{x}_\rho|_g\,\mathrm{d}\rho - \tfrac{1}{2}\int_I [(\varkappa_g)_s\,(\ln g)_s + 2\,\varkappa_g\,\varkappa\,\mathfrak{z} + \varkappa_g\,\vec{x}_s\,.\,(\nabla\,\ln g)_s]\,\mathcal{V}\,|\vec{x}_\rho|\,\mathrm{d}\rho\\ &\quad - \tfrac{1}{2}\int_I \varkappa_g\,[((\nabla\,\ln g)_t - (\vec{x}_s\,.\,\vec{x}_t)\,(\nabla\,\ln g)_s)\,.\,\vec{\nu}]\,|\vec{x}_\rho|\,\mathrm{d}\rho\,.\end{aligned} \tag{2.52}$$

Combining (2.48) and (2.52) we have, on noting (2.13), (2.15), (2.1) and (2.46),

$$\begin{aligned}
\frac{\mathrm{d}}{\mathrm{d}t}\, W_g(\vec{x}(t)) &= \int_I \Big[\tfrac{1}{2}\,\varkappa_g^3 - g^{-\frac{1}{2}}\,\varkappa\,\varkappa_g^2 + (\varkappa_g)_{s_g s_g} - (g^{-\frac{1}{2}})_s\,(\varkappa_g)_{s_g} + g^{-1}\,\varkappa^2\,\varkappa_g\Big]\,\mathcal{V}_g\,|\vec{x}_\rho|_g\,\mathrm{d}\rho \\
&\quad + \int_I [(\varkappa_g)_{s_g}\,(g^{-\frac{1}{2}})_s - g^{-1}\,\varkappa_g\,\varkappa\,\mathfrak{z}]\,\mathcal{V}_g\,|\vec{x}_\rho|_g\,\mathrm{d}\rho \\
&\quad - \tfrac{1}{2}\int_I \varkappa_g\,[((\nabla\,\ln g)_t - (\vec{x}_s\,.\,\vec{x}_t)\,(\nabla\,\ln g)_s)\,.\,\vec{\nu} + \vec{x}_s\,.\,(\nabla\,\ln g)_s\,\mathcal{V}\,]\,|\vec{x}_\rho|\,\mathrm{d}\rho \\
&= \int_I \Big[(\varkappa_g)_{s_g s_g} + \tfrac{1}{2}\,\varkappa_g^3 - g^{-1}\,\varkappa\,\varkappa_g\,\Big(g^{\frac{1}{2}}\,\varkappa_g - \varkappa + \mathfrak{z}\Big)\Big]\,\mathcal{V}_g\,|\vec{x}_\rho|_g\,\mathrm{d}\rho \\
&\quad - \tfrac{1}{2}\int_I \varkappa_g\,[((\nabla\,\ln g)_t - (\vec{x}_s\,.\,\vec{x}_t)\,(\nabla\,\ln g)_s)\,.\,\vec{\nu} + \vec{x}_s\,.\,(\nabla\,\ln g)_s\,\mathcal{V}\,]\,|\vec{x}_\rho|\,\mathrm{d}\rho \\
&= \int_I \Big[(\varkappa_g)_{s_g s_g} + \tfrac{1}{2}\,\varkappa_g^3\Big]\,\mathcal{V}_g\,|\vec{x}_\rho|_g\,\mathrm{d}\rho \\
&\quad - \tfrac{1}{2}\int_I \varkappa_g\,[((\nabla\,\ln g)_t - (\vec{x}_s\,.\,\vec{x}_t)\,(\nabla\,\ln g)_s)\,.\,\vec{\nu} + \vec{x}_s\,.\,(\nabla\,\ln g)_s\,\mathcal{V}\,]\,|\vec{x}_\rho|\,\mathrm{d}\rho\,. \qquad (2.53)
\end{aligned}$$

It remains to deal with the final integral in (2.53). To this end, we note that

$$\begin{aligned}
&((\nabla\,\ln g)_t - (\vec{x}_s\,.\,\vec{x}_t)\,(\nabla\,\ln g)_s)\,.\,\vec{\nu} + \vec{x}_s\,.\,(\nabla\,\ln g)_s\,\mathcal{V} \\
&\quad = \vec{\nu}\,.\,(D^2\,\ln g)\,\vec{x}_t - (\vec{x}_s\,.\,\vec{x}_t)\,\vec{\nu}\,.\,(D^2\,\ln g)\,\vec{x}_s + \mathcal{V}\,\vec{x}_s\,.\,(D^2\,\ln g)\,\vec{x}_s \\
&\quad = \mathcal{V}\,\vec{\nu}\,.\,(D^2\,\ln g)\,\vec{\nu} + \mathcal{V}\,\vec{x}_s\,.\,(D^2\,\ln g)\,\vec{x}_s = \mathcal{V}\,\Delta\,\ln g \qquad \text{in } I\,. \qquad (2.54)
\end{aligned}$$

Combining (2.53) and (2.54) yields, on noting (2.15), (2.1) and (2.9), that

$$\begin{aligned}
\frac{\mathrm{d}}{\mathrm{d}t}\, W_g(\vec{x}(t)) &= \int_I \Big[(\varkappa_g)_{s_g s_g} + \tfrac{1}{2}\,\varkappa_g^3\Big]\,\mathcal{V}_g\,|\vec{x}_\rho|_g\,\mathrm{d}\rho - \tfrac{1}{2}\int_I \varkappa_g\,(\Delta\,\ln g)\,\mathcal{V}\,|\vec{x}_\rho|\,\mathrm{d}\rho \\
&= \int_I \Big[(\varkappa_g)_{s_g s_g} + \tfrac{1}{2}\,\varkappa_g^3 + S_0(\vec{x})\,\varkappa_g\Big]\,\mathcal{V}_g\,|\vec{x}_\rho|_g\,\mathrm{d}\rho\,. \qquad (2.55)
\end{aligned}$$

It follows from (2.55) that elastic flow is given by

$$\mathcal{V}_g = -(\varkappa_g)_{s_g s_g} - \tfrac{1}{2}\,\varkappa_g^3 - S_0(\vec{x})\,\varkappa_g \qquad \text{in } I\,. \qquad (2.56)$$

REMARK 2.1 We note that in the special case (2.6b), it follows from (2.18) and (2.9) that $\varkappa_g = \varkappa$ and $S_0 = 0$, and so (2.56) collapses to

$$\mathcal{V} = -\varkappa_{ss} - \tfrac{1}{2}\,\varkappa^3 \qquad \text{in } I\,,$$

i.e. to elastic flow in the Euclidean plane; compare, e.g., Barrett *et al.* (2008, (1.8)).

REMARK 2.2 In the special case (2.6a), i.e. (2.7) with $\mu = 1$, it follows from (2.10) that sectional curvature $S_0 = -1$ is constant, and so (2.56) collapses to

$$\mathcal{V}_g = -(\varkappa_g)_{s_g s_g} - \tfrac{1}{2}\,\varkappa_g^3 + \varkappa_g \qquad \text{in } I\,, \tag{2.57}$$

which is also called hyperbolic elastic flow. In order to show that (2.57) is equivalent to Dall'Acqua & Spener (2017, (5)), for the length parameter $\lambda = 0$, i.e. to

$$\vec{x}_t = -\left(\nabla^{\perp}_{s_g}\right)^2 \vec{\varkappa}_g - \tfrac{1}{2}\,|\vec{\varkappa}_g|_g^2\,\vec{\varkappa}_g + \vec{\varkappa}_g = -\left(\nabla^{\perp}_{s_g}\right)^2 \vec{\varkappa}_g - \tfrac{1}{2}\,\varkappa_g^3\,\vec{\nu}_g + \varkappa_g\,\vec{\nu}_g \qquad \text{in } I\,, \tag{2.58}$$

we make the following observations. It follows from (2.32), (2.19) for $\mu = 1$, (2.13), (2.14) and $\vec{e}_2^{\,\perp} = \vec{e}_1$ that

$$\begin{aligned}
\vec{\varkappa}_g &= (\vec{x}\,.\,\vec{e}_2)^2 \left[\varkappa + \frac{\vec{\nu}\,.\,\vec{e}_2}{\vec{x}\,.\,\vec{e}_2}\right]\vec{\nu} = \vec{x}\,.\,\vec{e}_2\,\big[(\vec{x}\,.\,\vec{e}_2)\,\vec{x}_s\big]_s - \vec{x}\,.\,\vec{e}_2\,(\vec{x}_s\,.\,\vec{e}_2)\,\vec{x}_s + \vec{x}\,.\,\vec{e}_2\,(\vec{\nu}\,.\,\vec{e}_2)\,\vec{\nu} \\
&= \vec{x}_{s_g s_g} - \vec{x}\,.\,\vec{e}_2\,\big[(\vec{x}_s\,.\,\vec{e}_2)\,\vec{x}_s - (\vec{\nu}\,.\,\vec{e}_2)\,\vec{\nu}\big] = \vec{x}_{s_g s_g} - (\vec{x}\,.\,\vec{e}_2)^{-1}\left[(\vec{x}_{s_g}\,.\,\vec{e}_2)\,\vec{x}_{s_g} - (\vec{\nu}_g\,.\,\vec{e}_2)\,\vec{\nu}_g\right] \\
&= \vec{x}_{s_g s_g} - (\vec{x}\,.\,\vec{e}_2)^{-1}\left[(\vec{x}_{s_g}\,.\,\vec{e}_2)\,\vec{x}_{s_g} - (\vec{x}^{\,\perp}_{s_g}\,.\,\vec{e}_2)\,\vec{x}^{\,\perp}_{s_g}\right] = \vec{x}_{s_g s_g} - (\vec{x}\,.\,\vec{e}_2)^{-1}\left[(\vec{x}_{s_g}\,.\,\vec{e}_2)\,\vec{x}_{s_g} + (\vec{x}_{s_g}\,.\,\vec{e}_1)\,\vec{x}^{\,\perp}_{s_g}\right] \\
&= \vec{x}_{s_g s_g} + (\vec{x}\,.\,\vec{e}_2)^{-1}\left[-2\,\vec{x}_{s_g}\,.\,\vec{e}_1\,(\vec{x}_{s_g}\,.\,\vec{e}_2)\,\vec{e}_1 + \Big((\vec{x}_{s_g}\,.\,\vec{e}_1)^2 - (\vec{x}_{s_g}\,.\,\vec{e}_2)^2\Big)\,\vec{e}_2\right] \qquad \text{in } I\,,
\end{aligned} \tag{2.59}$$

which agrees with Dall'Acqua & Spener (2017, (12)). Alternatively, one can also write (2.59), on noting the last equation on its second line, as

$$\vec{\varkappa}_g = \nabla_{s_g}\,\vec{x}_{s_g} \qquad \text{in } I\,, \tag{2.60}$$

where the covariant derivative is defined by

$$\nabla_{s_g}\vec{f} = \vec{f}_{s_g} + (\vec{x}\,.\,\vec{e}_2)^{-1}\left[(\vec{f}\,.\,\vec{e}_1)\,\vec{\nu}_g - (\vec{f}\,.\,\vec{e}_2)\,\vec{x}_{s_g}\right] \qquad \text{in } I\,, \tag{2.61}$$

on recalling (2.14) and that $\vec{e}_1^{\,\perp} = -\vec{e}_2$. We remark that (2.60) agrees with Dall'Acqua & Spener (2017, expression under (1)), on noting the expression for ∇_{s_g} in Dall'Acqua & Spener (2017, on the top of page 5). In addition, we define

$$\nabla^{\perp}_{s_g}\vec{f} = \nabla_{s_g}\vec{f} - (\nabla_{s_g}\vec{f}, \vec{x}_{s_g})_g\,\vec{x}_{s_g} = (\nabla_{s_g}\vec{f}, \vec{\nu}_g)_g\,\vec{\nu}_g \qquad \text{in } I; \tag{2.62}$$

see Dall'Acqua & Spener (2017, (13)). It follows from (2.62) and (2.61), on recalling (2.14), that

$$\nabla^{\perp}_{s_g}\vec{f} = \left[(\vec{f}_{s_g}, \vec{\nu}_g)_g + (\vec{x}\,.\,\vec{e}_2)^{-1}\vec{f}\,.\,\vec{e}_1\right]\vec{\nu}_g \qquad \text{in } I\,. \tag{2.63}$$

We now compute $\nabla_{s_g}^{\perp}\,\vec{\varkappa}_g$. On recalling (2.14) and (2.32), we have $(\vec{\varkappa}_g)_{s_g} = (\varkappa_g\,\vec{\nu}_g)_{s_g} = (\vec{x}\,.\,\vec{e}_2\,\varkappa_g\,\vec{\nu})_{s_g}$, and so, on recalling (2.13), we have

$$((\vec{\varkappa}_g)_{s_g},\vec{\nu}_g)_g = (\vec{x}\,.\,\vec{e}_2)^{-1}\left[(\vec{x}\,.\,\vec{e}_2)\,\varkappa_g\,\vec{\nu}\right]_{s_g}\vec{\nu} = (\vec{x}\,.\,\vec{e}_2)^{-1}\left[\vec{x}\,.\,\vec{e}_2\,\varkappa_g\right]_{s_g} = (\varkappa_g)_{s_g} + \vec{x}_s\,.\,\vec{e}_2\,\varkappa_g \quad \text{in } I\,. \tag{2.64}$$

Hence it follows from (2.63), (2.64), (2.14), (2.32) and (1.1) that

$$\begin{aligned}\nabla_{s_g}^{\perp}\,\vec{\varkappa}_g &= \left[(\varkappa_g)_{s_g} + \left[\vec{x}_s\,.\,\vec{e}_2 + (\vec{x}\,.\,\vec{e}_2)^{-1}\,\vec{\nu}_g\,.\,\vec{e}_1\right]\varkappa_g\right]\vec{\nu}_g = \left[(\varkappa_g)_{s_g} + \left[\vec{x}_s\,.\,\vec{e}_2 + \vec{\nu}\,.\,\vec{e}_1\right]\varkappa_g\right]\vec{\nu}_g\\ &= (\varkappa_g)_{s_g}\,\vec{\nu}_g \qquad \text{in } I\,.\end{aligned} \tag{2.65}$$

Therefore, (2.32) and (2.65) yield

$$\left(\nabla_{s_g}^{\perp}\right)^2\,\vec{\varkappa}_g = \nabla_{s_g}^{\perp}\left[\nabla_{s_g}^{\perp}\,(\varkappa_g\,\vec{\nu}_g)\right] = \nabla_{s_g}^{\perp}\left[(\varkappa_g)_{s_g}\,\vec{\nu}_g\right] = (\varkappa_g)_{s_g s_g}\,\vec{\nu}_g \qquad \text{in } I\,. \tag{2.66}$$

On combining (2.66) and (2.58), we have that

$$\vec{x}_t = \left[-(\varkappa_g)_{s_g s_g} - \tfrac{1}{2}\,\varkappa_g^3 + \varkappa_g\right]\vec{\nu}_g \qquad \text{in } I\,,$$

which agrees with (2.57) in the normal direction on noting (2.15).

Our weak formulations of (2.56) are going be to based on the equivalent equation

$$g(\vec{x})\,\vec{x}_t\,.\,\vec{\nu} = -\frac{1}{|\vec{x}_\rho|}\left(\frac{[\varkappa_g]_\rho}{g^{\frac{1}{2}}(\vec{x})\,|\vec{x}_\rho|}\right)_\rho - \tfrac{1}{2}g^{\frac{1}{2}}(\vec{x})\,\varkappa_g^3 - g^{\frac{1}{2}}(\vec{x})\,S_0(\vec{x})\,\varkappa_g \qquad \text{in } I\,, \tag{2.67}$$

where we have recalled (2.15) and (2.13). Note the similarity between (2.67) and (2.41). On recalling (2.18), we consider the following weak formulation of (2.67) and (1.5), in the spirit of ($\mathcal{E}$) for curve diffusion.

($\mathcal{U}$): Let $\vec{x}(0) \in [H^1(I)]^2$. For $t \in (0,T]$ find $\vec{x}(t) \in [H^1(I)]^2$ and $\varkappa(t) \in H^1(I)$ such that (2.22) holds and

$$\begin{aligned}\int_I g(\vec{x})\,\vec{x}_t\,.\,\vec{\nu}\,\chi\,|\vec{x}_\rho|\,\mathrm{d}\rho &= \int_I g^{-\frac{1}{2}}(\vec{x})\,\left(g^{-\frac{1}{2}}(\vec{x})\left[\varkappa - \tfrac{1}{2}\,\vec{\nu}\,.\,\nabla\,\ln g(\vec{x})\right]\right)_\rho\,\chi_\rho\,|\vec{x}_\rho|^{-1}\,\mathrm{d}\rho\\ &\quad - \tfrac{1}{2}\int_I g^{-1}(\vec{x})\left[\varkappa - \tfrac{1}{2}\,\vec{\nu}\,.\,\nabla\,\ln g(\vec{x})\right]^3\,\chi\,|\vec{x}_\rho|\,\mathrm{d}\rho\\ &\quad - \int_I S_0(\vec{x})\left[\varkappa - \tfrac{1}{2}\,\vec{\nu}\,.\,\nabla\,\ln g(\vec{x})\right]\chi\,|\vec{x}_\rho|\,\mathrm{d}\rho \quad \forall\,\chi \in H^1(I)\,.\end{aligned} \tag{2.68}$$

Similarly to ($\mathcal{F}$) for curve diffusion, we also introduce the following alternative weak formulation for elastic flow, which treats the curvature $\varkappa_g$ as an unknown, and so is based on (2.67) and (2.21).

($\mathcal{W}$): Let $\vec{x}(0) \in [H^1(I)]^2$. For $t \in (0,T]$ find $\vec{x}(t) \in [H^1(I)]^2$ and $\varkappa_g(t) \in H^1(I)$ such that (2.23) holds and

$$\int_I g(\vec{x})\,\vec{x}_t \,.\, \vec{\nu}\,\chi\,|\vec{x}_\rho|\,\mathrm{d}\rho = \int_I g^{-\frac{1}{2}}(\vec{x})\,[\varkappa_g]_\rho\,\chi_\rho\,|\vec{x}_\rho|^{-1}\,\mathrm{d}\rho - \tfrac{1}{2}\int_I g^{\frac{1}{2}}(\vec{x})\,\varkappa_g^3\,\chi\,|\vec{x}_\rho|\,\mathrm{d}\rho$$
$$- \int_I S_0(\vec{x})\,g^{\frac{1}{2}}(\vec{x})\,\varkappa_g\,\chi\,|\vec{x}_\rho|\,\mathrm{d}\rho \quad \forall\ \chi \in H^1(I)\,. \tag{2.69}$$

Clearly, the formulations ($\mathcal{U}$) and ($\mathcal{W}$) are very close to ($\mathcal{E}$) and ($\mathcal{F}$) for curve diffusion. Hence, the finite element schemes based on them will share the properties of the corresponding schemes for curve diffusion, and we have summarized these properties in Table 1. Moreover, we note that for our numerical approximations based on ($\mathcal{U}$) and ($\mathcal{W}$) it does not appear possible to prove stability results that show that discrete analogues of (2.45) decrease monotonically in time. Based on the techniques in Barrett *et al.* (2012), it is possible to introduce alternative weak formulations, for which semidiscrete continuous-in-time approximations admit such a stability result. We present and analyse these alternative discretizations in Barrett *et al.* (2018).

2.4 *Geodesic curve evolutions in manifolds via conformal maps*

Let $\vec{\Phi} : H \to \mathbb{R}^d$, $d \geqslant 3$ be a conformal parameterization of the embedded two-dimensional Riemannian manifold $\mathcal{M} \subset \mathbb{R}^d$, i.e. $\mathcal{M} = \vec{\Phi}(H)$ and $|\partial_{\vec{e}_1}\vec{\Phi}(\vec{z})|^2 = |\partial_{\vec{e}_2}\vec{\Phi}(\vec{z})|^2$ and $\partial_{\vec{e}_1}\vec{\Phi}(\vec{z}) \,.\, \partial_{\vec{e}_2}\vec{\Phi}(\vec{z}) = 0$ for all $\vec{z} \in H$. While such a parameterization in general does not exist, we recall from Taylor (2011, §5.10) that any orientable two-dimensional Riemannian manifold can be covered with finitely many conformally parameterized patches. But below we give some examples for $\mathcal{M} \subset \mathbb{R}^3$, where such a conformal parameterization exists. Given a conformal parameterization of $\mathcal{M}$, the corresponding metric tensor is given by $g_{ij} = \partial_{\vec{e}_1}\vec{\Phi} \,.\, \partial_{\vec{e}_2}\vec{\Phi} = g\,\delta_{ij}$ for the metric

$$g(\vec{z}) = |\partial_{\vec{e}_1}\vec{\Phi}(\vec{z})|^2 = |\partial_{\vec{e}_2}\vec{\Phi}(\vec{z})|^2, \qquad \vec{z} \in H\,. \tag{2.70}$$

We recall from Kühnel (2015, 4.26 in §4E) that for (2.70) it holds that

$$S_0(\vec{z}) = -\frac{\Delta\,\ln g(\vec{z})}{2g(\vec{z})} = \mathcal{K}\,(\vec{\Phi}(\vec{z})), \qquad \vec{z} \in H\,, \tag{2.71}$$

where $\mathcal{K}$ denotes the Gaussian curvature of $\mathcal{M}$.

An example for (2.70) is the stereographic projection of the unit sphere, without the north pole, onto the plane, where

$$\vec{\Phi}(\vec{z}) = (1+|\vec{z}|^2)^{-1}\,(2\,\vec{z}\,.\,\vec{e}_1, 2\,\vec{z}\,.\,\vec{e}_2, |\vec{z}|^2 - 1)^T\,,$$
$$g(\vec{z}) = 4\,(1+|\vec{z}|^2)^{-2} \quad \text{and} \quad H = \mathbb{R}^2\,, \tag{2.72a}$$

which yields a geometric interpretation to (2.8) with $\alpha = -1$. Further examples are the Mercator projection of the unit sphere, without the north and south poles, where

$$\begin{aligned} \vec{\Phi}(\vec{z}) &= \cosh^{-1}(\vec{z}\,.\,\vec{e}_1)\,(\cos(\vec{z}\,.\,\vec{e}_2), \sin(\vec{z}\,.\,\vec{e}_2), \sinh(\vec{z}\,.\,\vec{e}_1))^T\,, \\ g(\vec{z}) &= \cosh^{-2}(\vec{z}\,.\,\vec{e}_1) \quad \text{and} \quad H = \mathbb{R}^2\,, \end{aligned} \tag{2.72b}$$

as well as the catenoid parameterization

$$\begin{aligned} \vec{\Phi}(\vec{z}) &= (\cosh(\vec{z}\,.\,\vec{e}_1)\,\cos(\vec{z}\,.\,\vec{e}_2), \cosh(\vec{z}\,.\,\vec{e}_1)\,\sin(\vec{z}\,.\,\vec{e}_2), \vec{z}\,.\,\vec{e}_1)^T\,, \\ g(\vec{z}) &= \cosh^2(\vec{z}\,.\,\vec{e}_1) \quad \text{and} \quad H = \mathbb{R}^2\,. \end{aligned} \tag{2.72c}$$

Based on Sullivan (2011, p. 593) we introduce the following conformal parameterization of a torus with large radius $R > 1$ and small radius $r = 1$. In particular, we let $\mathfrak{s} = [R^2 - 1]^{\frac{1}{2}}$ and define

$$\begin{aligned} \vec{\Phi}(\vec{z}) &= \mathfrak{s}\,\left([\mathfrak{s}^2 + 1]^{\frac{1}{2}} - \cos(\vec{z}\,.\,\vec{e}_2)\right)^{-1}\,\left(\mathfrak{s}\,\cos\tfrac{\vec{z}\,.\,\vec{e}_1}{\mathfrak{s}}, \mathfrak{s}\,\sin\tfrac{\vec{z}\,.\,\vec{e}_1}{\mathfrak{s}}, \sin(\vec{z}\,.\,\vec{e}_2)\right)^T\,, \\ g(\vec{z}) &= \mathfrak{s}^2\,\left([\mathfrak{s}^2 + 1]^{\frac{1}{2}} - \cos(\vec{z}\,.\,\vec{e}_2)\right)^{-2} \quad \text{and} \quad H = \mathbb{R}^2\,. \end{aligned} \tag{2.72d}$$

We observe that the parameterizations given in (2.72b), (2.72c) and (2.72d) are not bijective, since $\vec{\Phi}(H)$ covers the hypersurface $\mathcal{M} \subset \mathbb{R}^3$ infinitely many times.

It can be shown that geodesic curvature flow, geodesic curve diffusion and geodesic elastic flow in $\mathcal{M} = \vec{\Phi}(H)$ reduce to (2.24), (2.38) and (2.56) for the metric g in H, respectively. See Appendix B for details. Hence, the numerical schemes introduced in this paper yield novel numerical approximations for these geodesic evolution equations. As all the computations take place in H, the discrete curve that approximates $\vec{\Phi}(\vec{x}(I))$ will always lie in $\mathcal{M}$. This is similar to the approach in Mikula & Ševčovič (2006), where a (local) graph formulation for $\mathcal{M} \subset \mathbb{R}^3$ is employed. But it is fundamentally different from the direct approach considered in Barrett *et al.* (2010), where the three-dimensional curve $\vec{\Phi}(\vec{x}(I)) \subset \mathbb{R}^3$ is discretized. An advantage of the approach in this paper is that one always stays in $\mathcal{M}$, whereas in the approach of Barrett *et al.* (2010) the curve can leave $\mathcal{M}$ by a small error. A disadvantage of the strategy in this paper, compared to Barrett *et al.* (2010), is that if $\overline{\mathcal{M}} \setminus \vec{\Phi}(H)$ is nonempty, then curves going through these singular points cannot be considered, and curves coming close to these singular points pose numerical challenges. For example, the north pole of the unit sphere, i.e. $\vec{e}_3 \in \mathbb{R}^3$, is such a singular point for (2.72a), while both the north and south poles, i.e. $\pm\vec{e}_3 \in \mathbb{R}^3$, are such singular points for (2.72b). We also note that in the examples (2.72c) and (2.72d), any closed curve $\vec{x}(I)$ in H will correspond to a curve $\vec{\Phi}(\vec{x}(I))$ on the hypersurface $\mathcal{M}$ that is homotopic to a point. In order to model other curves, the domain H needs to be embedded in an algebraic structure different to $\mathbb{R}^2$. In particular, $H = \mathbb{R} \times \mathbb{R}/(2\,\pi\,\mathbb{Z})$ for (2.72c) and $H = \mathbb{R}/(2\,\pi\,\mathfrak{s}\,\mathbb{Z}) \times \mathbb{R}/(2\,\pi\,\mathbb{Z})$ for (2.72d), respectively.

2.5 *Geometric evolution equations for axisymmetric hypersurfaces*

We recall that the metric (2.6c) is of relevance when considering geometric evolution equations for axisymmetric hypersurfaces in $\mathbb{R}^3$. However, the natural gradient flows considered in that setting differ from the flows considered in this paper. Let us briefly recall some geometric evolution equations for closed hypersurfaces $\mathcal{S}(t)$ in $\mathbb{R}^d$, $d \geqslant 3$. We refer to the review article by Deckelnick *et al.* (2005) for

more details. The mean curvature flow for $\mathcal{S}(t)$, i.e. the $L^2|_{\mathcal{S}}$-gradient flow of surface area, is given by the evolution law

$$\mathcal{V}_{\mathcal{S}} = k_m \qquad \text{on } \mathcal{S}(t)\,, \tag{2.73}$$

where $\mathcal{V}_{\mathcal{S}}$ denotes the normal velocity of $\mathcal{S}(t)$ in the direction of the normal $\vec{n}_{\mathcal{S}}$. Moreover, k_m is the mean curvature of $\mathcal{S}(t)$, i.e. the sum of the principal curvatures of $\mathcal{S}(t)$. The surface diffusion flow for $\mathcal{S}(t)$ is given by the evolution law

$$\mathcal{V}_{\mathcal{S}} = -\Delta_{\mathcal{S}}\, k_m \qquad \text{on } \mathcal{S}(t)\,, \tag{2.74}$$

where $\Delta_{\mathcal{S}}$ is the Laplace–Beltrami operator on $\mathcal{S}(t)$.

For an axisymmetric hypersurface in $\mathbb{R}^3$ that is generated from the curve $\Gamma(t) = \vec{x}(t)$ by rotation around the x_1-axis, the total surface area is given by (2.5). Moreover, the mean curvature flow (2.73) can be written in terms of the metric (2.6c) as

$$\mathcal{V} = \varkappa - \frac{\vec{\nu}\,.\,\vec{e}_2}{\vec{x}\,.\,\vec{e}_2} = g^{\frac{1}{2}}(\vec{x})\,\varkappa_g \quad \Longleftrightarrow \quad \mathcal{V}_g = g(\vec{x})\,\varkappa_g \qquad \text{in } I\,; \tag{2.75}$$

see Barrett *et al.* (2019a, (2.18a)), where we have noted (2.18), (2.14) and (2.15). Hence, (2.75) differs from the curvature flow (2.24) for (2.6c) by a space-dependent weighting factor. We note that, in contrast to (2.24), the flow (2.75) is invariant under constant rescalings of g. For example, both (2.6c) and (2.7) with $\mu = -1$ lead to the same flow (2.75).

Moreover, surface diffusion, (2.74), for axisymmetric hypersurfaces in $\mathbb{R}^3$ can be written, in terms of the metric (2.6c), as

$$\begin{aligned} &2\,\pi\,\vec{x}\,.\,\vec{e}_2\,\mathcal{V} = -2\,\pi\left[\vec{x}\,.\,\vec{e}_2\left[\varkappa - \frac{\vec{\nu}\,.\,\vec{e}_2}{\vec{x}\,.\,\vec{e}_2}\right]_s\right]_s = -2\,\pi\left[\vec{x}\,.\,\vec{e}_2\left[g^{\frac{1}{2}}(\vec{x})\,\varkappa_g\right]_s\right]_s \\ &\Longleftrightarrow \quad \mathcal{V}_g = -\left[g^{\frac{1}{2}}(\vec{x})\left[g^{\frac{1}{2}}(\vec{x})\,\varkappa_g\right]_s\right]_s \qquad \text{in } I\,; \end{aligned} \tag{2.76}$$

see Barrett *et al.* (2019b, (2.18), (2.11)), where we have noted (2.18), (2.14) and (2.15). Hence, (2.76) is dramatically different from the curve diffusion flow (2.38) for (2.6c). Once again we note that, in contrast to (2.38), the flow (2.76) is invariant under constant rescalings of g. For example, both (2.6c) and (2.7) with $\mu = -1$ lead to the same flow (2.76). Solutions of (2.76) conserve the quantity $2\,\pi\,\int_{\Omega(t)} \vec{z}\,.\,\vec{e}_2\,\mathrm{d}\vec{z} = \int_{\Omega(t)} g^{\frac{1}{2}}(\vec{z})\,\mathrm{d}\vec{z}$ in time, which again differs from (2.40); recall (2.4).

Remark 2.3 The metric (2.6c) can be generalized to model the evolution of axisymmetric hypersurfaces $\mathcal{S}(t)$ in $\mathbb{R}^d$, $d \geqslant 3$. In particular, we let

$$g(\vec{z}) = [\varsigma(d-1)]^2\,(\vec{z}\,.\,\vec{e}_2)^{2\,(d-2)} \quad \text{and} \quad H = \mathbb{H}^2\,, \tag{2.77}$$

where $\varsigma(n) = 2\,\pi^{\frac{n}{2}}[\Gamma(\frac{n}{2})]^{-1}$ denotes the surface area of the n-dimensional unit ball. Then mean curvature flow, (2.73), is given by

$$\mathcal{V} = \varkappa - (d-2)\,\frac{\vec{\nu}\,.\,\vec{e}_2}{\vec{x}\,.\,\vec{e}_2} = g^{\frac{1}{2}}(\vec{x})\,\varkappa_g \quad \Longleftrightarrow \quad \mathcal{V}_g = g(\vec{x})\,\varkappa_g \qquad \text{in } I\,, \tag{2.78}$$

in terms of the metric (2.77), where we have recalled (2.18), (2.14) and (2.15). We note that (2.78) collapses to (2.75) in the case $d = 3$. Surface diffusion, (2.74), is still given by the last equation in (2.76), now for the metric (2.77). These results can be rigorously shown by extending the results in Barrett *et al.* (2019b, Appendix B) from $\mathbb{R}^3$ to $\mathbb{R}^d$, with the help of generalized spherical coordinates.

Using the techniques developed in the present paper, it is then possible to derive weak formulations and stable finite element schemes for mean curvature flow and surface diffusion of axisymmetric hypersurfaces in $\mathbb{R}^d$, $d \geqslant 3$, similarly to the special case $d = 3$ treated in Barrett *et al.* (2019a,b).

In the recent paper Barrett *et al.* (2019b), the authors considered numerical approximations of Willmore flow for axisymmetric hypersurfaces in $\mathbb{R}^3$. The Willmore energy for the hypersurface $\mathcal{S}$ generated by $\Gamma(t)$ through rotation around the x_1-axis is given by

$$W_{\mathcal{S}}(\vec{x}) = \tfrac{1}{2} \int_{\mathcal{S}} k_m^2 \,\mathrm{d}\mathcal{H}^{\,2} = \pi \int_I \vec{x} \,.\, \vec{e}_2 \left(\varkappa - \frac{\vec{\nu} \,.\, \vec{e}_2}{\vec{x} \,.\, \vec{e}_2} \right)^2 |\vec{x}_\rho| \,\mathrm{d}\rho \,, \tag{2.79}$$

where $\mathcal{H}^{\,2}$ denotes the two-dimensional Hausdorff measure in $\mathbb{R}^3$; see Barrett *et al.* (2019b, §2.3, (2.11)). In terms of the metric (2.6c), on recalling (2.18), (2.14) and (2.1), this can be rewritten as

$$W_{\mathcal{S}}(\vec{x}) = \tfrac{1}{2} \int_I g(\vec{x})\, \varkappa_g^2 \, |\vec{x}_\rho|_g \,\mathrm{d}\rho \,,$$

which clearly differs from $W_g(\vec{x}) = \frac{1}{2} \int_I \varkappa_g^2 \, |\vec{x}_\rho|_g \,\mathrm{d}\rho$, as defined in (2.45). Hence, the flow (2.56), for (2.7) with $\mu = -1$, has no relation at all to the Willmore flow of axisymmetric hypersurfaces in $\mathbb{R}^3$. However, for the metric (2.6a) it holds, on recalling (2.19) for $\mu = 1$, (2.1), (2.79), (1.5) and as I is periodic, that

$$\begin{aligned} W_g(\vec{x}) &= \tfrac{1}{2} \int_I \varkappa_g^2 \, |\vec{x}_\rho|_g \,\mathrm{d}\rho = \tfrac{1}{2} \int_I \vec{x} \,.\, \vec{e}_2 \left(\varkappa + \frac{\vec{\nu} \,.\, \vec{e}_2}{\vec{x} \,.\, \vec{e}_2} \right)^2 |\vec{x}_\rho| \,\mathrm{d}\rho = (2\pi)^{-1} W_{\mathcal{S}}(\vec{x}) + 2 \int_I \varkappa\, \vec{\nu} \,.\, \vec{e}_2 \, |\vec{x}_\rho| \,\mathrm{d}\rho \\ &= (2\pi)^{-1} W_{\mathcal{S}}(\vec{x}) + 2 \int_I \vec{x}_{ss} \,.\, \vec{e}_2 \, |\vec{x}_\rho| \,\mathrm{d}\rho = (2\pi)^{-1} W_{\mathcal{S}}(\vec{x}) \,; \end{aligned} \tag{2.80}$$

see also Dall'Acqua & Spener (2017, §2.2.1). Hence, there is a close relation between the hyperbolic elastic flow, (2.57), and Willmore flow for axisymmetric hypersurfaces in $\mathbb{R}^3$. In particular, on recalling (2.80), (2.55), (2.10) and (2.7) for $\mu = 1$, (2.15) and (2.1), it holds that

$$\begin{aligned} \frac{\mathrm{d}}{\mathrm{d}t} W_S(\vec{x}(t)) &= 2\pi \frac{\mathrm{d}}{\mathrm{d}t} W_g(\vec{x}(t)) = 2\pi \int_I \left[(\varkappa_g)_{s_g s_g} + \tfrac{1}{2} \varkappa_g^3 - \varkappa_g \right] \mathcal{V}_g \, |\vec{x}_\rho|_g \,\mathrm{d}\rho \\ &= 2\pi \int_I \left[(\varkappa_g)_{s_g s_g} + \tfrac{1}{2} \varkappa_g^3 - \varkappa_g \right] g(\vec{x})\, \mathcal{V} \, |\vec{x}_\rho| \,\mathrm{d}\rho \\ &= 2\pi \int_I \left[(\varkappa_g)_{s_g s_g} + \tfrac{1}{2} \varkappa_g^3 - \varkappa_g \right] g^{\frac{3}{2}}(\vec{x})\, \vec{x} \,.\, \vec{e}_2 \, \mathcal{V} \, |\vec{x}_\rho| \,\mathrm{d}\rho \,. \end{aligned}$$

Hence, Willmore flow for axisymmetric hypersurfaces in $\mathbb{R}^3$, i.e. the $L^2|_{\mathcal{S}}$-gradient flow of (2.79), can be written as

$$\mathcal{V} = g^{\frac{3}{2}}(\vec{x})\left(-(\varkappa_g)_{s_g s_g} - \tfrac{1}{2}\varkappa_g^3 + \varkappa_g\right) \iff g^{-2}(\vec{x})\,\mathcal{V}_g = -(\varkappa_g)_{s_g s_g} - \tfrac{1}{2}\varkappa_g^3 + \varkappa_g \qquad \text{in } I\,,$$

i.e. the two flows differ only via a space-dependent weighting; recall (2.57). In particular, steady states and minimizers of the two flows agree.

3. Finite element approximations

Let $[0,1] = \cup_{j=1}^{J} I_j$, $J \geqslant 3$ be a decomposition of $[0,1]$ into intervals given by the nodes q_j, $I_j = [q_{j-1}, q_j]$. For simplicity, and without loss of generality, we assume that the subintervals form an equipartitioning of $[0,1]$, i.e. that

$$q_j = j\,h \quad \text{with} \quad h = J^{-1}\,,\ j = 0,\dots,J\,. \tag{3.1}$$

Clearly, as $I = \mathbb{R}/\mathbb{Z}$ we identify $0 = q_0 = q_J = 1$.

The necessary finite element spaces are defined as follows:

$$V^h = \{\chi \in C(I) : \chi|_{I_j} \text{ is affine for } j = 1,\dots,J\} \quad \text{and} \quad \underline{V}^h = [V^h]^2\,.$$

Let $\{\chi_j\}_{j=1}^J$ denote the standard basis of V^h, and let $\pi^h : C(I) \to V^h$ and $\vec{\pi}^h : [C(I)]^2 \to \underline{V}^h$ be the standard interpolation operators at the nodes $\{q_j\}_{j=1}^J$.

Let $(\cdot,\cdot)$ denote the L^2-inner product on I, and define the mass lumped L^2-inner product $(u,v)^h$, for two piecewise continuous functions, with possible jumps at the nodes $\{q_j\}_{j=1}^J$, via

$$(u,v)^h = \tfrac{1}{2}h \sum_{j=1}^{J} \left[(u\,v)(q_j^-) + (u\,v)\left(q_{j-1}^+\right)\right], \tag{3.2}$$

where we define $u(q_j^{\pm}) = \lim_{\delta \searrow 0} u(q_j \pm \delta)$. The definition (3.2) naturally extends to vector-valued functions.

Let $0 = t_0 < t_1 < \cdots < t_{M-1} < t_M = T$ be a partitioning of $[0,T]$ into possibly variable time steps $\Delta t_m = t_{m+1} - t_m$, $m = 0,\dots,M-1$. We set $\Delta t = \max_{m=0,\dots,M-1} \Delta t_m$. For a given $\vec{X}^m \in \underline{V}^h$ we set $\vec{\nu}^m = -\frac{[\vec{X}^m_\rho]^\perp}{|\vec{X}^m_\rho|}$, as the discrete analogue to (1.1). Given $\vec{X}^m \in \underline{V}^h$, the fully discrete approximations we propose in this section will always seek a parameterization $\vec{X}^{m+1} \in \underline{V}^h$ at the new time level, together with a suitable approximation of curvature. One class of schemes will rely on the following discrete analogue of (2.22). Let $\kappa^{m+1} \in V^h$ be such that

$$\left(\kappa^{m+1}\,\vec{\nu}^m, \vec{\eta}\,|\vec{X}^m_\rho|\right)^h + \left(\vec{X}^{m+1}_\rho, \vec{\eta}_\rho\,|\vec{X}^m_\rho|^{-1}\right) = 0 \quad \forall\ \vec{\eta} \in \underline{V}^h\,. \tag{3.3}$$

We note that any of the schemes featuring the side constraint (3.3), i.e. $(\mathcal{A}_m)^h$, $(\mathcal{E}_m)^h$ and $(\mathcal{U}_m)^h$, below, exhibit a discrete tangential velocity that leads to a good distribution of vertices. In particular, a steady

state $\Gamma^m = \vec{X}^m(I)$ will satisfy a weak equidistribution property, i.e. any two neighbouring elements are either parallel or of the same length. Moreover, for general evolutions the distribution of vertices tends to equidistribution, with the convergence being faster for smaller time-step sizes. The reason is that any curve $\Gamma^m = \vec{X}^m(I)$, for which there exists a $\kappa \in V^h$ such that

$$\left(\kappa\, \vec{\nu}^m, \vec{\eta}\, |\vec{X}^m_\rho|\right)^h + \left(\vec{X}^m_\rho, \vec{\eta}_\rho\, |\vec{X}^m_\rho|^{-1}\right) = 0 \quad \forall\, \vec{\eta} \in \underline{V}^h\,, \tag{3.4}$$

can be shown to satisfy the weak equidistribution property. In particular, the obvious semidiscrete variants of $(\mathcal{A}_m)^h$, $(\mathcal{E}_m)^h$ and $(\mathcal{U}_m)^h$ satisfy the weak equidistribution property at every time $t > 0$. We refer to Barrett *et al.* (2007a, Rem. 2.4) and to Barrett *et al.* (2011) for more details.

Two other classes of schemes, which will also exhibit nontrivial discrete tangential motions, will be based on discrete analogues of (2.23). The first variant is given as follows. Let $\kappa_g^{m+1} \in V^h$ be such that

$$\left(g(\vec{X}^m)\, \kappa_g^{m+1}\, \vec{\nu}^m, \vec{\eta}\, |\vec{X}^m_\rho|\right)^h + \left(\nabla\, g^{\frac{1}{2}}(\vec{X}^m), \vec{\eta}\, |\vec{X}^m_\rho|\right)^h + \left(g^{\frac{1}{2}}(\vec{X}^m)\, \vec{X}^{m+1}_\rho, \vec{\eta}_\rho\, |\vec{X}^m_\rho|^{-1}\right)^h = 0 \quad \forall\, \vec{\eta} \in \underline{V}^h\,. \tag{3.5}$$

Schemes based on (3.5) will still be linear, but their induced tangential motion does not lead to equidistribution. In order to allow for stability proofs, we now adapt the time discretization in (3.5). In particular, we make use of a convex/concave splitting of the energy density $g^{\frac{1}{2}}$ in (2.3). This idea, for the case of a scalar potential $\Psi : \mathbb{R} \to \mathbb{R}$, goes back to Elliott & Stuart (1993), and we adapt their approach to the situation here, i.e. $g^{\frac{1}{2}} : \mathbb{R}^2 \supset H \to \mathbb{R}_{>0}$. In particular, we assume that we can split $g^{\frac{1}{2}}$ into

$$g^{\frac{1}{2}} = g_+^{\frac{1}{2}} + g_-^{\frac{1}{2}} \quad \text{such that } \pm g_\pm^{\frac{1}{2}} \text{ is convex in } H. \tag{3.6}$$

Note that such a splitting exists if $D^2 g^{\frac{1}{2}}$ is bounded from below on H, in the sense that there exists a symmetric positive semidefinite matrix $A \in \mathbb{R}^{2\times 2}$ such that $D^2 g^{\frac{1}{2}}(\vec{z}) + A$ is symmetric positive semidefinite for all $\vec{z} \in H$. For example, the splitting can then be chosen such that $g_+^{\frac{1}{2}}(\vec{z}) = g^{\frac{1}{2}}(\vec{z}) + \frac{1}{2}\,\vec{z}\,.A\,\vec{z}$ and $g_-^{\frac{1}{2}}(\vec{z}) = -\frac{1}{2}\,\vec{z}\,.A\,\vec{z}$. It follows from the splitting in (3.6) that

$$\nabla \left[g_+^{\frac{1}{2}}(\vec{u}) + g_-^{\frac{1}{2}}(\vec{v})\right].(\vec{u} - \vec{v}) \geqslant g^{\frac{1}{2}}(\vec{u}) - g^{\frac{1}{2}}(\vec{v}) \quad \forall\, \vec{u}, \vec{v} \in H\,. \tag{3.7}$$

The alternative discrete analogue of (2.23), compared to (3.5), is then given as follows. Let $\kappa_g^{m+1} \in V^h$ be such that

$$\left(g(\vec{X}^m)\, \kappa_g^{m+1}\, \vec{\nu}^m, \vec{\eta}\, |\vec{X}^m_\rho|\right)^h + \left(\nabla\, [g_+^{\frac{1}{2}}(\vec{X}^{m+1}) + g_-^{\frac{1}{2}}(\vec{X}^m)], \vec{\eta}\, |\vec{X}^{m+1}_\rho|\right)^h + \left(g^{\frac{1}{2}}(\vec{X}^m)\, \vec{X}^{m+1}_\rho, \vec{\eta}_\rho\, |\vec{X}^m_\rho|^{-1}\right)^h$$
$$= 0 \quad \forall\, \vec{\eta} \in \underline{V}^h\,. \tag{3.8}$$

We note that, in contrast to (3.5), the side constraint (3.8) will lead to nonlinear schemes.

We observe that in the cases (2.6) and (2.7) with $\mu \in \mathbb{R} \setminus (-1, 0)$ a splitting of the form (3.6) exists. In particular, for $\mu \in \mathbb{R} \setminus (-1, 0)$ the function $g^{\frac{1}{2}}(\vec{z}) = (\vec{z}\,.\,\vec{e}_2)^{-\mu}$ is convex on $H = \mathbb{H}^2$, since

$D^2\, g^{\frac{1}{2}}(\vec{z}) = \mu\,(\mu+1)\,(\vec{z}\,.\,\vec{e}_2)^{-(\mu+2)}\,\vec{e}_2\otimes\vec{e}_2$ is positive semidefinite for $\vec{z}\in\mathbb{H}^2$. Here $\otimes$ denotes the outer or tensor product in $\mathbb{R}^2$. Hence, we can choose

$$g_+^{\frac{1}{2}}(\vec{z}) = g^{\frac{1}{2}}(\vec{z}) = (\vec{z}\,.\,\vec{e}_2)^{-\mu} \quad \text{and} \quad g_-^{\frac{1}{2}}(\vec{z}) = 0\,, \tag{3.9}$$

with $\nabla\, g_+^{\frac{1}{2}}(\vec{z}) = -\mu\,(\vec{z}\,.\,\vec{e}_2)^{-(\mu+1)}\,\vec{e}_2$. Moreover, for the class of metrics (2.8) a splitting of the form (3.6) also exists. To this end, we note that $D^2\, g^{\frac{1}{2}}(\vec{z}) = 16\,\alpha^2\,(1-\alpha\,|\vec{z}|^2)^{-3}\,\vec{z}\otimes\vec{z} + 4\,\alpha\,(1-\alpha\,|\vec{z}|^2)^{-2}\,\underline{\underline{\mathrm{Id}}}$, where $\underline{\underline{\mathrm{Id}}}\in\mathbb{R}^{2\times 2}$ denotes the identity matrix. Clearly, if $\alpha > 0$ then $g^{\frac{1}{2}}$ is convex in H. If $\alpha \leqslant 0$, on the other hand, then $D^2\, g^{\frac{1}{2}}$ is clearly the sum of a positive semidefinite and a negative semidefinite matrix, with $A = -4\,\alpha\,\underline{\underline{\mathrm{Id}}}$ being such that $D^2\, g^{\frac{1}{2}} + A$ is symmetric positive semidefinite in H. Hence, we can choose

$$\begin{cases} g_+^{\frac{1}{2}}(\vec{z}) = g^{\frac{1}{2}}(\vec{z}) \quad \text{and} \quad g_-^{\frac{1}{2}}(\vec{z}) = 0\,, & \alpha > 0\,, \\ g_+^{\frac{1}{2}}(\vec{z}) = g^{\frac{1}{2}}(\vec{z}) - 2\,\alpha\,|\vec{z}|^2 \quad \text{and} \quad g_-^{\frac{1}{2}}(\vec{z}) = 2\,\alpha\,|\vec{z}|^2, & \alpha \leqslant 0\,. \end{cases}$$

Similarly, for the metric (2.72b) we note that

$$D^2 g^{\frac{1}{2}}(\vec{z}) = (\tanh^2(\vec{z}\,.\,\vec{e}_1) - \cosh^{-2}(\vec{z}\,.\,\vec{e}_1))\,\cosh^{-1}(\vec{z}\,.\,\vec{e}_1)\,\vec{e}_1\otimes\vec{e}_1\,,$$

and so we can choose

$$g_+^{\frac{1}{2}}(\vec{z}) = g^{\frac{1}{2}}(\vec{z}) + \tfrac{1}{2}\,(\vec{z}\,.\,\vec{e}_1)^2 \quad \text{and} \quad g_-^{\frac{1}{2}}(\vec{z}) = -\tfrac{1}{2}\,(\vec{z}\,.\,\vec{e}_1)^2\,.$$

For the metric (2.72c) we observe that $D^2\, g^{\frac{1}{2}}(\vec{z}) = \cosh(\vec{z}\,.\,\vec{e}_1)\,\vec{e}_1\otimes\vec{e}_1$, and so we can choose

$$g_+^{\frac{1}{2}}(\vec{z}) = g^{\frac{1}{2}}(\vec{z}) \quad \text{and} \quad g_-^{\frac{1}{2}}(\vec{z}) = 0\,.$$

Finally, for the metric (2.72d) we note that

$$D^2 g^{\frac{1}{2}}(\vec{z}) = \mathfrak{s}\left[\frac{2\,\sin^2(\vec{z}\,.\,\vec{e}_2)}{([\mathfrak{s}^2+1]^{\frac{1}{2}} - \cos(\vec{z}\,.\,\vec{e}_2))^3} - \frac{\cos(\vec{z}\,.\,\vec{e}_2)}{([\mathfrak{s}^2+1]^{\frac{1}{2}} - \cos(\vec{z}\,.\,\vec{e}_2))^2}\right]\vec{e}_2\otimes\vec{e}_2\,,$$

and so we can choose

$$g_+^{\frac{1}{2}}(\vec{z}) = g^{\frac{1}{2}}(\vec{z}) + \tfrac{1}{2}\,\mathfrak{s}\left([\mathfrak{s}^2+1]^{\frac{1}{2}} - 1\right)^{-2}(\vec{z}\,.\,\vec{e}_2)^2 \quad \text{and} \quad g_-^{\frac{1}{2}}(\vec{z}) = g^{\frac{1}{2}}(\vec{z}) - g_+^{\frac{1}{2}}(\vec{z})\,.$$

For the metrics we consider in this paper, we summarize in Table 1 the quantities that are necessary in order to implement the numerical schemes presented below. In addition, for the reader's convenience, Table 2 summarizes the main properties of all the schemes that will be introduced in this section.

TABLE 1 *Expressions for terms that are relevant for the implementation of the presented finite element approximations. Here* $[\alpha]_- = \min\{0, \alpha\}$

g	$\frac{1}{2}\vec{\nu}\,.\,\nabla\, g(\vec{x})$	$\nabla\, g^{\frac{1}{2}}(\vec{x})$	$\nabla\, g^{\frac{1}{2}}_{-(\vec{x})}$	$S_0(\vec{x})$
(2.7)	$-\mu\,\frac{\vec{\nu}\,.\,\vec{e}_2}{\vec{x}\,.\,\vec{e}_2}$	$-\frac{\mu}{(\vec{x}\,.\,\vec{e}_2)^{\mu+1}}\,\vec{e}_2$	0	$-\mu\,(\vec{x}\,.\,\vec{e}_2)^{2\,(\mu-1)}$
(2.8)	$\frac{2\,\alpha\,\vec{x}\,.\,\vec{\nu}}{1-\alpha\,\vec{x}\vert^2}$	$\frac{4\,\alpha}{(1-\alpha\,\vec{x}\vert^2)^2}\,\vec{x}$	$4\,[\alpha]_-\,\vec{x}$	$-\alpha$
(2.72b)	$-\tanh(\vec{x}\,.\,\vec{e}_1)\,\vec{\nu}\,.\,\vec{e}_1$	$-\frac{\tanh(\vec{x}\,.\,\vec{e}_1)}{\cosh(\vec{x}\,.\,\vec{e}_1)}\,\vec{e}_1$	$-(\vec{x}\,.\,\vec{e}_1)\,\vec{e}_1$	1
(2.72c)	$\tanh(\vec{x}\,.\,\vec{e}_1)\,\vec{\nu}\,.\,\vec{e}_1$	$\sinh(\vec{x}\,.\,\vec{e}_1)\,\vec{e}_1$	0	$-\cosh^{-4}(\vec{x}\,.\,\vec{e}_1)$
(2.72d)	$-\frac{\sin(\vec{x}\,.\,\vec{e}_2)\,\vec{\nu}\,.\,\vec{e}_2}{[\mathfrak{s}^2+1]^{\frac{1}{2}}-\cos(\vec{x}\,.\,\vec{e}_2)}$	$-\frac{\mathfrak{s}\,\sin(\vec{x}\,.\,\vec{e}_2)}{([\mathfrak{s}^2+1]^{\frac{1}{2}}-\cos(\vec{x}\,.\,\vec{e}_2))^2}\,\vec{e}_2$	$-\frac{\mathfrak{s}\,\vec{x}\,.\,\vec{e}_2}{([\mathfrak{s}^2+1]^{\frac{1}{2}}-1)^2}\,\vec{e}_2$	$\frac{[\mathfrak{s}^2+1]^{\frac{1}{2}}\cos(\vec{x}\,.\,\vec{e}_2)-1}{\mathfrak{s}^2}$

TABLE 2 *Properties of the different schemes for curvature flow, curve diffusion and elastic flow. Here 'equidistribution' refers to the property discussed around (3.4), and 'linear' indicates whether the systems of equations arising at each time level are linear or not*

Scheme	Flow	Stability proof	Implicit tangential motion	Equidistribution	Linear
$(\mathcal{A}_m)^h$	Section 2.1	no	yes	yes	yes
$(\mathcal{B}_m)^h$	Section 2.1	no	no	no	yes
$(\mathcal{C}_m)^h$	Section 2.1	no	yes	no	yes
$(\mathcal{D}_m)^h$	Section 2.1	no	no	no	yes
$(\mathcal{C}_{m,\star})^h$	Section 2.1	yes	yes	no	no
$(\mathcal{D}_{m,\star})^h$	Section 2.1	yes	no	no	no
$(\mathcal{E}_m)^h$	Section 2.2	no	yes	yes	yes
$(\mathcal{F}_m)^h$	Section 2.2	no	yes	no	yes
$(\mathcal{F}_{m,\star})^h$	Section 2.2	yes	yes	no	no
$(\mathcal{U}_m)^h$	Section 2.3	no	yes	yes	yes
$(\mathcal{W}_m)^h$	Section 2.3	no	yes	no	yes

3.1 *Curvature flow*

We consider the following fully discrete analogue of $(\mathcal{A})$, i.e. (2.27), (2.22).
$(\mathcal{A}_m)^h$: Let $\vec{X}^0 \in \underline{V}^h$. For $m = 0, \ldots, M-1$, find $(\vec{X}^{m+1}, \kappa^{m+1}) \in \underline{V}^h \times V^h$ such that (3.3) holds and

$$\left(g(\vec{X}^m)\,\frac{\vec{X}^{m+1}-\vec{X}^m}{\Delta t_m}, \chi\,\vec{\nu}^m\,\vert\vec{X}^m_\rho\vert\right)^h = \left(\kappa^{m+1} - \tfrac{1}{2}\,\vec{\nu}^m\,.\,\nabla\,\ln g(\vec{X}^m), \chi\,\vert\vec{X}^m_\rho\vert\right)^h \quad \forall\,\chi \in V^h\,. \tag{3.10}$$

We remark that the scheme $(\mathcal{A}_m)^h$, in the case (2.6b), collapses to the scheme Barrett *et al.* (2007b, (2.3a,b)), with $f = \mathrm{id}$, for Euclidean curvature flow.

We make the following mild assumption.

$(\mathfrak{A})^h$ Let $|\vec{X}^m_\rho| > 0$ for almost all $\rho \in I$, and let $\dim \mathcal{Z}^h = 2$, where $\mathcal{Z}^h = \left\{ \int_I \pi^h[g(\vec{X}^m)\chi]\,|\vec{X}^m_\rho|\,\vec{\nu}^m \,\mathrm{d}\rho : \chi \in V^h \right\} \subset \mathbb{R}^2$.

In order to interpret this assumption, we let $\vec{\omega}^m \in \underline{V}^h$ be the mass-lumped L^2-projection of $\vec{\nu}^m$ onto $\underline{V}^h$, i.e.

$$\left(\vec{\omega}^m, \vec{\varphi}\,|\vec{X}^m_\rho|\right)^h = \left(\vec{\nu}^m, \vec{\varphi}\,|\vec{X}^m_\rho|\right) = \left(\vec{\nu}^m, \vec{\varphi}\,|\vec{X}^m_\rho|\right)^h \quad \forall\, \vec{\varphi} \in \underline{V}^h\,. \tag{3.11}$$

Then it follows from the definition of $\mathcal{Z}^h$, (3.11) and (3.2) that

$$\begin{aligned}\mathcal{Z}^h &= \operatorname{span}\left\{ \int_I \pi^h\,[g(\vec{X}^m)\,\chi_j]\,|\vec{X}^m_\rho|\,\vec{\nu}^m \,\mathrm{d}\rho : j = 1,\dots,J \right\} \\ &= \operatorname{span}\left\{ \int_I \pi^h\,[g(\vec{X}^m)\,\chi_j\,\vec{\omega}^m]\,|\vec{X}^m_\rho| \,\mathrm{d}\rho : j = 1,\dots,J \right\} = \operatorname{span}\left\{ \vec{\omega}^m(q_j) : j = 1,\dots,J \right\},\end{aligned}$$

which means that the assumption $(\mathfrak{A})^h$ is only violated, if the J vertex normals $\vec{\omega}^m(q_j)$ of Γ^m are all collinear. Clearly, this almost never happens in practice, and it certainly cannot happen if Γ^m has no self-intersections. See also Barrett *et al.* (2007a, Remark 2.2) for more details.

LEMMA 3.1 Let the assumption $(\mathfrak{A})^h$ hold. Then there exists a unique solution $(\vec{X}^{m+1}, \kappa^{m+1}) \in \underline{V}^h \times V^h$ to $(\mathcal{A}_m)^h$.

Proof. As (3.10), (3.3) is linear, existence follows from uniqueness. To investigate the latter, we consider the following system. Find $(\vec{X}, \kappa) \in \underline{V}^h \times V^h$ such that

$$\left(g(\vec{X}^m)\,\frac{\vec{X}}{\Delta t_m}, \chi\,\vec{\nu}^m\,|\vec{X}^m_\rho| \right)^h = \left(\kappa, \chi\,|\vec{X}^m_\rho|\right)^h \quad \forall\, \chi \in V^h\,, \tag{3.12a}$$

$$\left(\kappa\,\vec{\nu}^m, \vec{\eta}\,|\vec{X}^m_\rho|\right)^h + \left(\vec{X}_\rho, \vec{\eta}_\rho\,|\vec{X}^m_\rho|^{-1}\right) = 0 \quad \forall\, \vec{\eta} \in \underline{V}^h\,. \tag{3.12b}$$

Choosing $\chi = \pi^h[g^{-1}(\vec{X}^m)\,\kappa] \in V^h$ in (3.12a) and $\vec{\eta} = \vec{X} \in \underline{V}^h$ in (3.12b) yields

$$\left(|\vec{X}_\rho|^2, |\vec{X}^m_\rho|^{-1}\right) + \Delta t_m \left(g^{-1}(\vec{X}^m)\,|\kappa|^2, |\vec{X}^m_\rho|\right)^h = 0\,. \tag{3.13}$$

It follows from (3.13) that $\kappa = 0$ and that $\vec{X}$ is constant. Hence, (3.12a) and (3.2) imply that

$$0 = \left(g(\vec{X}^m)\,\vec{X}, \chi\,\vec{\nu}^m\,|\vec{X}^m_\rho|\right)^h = \vec{X}\,.\int_I \pi^h\,[g(\vec{X}^m)\,\chi]\,|\vec{X}^m_\rho|\,\vec{\nu}^m \,\mathrm{d}\rho \quad \forall\, \chi \in V^h\,. \tag{3.14}$$

It follows from (3.14) and assumption $(\mathfrak{A})^h$ that $\vec{X} = \vec{0}$. Hence, we have shown that $(\mathcal{A}_m)^h$ has a unique solution $(\vec{X}^{m+1}, \kappa^{m+1}) \in \underline{V}^h \times V^h$. □

We consider the following fully discrete analogue of ($\mathcal{B}$), i.e. (2.29).
($\mathcal{B}_m$)^h: Let $\vec{X}^0 \in \underline{V}^h$. For $m = 0, \ldots, M-1$, find $(\vec{X}^{m+1}, \vec{\kappa}^{m+1}) \in \underline{V}^h \times \underline{V}^h$ such that

$$\left(g(\vec{X}^m)\, \frac{\vec{X}^{m+1} - \vec{X}^m}{\Delta t_m}, \vec{\chi}\, |\vec{X}^m_\rho| \right)^h = \left(\vec{\kappa}^{m+1} - \tfrac{1}{2}\, [\vec{v}^m \,.\, \nabla\, \ln g(\vec{X}^m)]\, \vec{\nu}^m, \vec{\chi}\, |\vec{X}^m_\rho| \right)^h \quad \forall\ \vec{\chi} \in \underline{V}^h\,, \tag{3.15a}$$

$$\left(\vec{\kappa}^{m+1}, \vec{\eta}\, |\vec{X}^m_\rho| \right)^h + \left(\vec{X}^{m+1}_\rho, \vec{\eta}_\rho\, |\vec{X}^m_\rho|^{-1} \right) = 0 \quad \forall\ \vec{\eta} \in \underline{V}^h\,. \tag{3.15b}$$

We remark that the scheme ($\mathcal{B}_m$)^h, in the case (2.6b), collapses to the scheme in Dziuk (1994, §6) for Euclidean curvature flow.

LEMMA 3.2 There exists a unique solution $(\vec{X}^{m+1}, \vec{\kappa}^{m+1}) \in \underline{V}^h \times \underline{V}^h$ to ($\mathcal{B}_m$)^h.

Proof. As (3.15) is linear, existence follows from uniqueness. To investigate the latter, we consider the following system. Find $(\vec{X}, \vec{\kappa}) \in \underline{V}^h \times \underline{V}^h$ such that

$$\left(g(\vec{X}^m)\, \frac{\vec{X}}{\Delta t_m}, \vec{\chi}\, |\vec{X}^m_\rho| \right)^h = \left(\vec{\kappa}, \vec{\chi}\, |\vec{X}^m_\rho| \right)^h \quad \forall\ \vec{\chi} \in \underline{V}^h\,, \tag{3.16a}$$

$$\left(\vec{\kappa}, \vec{\eta}\, |\vec{X}^m_\rho| \right)^h + \left(\vec{X}_\rho, \vec{\eta}_\rho\, |\vec{X}^m_\rho|^{-1} \right) = 0 \quad \forall\ \vec{\eta} \in \underline{V}^h\,. \tag{3.16b}$$

Choosing $\vec{\chi} = \vec{\pi}^h[g^{-1}(\vec{X}^m)\, \vec{\kappa}] \in \underline{V}^h$ in (3.16a) and $\vec{\eta} = \vec{X} \in \underline{V}^h$ in (3.16b) yields

$$\left(|\vec{X}_\rho|^2, |\vec{X}^m_\rho|^{-1} \right) + \Delta t_m \left(g^{-1}(\vec{X}^m)\, |\vec{\kappa}|^2, |\vec{X}^m_\rho| \right)^h = 0\,. \tag{3.17}$$

It follows from (3.17) that $\vec{\kappa} = \vec{0}$ and then from (3.16a) that $\vec{X} = \vec{0}$. Hence, we have shown that (3.15) has a unique solution $(\vec{X}^{m+1}, \vec{\kappa}^{m+1}) \in \underline{V}^h \times \underline{V}^h$. □

We consider the following two fully discrete analogues of ($\mathcal{C}$), i.e. (2.31), (2.23).
($\mathcal{C}_m$)^h: Let $\vec{X}^0 \in \underline{V}^h$. For $m = 0, \ldots, M-1$, find $(\vec{X}^{m+1}, \kappa_g^{m+1}) \in \underline{V}^h \times V^h$ such that (3.5) holds and

$$\left(g(\vec{X}^m)\, \frac{\vec{X}^{m+1} - \vec{X}^m}{\Delta t_m}, \chi\, \vec{\nu}^m\, |\vec{X}^m_\rho| \right)^h = \left(g^{\frac{1}{2}}(\vec{X}^m)\, \kappa_g^{m+1}, \chi\, |\vec{X}^m_\rho| \right)^h \quad \forall\ \chi \in V^h\,. \tag{3.18}$$

($\mathcal{C}_{m,\star}$)^h: Let $\vec{X}^0 \in \underline{V}^h$. For $m = 0, \ldots, M-1$, find $(\vec{X}^{m+1}, \kappa_g^{m+1}) \in \underline{V}^h \times V^h$ such that (3.8) and (3.18) hold.

We remark that the schemes ($\mathcal{C}_m$)^h and ($\mathcal{C}_{m,\star}$)^h, with (3.9), in the case (2.6b), collapse to the scheme Barrett *et al.* (2007b, (2.3a,b)), with $f = \mathrm{id}$, for Euclidean curvature flow.

We consider the following two fully discrete analogues of $(\mathcal{D})$, i.e. (2.34).
$(\mathcal{D}_m)^h$: Let $\vec{X}^0 \in \underline{V}^h$. For $m = 0, \dots, M-1$, find $(\vec{X}^{m+1}, \vec{\kappa}_g^{m+1}) \in \underline{V}^h \times \underline{V}^h$ such that

$$\left(g(\vec{X}^m)\, \frac{\vec{X}^{m+1} - \vec{X}^m}{\Delta t_m}, \vec{\chi}\, |\vec{X}^m_\rho| \right)^h = \left(g(\vec{X}^m)\, \vec{\kappa}_g^{m+1}, \vec{\chi}\, |\vec{X}^m_\rho| \right)^h \quad \forall\, \vec{\chi} \in \underline{V}^h\,, \tag{3.19a}$$

$$\left(g^{\frac{3}{2}}(\vec{X}^m)\, \vec{\kappa}_g^{m+1}, \vec{\eta}\, |\vec{X}^m_\rho| \right)^h + \left(\nabla\, g^{\frac{1}{2}}(\vec{X}^m), \vec{\eta}\, |\vec{X}^m_\rho| \right)^h + \left(g^{\frac{1}{2}}(\vec{X}^m)\, \vec{X}^{m+1}_\rho, \vec{\eta}_\rho\, |\vec{X}^m_\rho|^{-1} \right)^h = 0 \quad \forall\, \vec{\eta} \in \underline{V}^h\,. \tag{3.19b}$$

$(\mathcal{D}_{m,\star})^h$: Let $\vec{X}^0 \in \underline{V}^h$. For $m = 0, \dots, M-1$, find $(\vec{X}^{m+1}, \vec{\kappa}_g^{m+1}) \in \underline{V}^h \times \underline{V}^h$ such that (3.19a) holds and

$$\left(g^{\frac{3}{2}}(\vec{X}^m)\, \vec{\kappa}_g^{m+1}, \vec{\eta}\, |\vec{X}^m_\rho| \right)^h + \left(\nabla\, [g_+^{\frac{1}{2}}(\vec{X}^{m+1}) + g_-^{\frac{1}{2}}(\vec{X}^m)], \vec{\eta}\, |\vec{X}^{m+1}_\rho| \right)^h + \left(g^{\frac{1}{2}}(\vec{X}^m)\, \vec{X}^{m+1}_\rho, \vec{\eta}_\rho\, |\vec{X}^m_\rho|^{-1} \right)^h = 0 \quad \forall\, \vec{\eta} \in \underline{V}^h\,. \tag{3.20}$$

We remark that the schemes $(\mathcal{D}_m)^h$ and $(\mathcal{D}_{m,\star})^h$, with (3.9), in the case (2.6b), collapse to the scheme in Dziuk (1994, §6) for Euclidean curvature flow.

Overall we observe that $(\mathcal{C}_m)^h$ and $(\mathcal{D}_m)^h$ are linear schemes, while $(\mathcal{C}_{m,\star})^h$ and $(\mathcal{D}_{m,\star})^h$ are nonlinear. For the linear schemes we can prove existence and uniqueness, while for the nonlinear schemes we can prove unconditional stability.

LEMMA 3.3 Let the assumption $(\mathfrak{A})^h$ hold. Then there exists a unique solution $(\vec{X}^{m+1}, \kappa_g^{m+1}) \in \underline{V}^h \times V^h$ to $(\mathcal{C}_m)^h$.

Proof. As (3.18), (3.5) is linear, existence follows from uniqueness. To investigate the latter, we consider the following system. Find $(\vec{X}, \kappa_g) \in \underline{V}^h \times V^h$ such that

$$\left(g(\vec{X}^m)\, \frac{\vec{X}}{\Delta t_m}, \chi\, \vec{\nu}^m\, |\vec{X}^m_\rho| \right)^h = \left(g^{\frac{1}{2}}(\vec{X}^m)\, \kappa_g, \chi\, |\vec{X}^m_\rho| \right)^h \quad \forall\, \chi \in V^h\,, \tag{3.21a}$$

$$\left(g(\vec{X}^m)\, \kappa_g\, \vec{\nu}^m, \vec{\eta}\, |\vec{X}^m_\rho| \right)^h + \left(g^{\frac{1}{2}}(\vec{X}^m)\, \vec{X}_\rho, \vec{\eta}_\rho\, |\vec{X}^m_\rho|^{-1} \right) = 0 \quad \forall\, \vec{\eta} \in \underline{V}^h\,. \tag{3.21b}$$

Choosing $\chi = \kappa_g \in V^h$ in (3.21a) and $\vec{\eta} = \vec{X} \in \underline{V}^h$ in (3.21b) yields

$$\left(g^{\frac{1}{2}}(\vec{X}^m)\, |\vec{X}_\rho|^2, |\vec{X}^m_\rho|^{-1} \right) + \Delta t_m \left(g^{\frac{1}{2}}(\vec{X}^m)\, |\kappa_g|^2, |\vec{X}^m_\rho| \right)^h = 0\,. \tag{3.22}$$

It immediately follows from (3.22) that $\kappa_g = 0$, and that $\vec{X}$ is constant. Similarly to the proof of Lemma 3.1 it then follows from (3.21a) and the assumption $(\mathfrak{A})^h$ that $\vec{X} = \vec{0}$. Hence, we have shown that $(\mathcal{C}_m)^h$ has a unique solution $(\vec{X}^{m+1}, \kappa_g^{m+1}) \in \underline{V}^h \times V^h$. □

LEMMA 3.4 Let $|\vec{X}^m_\rho| > 0$ for almost all $\rho \in I$. Then there exists a unique solution $(\vec{X}^{m+1}, \vec{\kappa}^{m+1}_g) \in \underline{V}^h \times \underline{V}^h$ to $(\mathcal{D}_m)^h$.

Proof. As (3.19) is linear, existence follows from uniqueness. To investigate the latter, we consider the following system. Find $(\vec{X}, \vec{\kappa}_g) \in \underline{V}^h \times \underline{V}^h$ such that

$$\left(g(\vec{X}^m) \frac{\vec{X}}{\Delta t_m}, \vec{\chi}\, |\vec{X}^m_\rho| \right)^h = \left(g(\vec{X}^m)\, \vec{\kappa}_g, \vec{\chi}\, |\vec{X}^m_\rho| \right)^h \quad \forall\ \vec{\chi} \in \underline{V}^h\,, \tag{3.23a}$$

$$\left(g^{\frac{3}{2}}(\vec{X}^m)\, \vec{\kappa}_g, \vec{\eta}\, |\vec{X}^m_\rho| \right)^h + \left(g^{\frac{1}{2}}(\vec{X}^m)\, \vec{X}_\rho, \vec{\eta}_\rho\, |\vec{X}^m_\rho|^{-1} \right) = 0 \quad \forall\ \vec{\eta} \in \underline{V}^h\,. \tag{3.23b}$$

Choosing $\vec{\chi} = \vec{\pi}^h[g^{\frac{1}{2}}(\vec{X}^m)\, \vec{\kappa}_g \in \underline{V}^h$ in (3.23a) and $\vec{\eta} = \vec{X} \in \underline{V}^h$ in (3.23b) yields

$$\left(g^{\frac{1}{2}}(\vec{X}^m)\, |\vec{X}_\rho|^2, |\vec{X}^m_\rho|^{-1} \right) + \Delta t_m \left(g^{\frac{3}{2}}(\vec{X}^m)\, |\vec{\kappa}_g|^2, |\vec{X}^m_\rho| \right)^h = 0\,, \tag{3.24}$$

It immediately follows from (3.24) that $\vec{\kappa}_g = \vec{0}$, and hence (3.23a) implies that $\vec{X} = \vec{0}$. Hence, we have shown that $(\mathcal{D}_m)^h$ has a unique solution $(\vec{X}^{m+1}, \vec{\kappa}^{m+1}_g) \in \underline{V}^h \times \underline{V}^h$. □

On recalling (2.3), for $\vec{Z} \in \underline{V}^h$ we let

$$L^h_g(\vec{Z}) = \left(g^{\frac{1}{2}}(\vec{Z}), |\vec{Z}_\rho| \right)^h.$$

We now prove discrete analogues of (2.25) and (2.35) for the schemes $(\mathcal{C}_{m,\star})^h$ and $(\mathcal{D}_{m,\star})^h$, respectively.

THEOREM 3.5 Let $(\vec{X}^{m+1}, \kappa^{m+1}_g)$ be a solution to $(\mathcal{C}_{m,\star})^h$, or let $(\vec{X}^{m+1}, \vec{\kappa}^{m+1}_g)$ be a solution to $(\mathcal{D}_{m,\star})^h$. Then it holds that

$$L^h_g(\vec{X}^{m+1}) + \Delta t_m \begin{cases} \left(g^{\frac{1}{2}}(\vec{X}^m)\, |\kappa^{m+1}_g|^2, |\vec{X}^m_\rho| \right)^h \\ \left(g^{\frac{3}{2}}(\vec{X}^m)\, |\vec{\kappa}^{m+1}_g|^2, |\vec{X}^m_\rho| \right)^h \end{cases} \leqslant L^h_g(\vec{X}^m)\,, \tag{3.25}$$

respectively.

Proof. Choosing $\chi = \Delta t_m \, \kappa_g^{m+1}$ in (3.18) and $\vec{\eta} = \vec{X}^{m+1} - \vec{X}^m$ in (3.8) yields

$$\begin{aligned}
-\Delta t_m \left(g^{\frac{1}{2}}(\vec{X}^m)\, |\kappa_g^{m+1}|^2, |\vec{X}_\rho^m| \right)^h &= \left(\nabla \left[g_+^{\frac{1}{2}}(\vec{X}^{m+1}) + g_-^{\frac{1}{2}}(\vec{X}^m) \right], (\vec{X}^{m+1} - \vec{X}^m)\, |\vec{X}_\rho^{m+1}| \right)^h \\
&\quad + \left(g^{\frac{1}{2}}(\vec{X}^m)\, \vec{X}_\rho^{m+1}, (\vec{X}_\rho^{m+1} - \vec{X}_\rho^m)\, |\vec{X}_\rho^m|^{-1} \right)^h \\
&\geqslant \left(g^{\frac{1}{2}}(\vec{X}^{m+1}) - g^{\frac{1}{2}}(\vec{X}^m), |\vec{X}_\rho^{m+1}| \right)^h + \left(g^{\frac{1}{2}}(\vec{X}^m), |\vec{X}_\rho^{m+1}| - |\vec{X}_\rho^m| \right)^h \\
&= \left(g^{\frac{1}{2}}(\vec{X}^{m+1})\, |\vec{X}_\rho^{m+1}| - g^{\frac{1}{2}}(\vec{X}^m)\, |\vec{X}_\rho^m|, 1 \right)^h \\
&= L_g^h(\vec{X}^{m+1}) - L_g^h(\vec{X}^m)\,, \qquad (3.26)
\end{aligned}$$

where we have used (3.7) and the inequality $\vec{a}\,.\,(\vec{a} - \vec{b}) \geqslant |\vec{b}|\,(|\vec{a}| - |\vec{b}|)$ for $\vec{a}, \vec{b} \in \mathbb{R}^2$. This proves the desired result (3.25) for $(\mathcal{C}_{m,\star})^h$. The proof for $(\mathcal{D}_{m,\star})^h$ is analogous. □

Remark 3.6 We observe that in most of the above fully discrete schemes it is possible to eliminate the discrete curvatures, κ_g^{m+1} or $\vec{\kappa}_g^{m+1}$, to derive discrete analogues of (2.36) and (2.37), respectively. In particular, on recalling (3.11) and on choosing $\chi = \pi^h[g^{\frac{1}{2}}(\vec{X}^m)\, \vec{\eta}\,.\,\vec{\omega}^m] \in V^h$ in (3.18) for $\vec{\eta} \in \underline{V}^h$, the scheme $(\mathcal{C}_{m,\star})^h$ reduces to the following. Find $\vec{X}^{m+1} \in \underline{V}^h$ such that

$$\begin{aligned}
&\left(g^{\frac{3}{2}}(\vec{X}^m)\, \frac{\vec{X}^{m+1} - \vec{X}^m}{\Delta t_m}\,.\,\vec{\omega}^m, \vec{\eta}\,.\,\vec{\omega}^m\, |\vec{X}_\rho^m| \right)^h + \left(\nabla \left[g_+^{\frac{1}{2}}(\vec{X}^{m+1}) + g_-^{\frac{1}{2}}(\vec{X}^m) \right], \vec{\eta}\, |\vec{X}_\rho^{m+1}| \right)^h \\
&\quad + \left(g^{\frac{1}{2}}(\vec{X}^m)\, \vec{X}_\rho^{m+1}, \vec{\eta}_\rho\, |\vec{X}_\rho^m|^{-1} \right)^h = 0 \quad \forall\, \vec{\eta} \in \underline{V}^h \qquad (3.27)
\end{aligned}$$

and similarly for $(\mathcal{C}_m)^h$, $(\mathcal{D}_m)^h$ and $(\mathcal{D}_{m,\star})^h$. A related variant to (3.27) is given by the following. Find $\vec{X}^{m+1} \in \underline{V}^h$ such that

$$\begin{aligned}
&\left(g^{\frac{3}{2}}(\vec{X}^m)\, \frac{\vec{X}^{m+1} - \vec{X}^m}{\Delta t_m}\,.\,\vec{\nu}^m, \vec{\eta}\,.\,\vec{\nu}^m\, |\vec{X}_\rho^m| \right)^h + \left(\nabla \left[g_+^{\frac{1}{2}}(\vec{X}^{m+1}) + g_-^{\frac{1}{2}}(\vec{X}^m) \right], \vec{\eta}\, |\vec{X}_\rho^{m+1}| \right)^h \\
&\quad + \left(g^{\frac{1}{2}}(\vec{X}^m)\, \vec{X}_\rho^{m+1}, \vec{\eta}_\rho\, |\vec{X}_\rho^m|^{-1} \right)^h = 0 \quad \forall\, \vec{\eta} \in \underline{V}^h\,. \qquad (3.28)
\end{aligned}$$

Similarly to Theorem 3.5, the scheme (3.28) can also be shown to be unconditionally stable, i.e. a solution to (3.28) satisfies

$$L_g^h(\vec{X}^{m+1}) + \Delta t_m \left(g^{\frac{3}{2}}(\vec{X}^m) \left| \frac{\vec{X}^{m+1} - \vec{X}^m}{\Delta t_m}\,.\,\vec{\nu}^m \right|^2, |\vec{X}_\rho^m| \right)^h \leqslant L_g^h(\vec{X}^m)\,.$$

REMARK 3.7 Note that in the case $\mu = -1$, the function $g_+^{\frac{1}{2}}(\vec{z}) = g^{\frac{1}{2}}(\vec{z}) = \vec{z}\,.\,\vec{e}_2$ is linear, and $\nabla\, g^{\frac{1}{2}}(\vec{z}) = \vec{e}_2$. As a consequence, the numerical integration in the second and third terms in (3.5), (3.8), (3.19b) and (3.20) plays no role. In fact, in this case the schemes $(\mathcal{C}_m)^h$, $(\mathcal{D}_m)^h$ and $(\mathcal{C}_{m,\star})^h$, $(\mathcal{D}_{m,\star})^h$, with (3.9), collapse to their namesakes in Barrett *et al.* (2019a), if we account for the space-dependent weighting factor that differentiates (2.75) from (2.24).

REMARK 3.8 Using the techniques from Barrett *et al.* (2019a), it is straightforward to adapt the presented schemes to deal with open curves, with fixed end points. These schemes then allow us to compute approximations to geodesics in the hyperbolic plane, for example. In particular, we replace $I = \mathbb{R}/\mathbb{Z}$ by $I = [0,1]$ and define $\underline{V}^h_\partial = \{\vec{\eta} \in \underline{V}^h : \vec{\eta}(0) = \vec{\eta}(1) = \vec{0}\}$. Then in place of $(\mathcal{A}_m)^h$ we seek $(\vec{X}^{m+1}, \kappa^{m+1}) \in \underline{V}^h \times V^h$, with $\vec{X}^{m+1} - \vec{X}^m \in \underline{V}^h_\partial$, such that (3.10) holds, as well as (3.3), with $\underline{V}^h$ replaced by $\underline{V}^h_\partial$. For later reference, we call this adapted scheme $(\mathcal{A}^\partial_m)^h$. Of course, this scheme will inherit all the properties from $(\mathcal{A}_m)^h$ as displayed in Table 2.

3.2 *Curve diffusion*

We consider the following fully discrete approximation of $(\mathcal{E})$, i.e. (2.42), (2.22), where, in order to make the approximation more practical, we introduce an auxiliary variable.
$(\mathcal{E}_m)^h$: Let $\vec{X}^0 \in \underline{V}^h$. For $m = 0, \ldots, M-1$, find $(\vec{X}^{m+1}, \kappa^{m+1}, \mathfrak{k}^{m+1}) \in \underline{V}^h \times V^h \times V^h$ such that (3.3) holds and

$$\left(g(\vec{X}^m)\, \frac{\vec{X}^{m+1} - \vec{X}^m}{\Delta t_m}, \chi\, \vec{\nu}^m\, |\vec{X}^m_\rho| \right)^h = \left(g^{-\frac{1}{2}}(\vec{X}^m) \left[\mathfrak{k}^{m+1} - Z^m \right]_\rho, \chi_\rho\, |\vec{X}^m_\rho|^{-1} \right)^h \quad \forall\, \chi \in V^h\,, \tag{3.29a}$$

$$\left(g^{\frac{1}{2}}(\vec{X}^m)\, \mathfrak{k}^{m+1}, \zeta\, |\vec{X}^m_\rho| \right)^h = \left(\kappa^{m+1}, \zeta\, |\vec{X}^m_\rho| \right)^h \quad \forall\, \zeta \in V^h\,, \tag{3.29b}$$

where $Z^m \in V^h$ is such that

$$\left(g^{\frac{1}{2}}(\vec{X}^m)\, Z^m, \xi\, |\vec{X}^m_\rho| \right)^h = \tfrac{1}{2} \left(\vec{\nu}^m\,.\,\nabla\, \ln g(\vec{X}^m), \xi\, |\vec{X}^m_\rho| \right)^h \quad \forall\, \xi \in V^h\,. \tag{3.29c}$$

We note that it does not appear possible to prove the existence of a unique solution to $(\mathcal{E}_m)^h$. However, in practice, in all our numerical experiments, the associated linear system is always nonsingular and so a unique solution exists.

We consider the following two fully discrete analogues of $(\mathcal{F})$, i.e. (2.43) and (2.23). The first scheme will be linear, while the second scheme will be nonlinear, and will admit a stability proof.
$(\mathcal{F}_m)^h$: Let $\vec{X}^0 \in \underline{V}^h$. For $m = 0, \ldots, M-1$, find $(\vec{X}^{m+1}, \kappa_g^{m+1}) \in \underline{V}^h \times V^h$ such that (3.5) holds and

$$\left(g(\vec{X}^m)\, \frac{\vec{X}^{m+1} - \vec{X}^m}{\Delta t_m}, \chi\, \vec{\nu}^m\, |\vec{X}^m_\rho| \right)^h = \left(g^{-\frac{1}{2}}(\vec{X}^m)\, [\kappa_g^{m+1}]_\rho, \chi_\rho\, |\vec{X}^m_\rho|^{-1} \right)^h \quad \forall\, \chi \in V^h\,. \tag{3.30}$$

$(\mathcal{F}_{m,\star})^h$: Let $\vec{X}^0 \in \underline{V}^h$. For $m = 0, \ldots, M-1$, find $(\vec{X}^{m+1}, \kappa_g^{m+1}) \in \underline{V}^h \times V^h$ such that (3.8) and (3.30) hold.

We remark that the schemes $(\mathcal{E}_m)^h$, $(\mathcal{F}_m)^h$ and $(\mathcal{F}_{m,\star})^h$, with (3.9), in the case (2.6b), collapse to the scheme Barrett *et al.* (2007a, (2.2a,b)) for Euclidean curve/surface diffusion.

LEMMA 3.9 Let the assumption $(\mathfrak{A})^h$ hold. Then there exists a unique solution $(\vec{X}^{m+1}, \kappa_g^{m+1}) \in \underline{V}^h \times V^h$ to $(\mathcal{F}_m)^h$.

Proof. As (3.30), (3.5) is linear, existence follows from uniqueness. To investigate the latter, we consider the following system. Find $(\vec{X}, \kappa_g) \in \underline{V}^h \times V^h$ such that

$$\left(g(\vec{X}^m)\, \frac{\vec{X}}{\Delta t_m}, \chi\, \vec{\nu}^m\, |\vec{X}^m_\rho| \right)^h = \left(g^{-\frac{1}{2}}(\vec{X}^m)\, [\kappa_g]_\rho, \chi_\rho\, |\vec{X}^m_\rho|^{-1} \right)^h \quad \forall\ \chi \in V^h\,, \tag{3.31a}$$

$$\left(g(\vec{X}^m)\, \kappa_g\, \vec{\nu}^m, \vec{\eta}\, |\vec{X}^m_\rho| \right)^h + \left(g^{\frac{1}{2}}(\vec{X}^m)\, \vec{X}_\rho, \vec{\eta}_\rho\, |\vec{X}^m_\rho|^{-1} \right)^h = 0 \quad \forall\ \vec{\eta} \in \underline{V}^h\,. \tag{3.31b}$$

Choosing $\chi = \kappa_g \in V^h$ in (3.31a) and $\vec{\eta} = \vec{X} \in \underline{V}^h$ in (3.31b) yields

$$\left(g^{\frac{1}{2}}(\vec{X}^m)\, |\vec{X}_\rho|^2, |\vec{X}^m_\rho|^{-1} \right)^h + \Delta t_m \left(g^{-\frac{1}{2}}(\vec{X}^m)\, |[\kappa_g]_\rho|^2, |\vec{X}^m_\rho|^{-1} \right)^h = 0\,. \tag{3.32}$$

It follows from (3.32) that κ_g and $\vec{X}$ are constant. Hence, it follows from (3.31a) and the assumption $(\mathfrak{A})^h$, similarly to the proof of Lemma 3.1, that $\vec{X} = \vec{0}$. Moreover, it follows from (3.31b) and the fact that $\mathcal{Z}^h$ must contain a nonzero vector that $\kappa_g = 0$. Hence, we have shown that $(\mathcal{F}_m)^h$ has a unique solution $(\vec{X}^{m+1}, \kappa_g^{m+1}) \in \underline{V}^h \times V^h$. □

We now prove a discrete analogue of (2.39), recall also (2.44), for the scheme $(\mathcal{F}_{m,\star})^h$.

THEOREM 3.10 Let $(\vec{X}^{m+1}, \kappa_g^{m+1})$ be a solution to $(\mathcal{F}_{m,\star})^h$. Then it holds that

$$L^h_g(\vec{X}^{m+1}) + \Delta t_m \left(g^{-\frac{1}{2}}(\vec{X}^m)\, |[\kappa_g^{m+1}]_\rho|^2, |\vec{X}^m_\rho|^{-1} \right)^h \leqslant L^h_g(\vec{X}^m)\,. \tag{3.33}$$

Proof. Choosing $\chi = \Delta t_m\, \kappa_g^{m+1}$ in (3.30) and $\vec{\eta} = \vec{X}^{m+1} - \vec{X}^m$ in (3.8) we obtain, similarly to (3.26), that

$$\begin{aligned} -\Delta t_m \left(g^{-\frac{1}{2}}(\vec{X}^m)\, |[\kappa_g^{m+1}]_\rho|^2, |\vec{X}^m_\rho|^{-1} \right)^h &= \left(\nabla\, [g_+^{\frac{1}{2}}(\vec{X}^{m+1}) + g_-^{\frac{1}{2}}(\vec{X}^m)], (\vec{X}^{m+1} - \vec{X}^m)\, |\vec{X}^{m+1}_\rho| \right)^h \\ &\quad + \left(g^{\frac{1}{2}}(\vec{X}^m)\, \vec{X}^{m+1}_\rho, (\vec{X}^{m+1}_\rho - \vec{X}^m_\rho)\, |\vec{X}^m_\rho|^{-1} \right)^h \\ &\geqslant L^h_g(\vec{X}^{m+1}) - L^h_g(\vec{X}^m)\,. \end{aligned}$$

This proves the desired result (3.33). □

3.3 *Elastic flow*

We consider the following fully discrete finite element approximation of $(\mathcal{U})$, i.e. (2.68) and (2.22), similarly to the approximation $(\mathcal{E}_m)^h$ for $(\mathcal{E})$.

$(\mathcal{U}_m)^h$: Let $\vec{X}^0 \in \underline{V}^h$ and $\kappa^0 \in V^h$. For $m = 0, \ldots, M-1$, find $(\vec{X}^{m+1}, \kappa^{m+1}, \mathfrak{k}^{m+1}) \in \underline{V}^h \times V^h \times V^h$ such that (3.3), (3.29b) hold and

$$\left(g(\vec{X}^m)\, \frac{\vec{X}^{m+1} - \vec{X}^m}{\Delta t_m}, \chi\, \vec{\nu}^m\, |\vec{X}^m_\rho| \right)^h = \left(g^{-\frac{1}{2}}(\vec{X}^m) \left[\mathfrak{k}^{m+1} - Z^m \right]_\rho, \chi_\rho\, |\vec{X}^m_\rho|^{-1} \right)^h - \tfrac{1}{2} \left(g^{-1}(\vec{X}^m) \left[\kappa^m - \tfrac{1}{2}\, \vec{\nu}^m \,.\, \nabla\, \ln g(\vec{X}^m) \right]^3, \chi\, |\vec{X}^m_\rho| \right)^h - \left(S_0(\vec{X}^m) \left[\kappa^m - \tfrac{1}{2}\, \vec{\nu}^m \,.\, \nabla\, \ln g(\vec{X}^m) \right], \chi\, |\vec{X}^m_\rho| \right)^h \quad \forall\, \chi \in V^h\,, \tag{3.34}$$

where $Z^m \in V^h$ is defined by (3.29c).

We consider the following fully discrete finite element approximation of $(\mathcal{W})$, i.e. (2.69) and (2.23). $(\mathcal{W}_m)^h$: Let $\vec{X}^0 \in \underline{V}^h$ and $\kappa_g^0 \in V^h$. For $m = 0, \ldots, M-1$, find $(\vec{X}^{m+1}, \kappa_g^{m+1}) \in \underline{V}^h \times V^h$ such that (3.5) holds and

$$\left(g(\vec{X}^m)\, \frac{\vec{X}^{m+1} - \vec{X}^m}{\Delta t_m}, \chi\, \vec{\nu}^m\, |\vec{X}^m_\rho| \right)^h = \left(g^{-\frac{1}{2}}(\vec{X}^m)\, [\kappa_g^{m+1}]_\rho, \chi_\rho\, |\vec{X}^m_\rho|^{-1} \right)^h - \tfrac{1}{2} \left(g^{\frac{1}{2}}(\vec{X}^m)\, (\kappa_g^m)^3, \chi\, |\vec{X}^m_\rho| \right)^h - \left(S_0(\vec{X}^m)\, g^{\frac{1}{2}}(\vec{X}^m)\, \kappa_g^m, \chi\, |\vec{X}^m_\rho| \right)^h \quad \forall\, \chi \in V^h\,. \tag{3.35}$$

Clearly, for the metric (2.6b) we have $S_0 = 0$, and so the last terms in (3.34) and (3.35) vanish. In fact, in this case the schemes $(\mathcal{U}_m)^h$ and $(\mathcal{W}_m)^h$ collapse to the scheme Barrett *et al.* (2007a, (2.45a,b)), with $\lambda_m = 0$, for Euclidean elastic flow.

REMARK 3.11 It is often of interest to add a length penalization term to the energy (2.45), and hence consider the L^2-gradient flow of

$$W_g^\lambda(\vec{x}) = W_g(\vec{x}) + \lambda\, L_g(\vec{x})\,,$$

recall (2.3), for some $\lambda \in \mathbb{R}_{\geqslant 0}$; see, e.g., Dall'Acqua & Spener (2017). It is straightforward to generalize our weak formulations and finite element approximations to this case. For example, the scheme $(\mathcal{W}_m)^h$ is adapted by adding the term $\lambda\, (g^{\frac{1}{2}}(\vec{X}^m)\, \kappa_g^{m+1}, \chi\, |\vec{X}^m_\rho|)^h$ to the right-hand side of (3.35), and we call this new scheme $(\mathcal{W}_m^\lambda)^h$ for later reference. Of course, this scheme will inherit all the properties from $(\mathcal{W}_m)^h$ as displayed in Table 2.

4. Numerical results

In this section we present some numerical computations for the introduced finite element approximations. We implemented the schemes within the finite element toolbox Alberta; see Schmidt & Siebert (2005). Where the arising systems of equations to be solved at each time level are linear, these are solved with the sparse factorization package UMFPACK; see Davis (2004). When the equations are nonlinear, we employ a standard Newton iteration and solve the

linear substeps with UMFPACK. In all our simulations, the Newton iteration never took more than two steps.

We recall from (2.4) that

$$A_g(\vec{x}) = \int_\Omega g(\vec{z})\,\mathrm{d}\vec{z} = \int_I \vec{\phi}_g(\vec{x})\,.\,\vec{\nu}\,|\vec{x}_\rho|\,\mathrm{d}\rho\,, \quad \text{where} \quad \nabla\,.\,\vec{\phi}_g = g \quad \text{in } H\,,$$

if $\nu \circ \vec{x}^{-1}$ denotes the outer normal on $\partial\Omega = \Gamma = \vec{x}(I)$. With this in mind, we define the following approximation of $A_g(\vec{X}^m)$:

$$A_g^h(\vec{X}^m) = \left(\vec{\phi}_g(\vec{X}^m)\,.\,\vec{\nu}^m, |\vec{X}^m_\rho|\right)^h. \tag{4.1}$$

For the different metrics we consider, the function $\vec{\phi}_g$ can be chosen as follows:

$$\text{(2.7)} \qquad \vec{\phi}_g(\vec{z}) = \begin{cases} (1-2\,\mu)^{-1}\,(\vec{z}\,.\,\vec{e}_2)^{1-2\,\mu}\,\vec{e}_2\,, & \mu \neq \frac{1}{2}\,, \\ \ln(\vec{z}\,.\,\vec{e}_2)\,\vec{e}_2\,, & \mu = \frac{1}{2}\,, \end{cases}$$

$$\text{(2.8)} \qquad \vec{\phi}_g(\vec{z}) = \begin{cases} 2\,[\alpha\,|\vec{z}|^2\,(1-\alpha\,|\vec{z}|^2)]^{-1}\,\vec{z}\,, & \alpha \neq 0\,, \\ 2\,\vec{z}\,, & \alpha = 0\,, \end{cases}$$

$$\text{(2.72b)} \qquad \vec{\phi}_g(\vec{z}) = \tanh(\vec{z}\,.\,\vec{e}_1)\,\vec{e}_1\,,$$

$$\text{(2.72c)} \qquad \vec{\phi}_g(\vec{z}) = \tfrac{1}{2}\,(\vec{z}\,.\,\vec{e}_1 + \sinh(\vec{z}\,.\,\vec{e}_1)\,\cosh(\vec{z}\,.\,\vec{e}_1))\,\vec{e}_1\,,$$

$$\text{(2.72d)} \qquad \vec{\phi}_g(\vec{z}) = \tfrac{2\,[\mathfrak{s}^2+1]^{\frac{1}{2}}}{\mathfrak{s}}\,\arctan\left(\tfrac{[\mathfrak{s}^2+1]^{\frac{1}{2}}+1}{\mathfrak{s}}\,\tan\tfrac{\vec{z}\,.\,\vec{e}_2}{2}\right) + \tfrac{\sin\vec{z}\,.\,\vec{e}_2}{[\mathfrak{s}^2+1]^{\frac{1}{2}}-\cos\vec{z}\,.\,\vec{e}_2}\,.$$

For solutions of the scheme $(\mathcal{U}_m)^h$, we define

$$W_g^m = \tfrac{1}{2}\left(g^{-\frac{1}{2}}(\vec{X}^m)\left[\kappa^m - \tfrac{1}{2}\,\vec{\nu}^m\,.\,\nabla\,\ln g(\vec{X}^m)\right]^2, |\vec{X}^m_\rho|\right)^h \tag{4.2}$$

as the natural discrete analogue of (2.45), while for solutions of the scheme $(\mathcal{W}_m)^h$ we define

$$\widetilde{W}_g^m = \tfrac{1}{2}\left(g^{\frac{1}{2}}(\vec{X}^m)\left[\kappa_g^m\right]^2, |\vec{X}^m_\rho|\right)^h.$$

On recalling (1.5), and given $\Gamma^0 = \vec{X}^0(\bar{I})$, we define the initial data $\kappa^0 \in V^h$ for the scheme $(\mathcal{U}_m)^h$ via $\kappa^0 = \pi^h\left[\frac{\vec{\kappa}^0\,.\,\vec{\omega}^0}{|\vec{\omega}^0|}\right]$, where we recall (3.11), and where $\vec{\kappa}^0 \in \underline{V}^h$ is such that

$$\left(\vec{\kappa}^0, \vec{\eta}\,|\vec{X}^0_\rho|\right)^h + \left(\vec{X}^0_\rho, \vec{\eta}_\rho\,|\vec{X}^0_\rho|^{-1}\right) = 0 \quad \forall\,\vec{\eta} \in \underline{V}^h\,.$$

With this definition of κ^0, we define the initial data $\kappa_g^0 \in V^h$ for the scheme $(\mathcal{W}_m)^h$ via

$$\kappa_g^0 = \pi^h \left[g^{-\frac{1}{2}}(\vec{X}^0) \left[\kappa^0 - \tfrac{1}{2}\, \vec{\omega}^0 \,.\, \nabla \, \ln g(\vec{X}^0) \right] \right].$$

We also consider the ratio

$$\mathfrak{r}^m = \frac{\max_{j=1,\ldots,J} |\vec{X}^m(q_j) - \vec{X}^m(q_{j-1})|}{\min_{j=1,\ldots,J} |\vec{X}^m(q_j) - \vec{X}^m(q_{j-1})|} \tag{4.3}$$

between the longest and shortest elements of Γ^m, and are often interested in the evolution of this ratio over time.

4.1 *The hyperbolic plane, and (2.7) for $\mu \in \mathbb{R}$*

Unless otherwise stated, all our computations in this section are for the hyperbolic plane, i.e. (2.6a) or, equivalently, (2.7) with $\mu = 1$.

4.1.1 *Curvature flow.* From Appendix A.1 we recall the true solution (A.1) with (A.5) for hyperbolic curvature flow, (2.24) in the case (2.6a). We use this true solution for a convergence test for the various schemes for curvature flow. Here we start with a nonuniform partitioning of a circle of radius $r(0) = 1$ centred at $a(0)\,\vec{e}_2$, where $a(0) = 2$. In particular, we choose $\vec{X}^0 \in \underline{V}^h$ with

$$\vec{X}^0(q_j) = a(0)\,\vec{e}_2 + r(0) \begin{pmatrix} \cos[2\,\pi\, q_j + 0.1\, \sin(2\,\pi\, q_j)] \\ \sin[2\,\pi\, q_j + 0.1\, \sin(2\,\pi\, q_j)] \end{pmatrix}, \quad j = 1, \ldots, J\,; \tag{4.4}$$

recall (3.1). We compute the error

$$\|\Gamma - \Gamma^h\|_{L^\infty} = \max_{m=1,\ldots,M} \max_{j=1,\ldots,J} ||\vec{X}^m(q_j) - a(t_m)\,\vec{e}_2| - r(t_m)|$$

over the time interval $[0, 0.1]$ between the true solution (A.1) and the discrete solutions for the schemes $(\mathcal{A}_m)^h$ and $(\mathcal{B}_m)^h$. We note that the extinction time for (A.5) is $T_0 = -\frac{1}{2}\, \ln \frac{3}{4} = 0.144$. Here we use the time-step size $\Delta t = 0.1\, h_{\Gamma^0}^2$, where h_{Γ^0} is the maximal edge length of Γ^0. The computed errors are reported in Table 3. The same errors for the schemes $(\mathcal{C}_m)^h$, $(\mathcal{D}_m)^h$, $(\mathcal{C}_{m,\star})^h$ and $(\mathcal{D}_{m,\star})^h$ can be seen in Tables 4 and 5, respectively. We observe that all schemes exhibit second-order convergence rates, with the smallest errors produced by $(\mathcal{A}_m)^h$ and $(\mathcal{C}_{m,\star})^h$. The CPU times of all the schemes are comparable, with the two nonlinear schemes $(\mathcal{C}_{m,\star})^h$ and $(\mathcal{D}_{m,\star})^h$ taking only slightly longer than the linear schemes. In particular, on an Intel Xeon E5-2643 3.30 GHz, with 16 GB main memory, the runs for $J = 512$ took about 15 s each for $(\mathcal{C}_{m,\star})^h$ and $(\mathcal{D}_{m,\star})^h$, and about 12 s for the remaining schemes.

For the scheme $(\mathcal{A}_m)^h$ we show the evolution of a cigar shape in Fig. 1. The discretization parameters are $J = 128$ and $\Delta t = 10^{-4}$. Rotating the initial shape by 90° yields the evolution in Fig. 2. We note that in both cases the curve shrinks to a point. The same computations for the remaining schemes, i.e.

TABLE 3 *Errors for the convergence test for* (A.1) *with* (A.5)*, with* $r(0) = 1$*,* $a(0) = 2$*, over the time interval* $[0, 0.1]$

J	h_{Γ^0}	$(\mathcal{A}_m)^h$ $\|\Gamma - \Gamma^h\|_{L^\infty}$	EOC	$(\mathcal{B}_m)^h$ $\|\Gamma - \Gamma^h\|_{L^\infty}$	EOC
32	2.1544e–01	2.7956e–02	—	4.7884e–02	—
64	1.0792e–01	7.6597e–03	1.87	1.3493e–02	1.83
128	5.3988e–02	1.9572e–03	1.97	3.4819e–03	1.96
256	2.6997e–02	4.9196e–04	1.99	8.7754e–04	1.99
512	1.3499e–02	1.2315e–04	2.00	2.1982e–04	2.00

TABLE 4 *Errors for the convergence test for* (A.1) *with* (A.5)*, with* $r(0) = 1$*,* $a(0) = 2$*, over the time interval* $[0, 0.1]$

J	h_{Γ^0}	$(\mathcal{C}_m)^h$ $\|\Gamma - \Gamma^h\|_{L^\infty}$	EOC	$(\mathcal{D}_m)^h$ $\|\Gamma - \Gamma^h\|_{L^\infty}$	EOC
32	2.1544e–01	3.4212e–02	—	5.2395e–02	—
64	1.0792e–01	9.3803e–03	1.87	1.4744e–02	1.83
128	5.3988e–02	2.3970e–03	1.97	3.8047e–03	1.96
256	2.6997e–02	6.0251e–04	1.99	9.5887e–04	1.99
512	1.3499e–02	1.5082e–04	2.00	2.4019e–04	2.00

TABLE 5 *Errors for the convergence test for* (A.1) *with* (A.5)*, with* $r(0) = 1$*,* $a(0) = 2$*, over the time interval* $[0, 0.1]$

J	h_{Γ^0}	$(\mathcal{C}_{m,\star})^h$ $\|\Gamma - \Gamma^h\|_{L^\infty}$	EOC	$(\mathcal{D}_{m,\star})^h$ $\|\Gamma - \Gamma^h\|_{L^\infty}$	EOC
32	2.1544e–01	2.7155e–02	—	4.9299e–02	—
64	1.0792e–01	7.5112e–03	1.86	1.3918e–02	1.83
128	5.3988e–02	1.9237e–03	1.97	3.5945e–03	1.95
256	2.6997e–02	4.8381e–04	1.99	9.0613e–04	1.99
512	1.3499e–02	1.2112e–04	2.00	2.2699e–04	2.00

$(\mathcal{B}_m)^h$, $(\mathcal{C}_m)^h$, $(\mathcal{D}_m)^h$, $(\mathcal{C}_{m,\star})^h$ and $(\mathcal{D}_{m,\star})^h$, yield very similar results, with the main difference being the evolution of the ratio (4.3). For the simulation in Fig. 1, we present the plots of this quantity for these alternative schemes in Fig. 3, where we observe that the obtained curves are far from being equidistributed. In particular, the ratio for the schemes $(\mathcal{B}_m)^h$, $(\mathcal{D}_m)^h$ $(\mathcal{D}_{m,\star})^h$ reaches almost 60, while it remains bounded below 3 for the schemes $(\mathcal{C}_m)^h$ and $(\mathcal{C}_{m,\star})^h$. This compares with a final ratio of about 1.2 in Fig. 1.

We now employ the scheme $(\mathcal{A}_m^{\partial})^h$ from Remark 3.8 to compute some geodesics. To this end, we use as initial data a straight line segment between the two fixed end points, and let the scheme run until time $T = 10$, at which point the discrete energy $L_g^h(\vec{X}^m)$ is almost constant in time. For each run the discretization parameters are $J = 128$ and $\Delta t = 10^{-4}$. For the hyperbolic plane, we show the final curves Γ^M in Fig. 4. Repeating the first of the two geodesic computations for the metric (2.7) with $\mu = 0.1$ and $\mu = 2$ yields the results in Fig. 5.

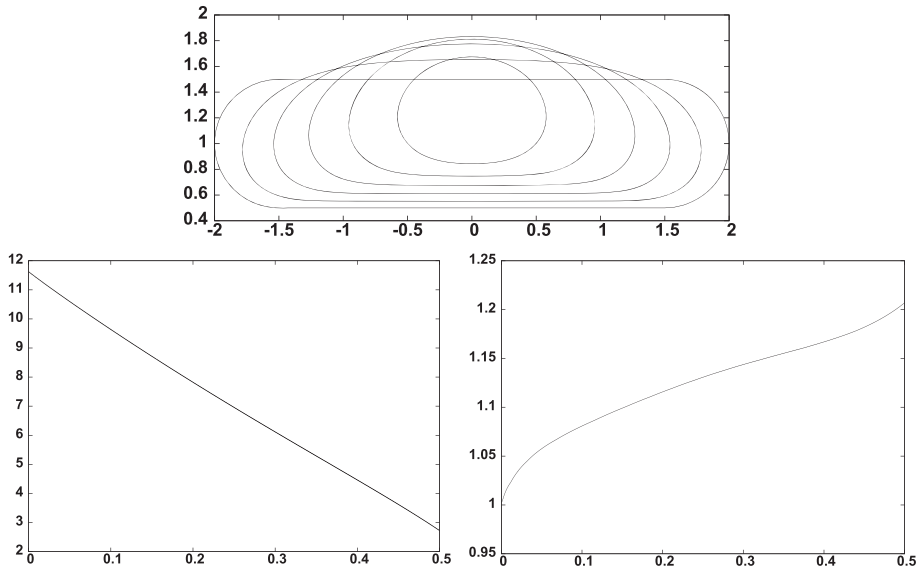

FIG. 1. $(\mathcal{A}_m)^h$: Curvature flow towards extinction. Solution at times $t = 0, 0.1, \ldots, 0.5$. Below are plots of the discrete energy $L_g^h(\vec{X}^m)$ and of the ratio (4.3).

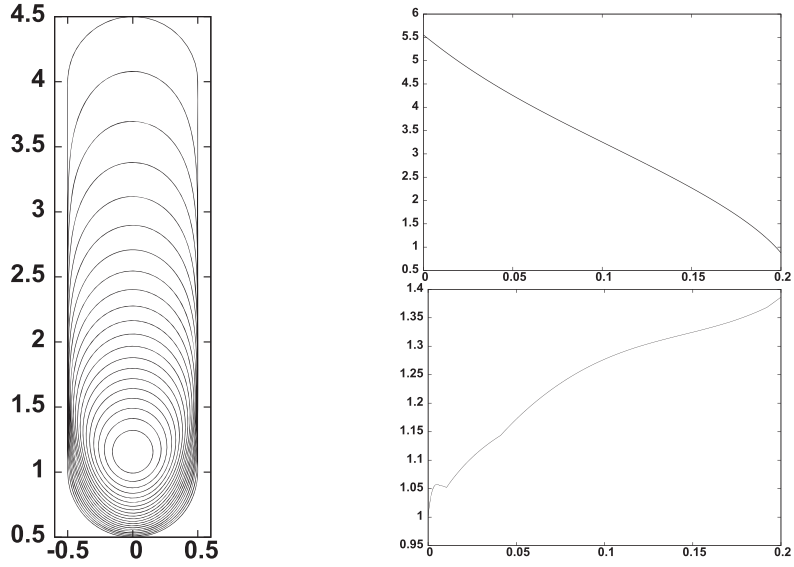

FIG. 2. $(\mathcal{A}_m)^h$: Curvature flow towards extinction. Solution at times $t = 0, 0.01, \ldots, 0.2$. On the right are plots of the discrete energy $L_g^h(\vec{X}^m)$ and of the ratio (4.3).

4.1.2 *Curve diffusion.* For curve diffusion in the hyperbolic plane, circles are steady state solutions. This follows from the fact that, analogously to the Euclidean case, circles in the hyperbolic plane have constant curvature; see (A.2) in Appendix A.1. For the scheme $(\mathcal{E}_m)^h$ we now show the evolutions of

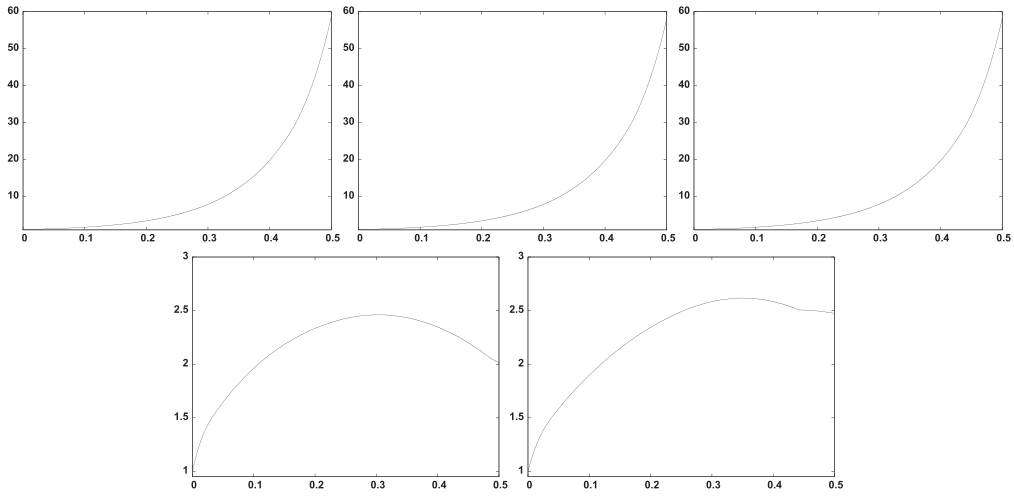

FIG. 3. The ratio plots (4.3) for the schemes $(\mathcal{B}_m)^h$, $(\mathcal{D}_m)^h$, $(\mathcal{D}_{m,\star})^h$, $(\mathcal{C}_m)^h$ and $(\mathcal{C}_{m,\star})^h$ for simulations as in Fig. 1.

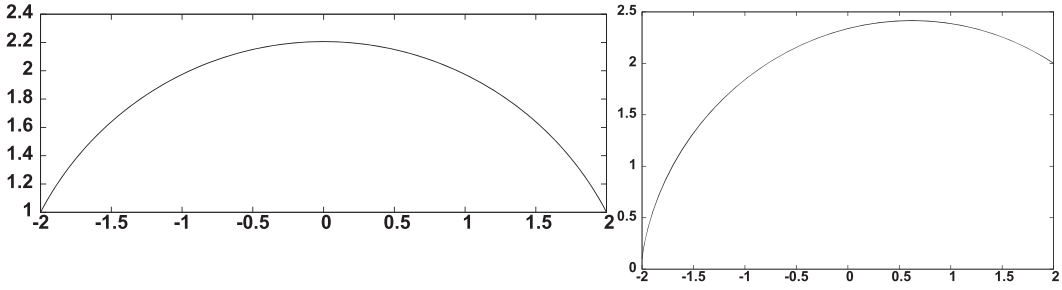

FIG. 4. $(\mathcal{A}_m^\vartheta)^h$: Geodesics in the hyperbolic plane, obtained with curvature flow. The left geodesic connects the points $(\pm 2, 1)^T$, with $L_g^h(\vec{X}^M) = 2.887$, while the right geodesics connects $(-2, 0.1)^T$ and $(2, 2)^T$, with $L_g^h(\vec{X}^M) = 4.620$.

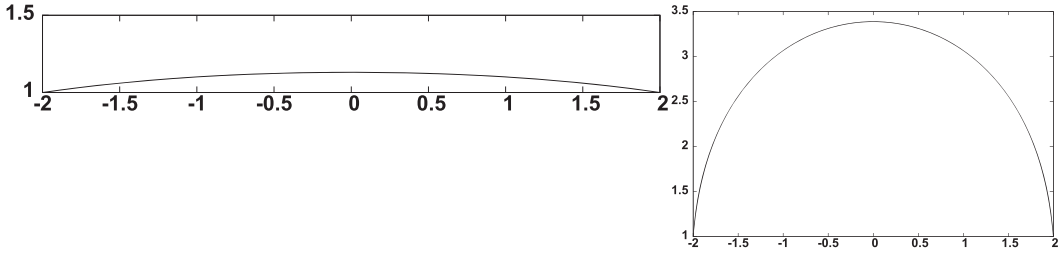

FIG. 5. $(\mathcal{A}_m^\vartheta)^h$: Geodesics connecting the points $(\pm 2, 1)^T$ for (2.7) with $\mu = 0.1$ (left) and $\mu = 2$ (right). The discrete lengths are $L_g^h(\vec{X}^M) = 3.977$ and $L_g^h(\vec{X}^M) = 1.645$, respectively.

two cigar shapes towards a circle. The discretization parameters are $J = 128$ and $\Delta t = 10^{-4}$. In Fig. 6 the initial shape is aligned horizontally, whereas in Fig. 7 it is aligned vertically. The relative area losses, measured in terms of (4.1), were -0.24% and 0.04% for these two simulations. Repeating

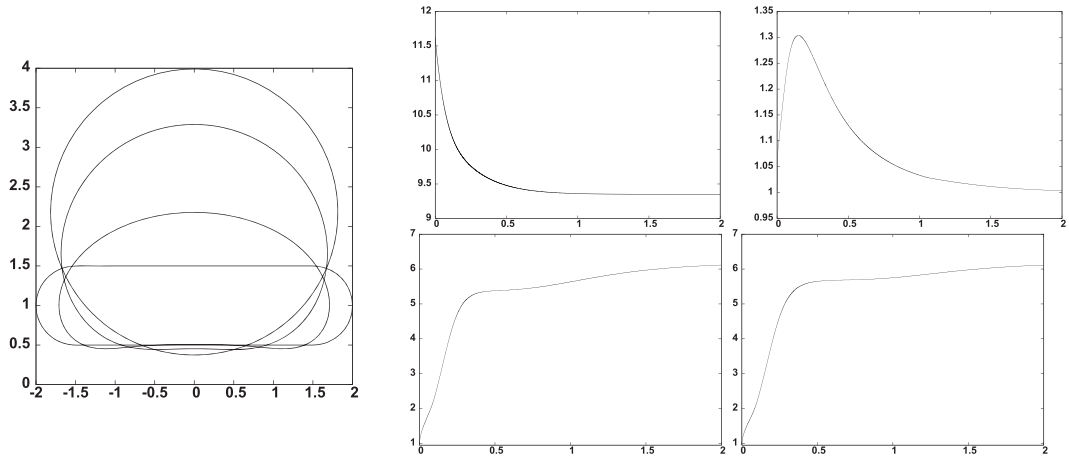

FIG. 6. $(\mathcal{E}_m)^h$: Curve diffusion towards a circle. Solution at times $t = 0, 0.1, 0.5, 2$. On the right are plots of the discrete energy $L_g^h(\vec{X}^m)$ and of the ratio (4.3), with plots of the ratio (4.3) for the schemes $(\mathcal{F}_m)^h$ and $(\mathcal{F}_{m,\star})^h$ below.

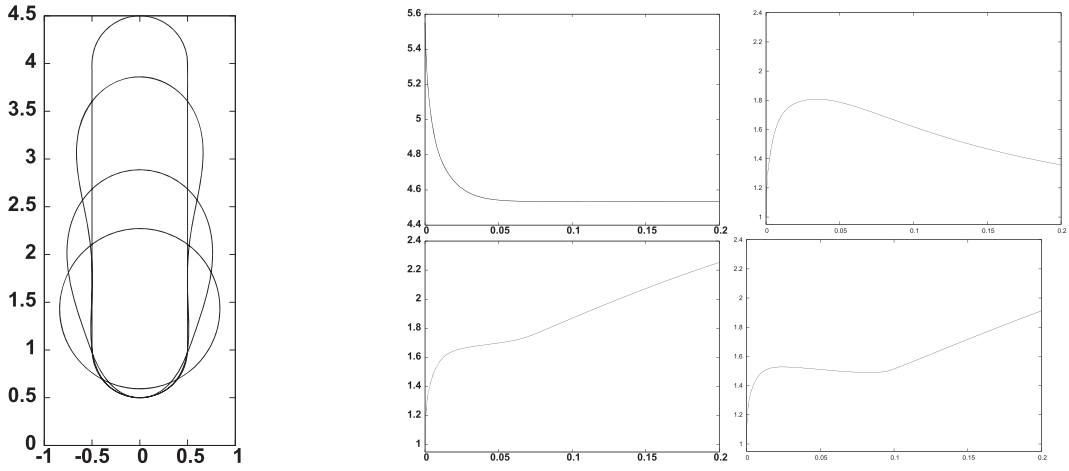

FIG. 7. $(\mathcal{E}_m)^h$: Curve diffusion towards a circle. Solution at times $t = 0, 10^{-3}, 10^{-2}, 0.2$. On the right are plots of the discrete energy $L_g^h(\vec{X}^m)$ and of the ratio (4.3), with plots of the ratio (4.3) for the schemes $(\mathcal{F}_m)^h$ and $(\mathcal{F}_{m,\star})^h$ below.

the simulations for the schemes $(\mathcal{F}_m)^h$ and $(\mathcal{F}_{m,\star})^h$ produces nearly identical results, with the main difference being the larger ratios (4.3). For the simulations corresponding to Fig. 6, the ratio reaches a value of about 6, and the relative area loss is -0.01% for both $(\mathcal{F}_m)^h$ and $(\mathcal{F}_{m,\star})^h$. For the runs shown in Fig. 7 the ratio (4.3) reaches a value around 2, and the relative area losses are 0.13% and 0.14%, respectively.

For the metric (2.7) with $\mu \notin \{0, 1\}$, circles are in general not steady state solutions for curve diffusion. We demonstrate this with numerical experiments for the metrics (2.7) with $\mu = 0.1$ and $\mu = 2$. For the case $\mu = 0.1$ we start from the initial data (4.4) with $a(0) = 1.01$ and $r(0) = 1$, and compute the evolution with the scheme $(\mathcal{E}_m)^h$ with the discretization parameters $J = 128$ and

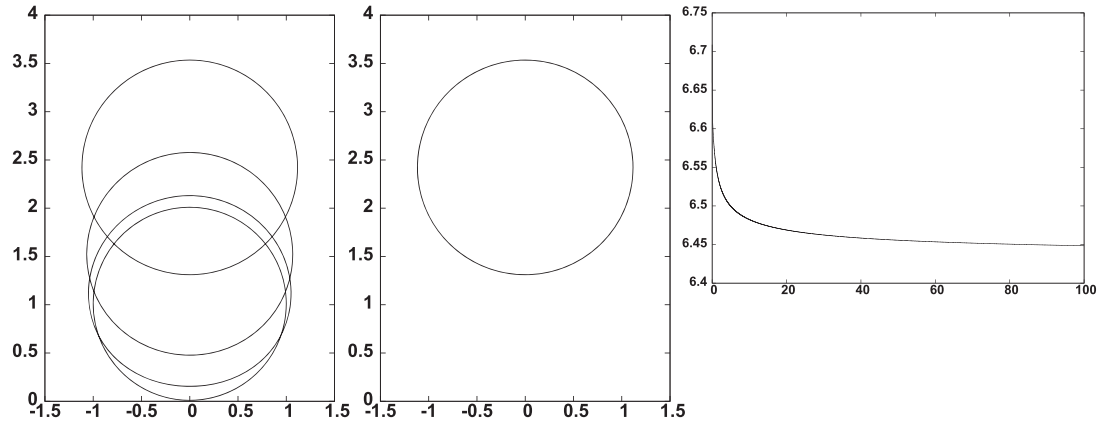

FIG. 8. $(\mathcal{E}_m)^h$: Curve diffusion for (2.7) with $\mu = 0.1$, starting from a circle. Solution at times $t = 0, 1, 10, 100$, and separately at time $t = 100$. On the right is a plot of the discrete energy $L_g^h(\vec{X}^m)$.

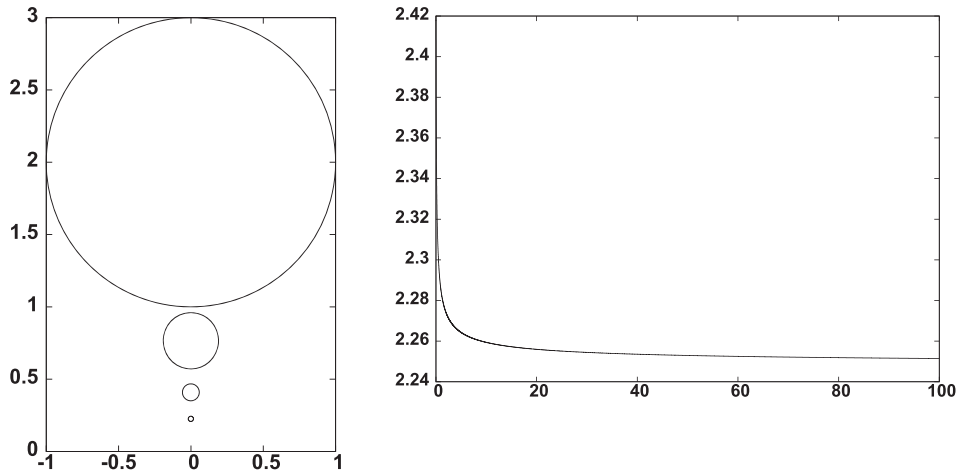

FIG. 9. $(\mathcal{E}_m)^h$: Curve diffusion for (2.7) with $\mu = 2$, starting from a circle. Solution at times $t = 0, 1, 10, 100$. On the right is a plot of the discrete energy $L_g^h(\vec{X}^m)$.

$\Delta t = 10^{-3}$. The results are shown in Fig. 8, where we note that the relative area loss, measured in terms of (4.1), was -0.04% for this experiment. The final shape has height 2.224 and width 2.233. For the case $\mu = 2$ we use the initial data (4.4) with $a(0) = 2$ and $r(0) = 1$, and leave all the remaining parameters unchanged. The evolution is shown in Fig. 9, with a relative area loss of 0.22%. The final shape has height 0.03617 and width 0.03609.

4.1.3 *Elastic flow.* For hyperbolic elastic flow, (2.57), we recall the true solution (A.1) with (A.10) from Appendix A.1. We use this true solution for a convergence test for our two schemes for elastic flow. Similarly to Table 3 we start with the initial data (4.4) with $r(0) = 1$ and $a(0) = 1.1$. We compute the error $\|\Gamma - \Gamma^h\|_{L^\infty}$ over the time interval $[0, 1]$ between the true solution (A.1) and the discrete solutions

TABLE 6 *Errors for the convergence test for* (A.1) *with* (A.10)*, with* $r(0) = 1$, $a(0) = 1.1$, *over the time interval* $[0, 1]$

J	h_{Γ^0}	$(\mathcal{U}_m)^h$ $\|\Gamma - \Gamma^h\|_{L^\infty}$	EOC	$(\mathcal{W}_m)^h$ $\|\Gamma - \Gamma^h\|_{L^\infty}$	EOC
32	2.1544e–01	3.5987e–02	—	3.1536e–02	—
64	1.0792e–01	8.7266e–03	2.05	7.9745e–03	1.99
128	5.3988e–02	2.1624e–03	2.01	1.9958e–03	2.00
256	2.6997e–02	5.3929e–04	2.00	4.9957e–04	2.00
512	1.3499e–02	1.3474e–04	2.00	1.2489e–04	2.00

TABLE 7 *Errors for the convergence test for* (A.1) *with* (A.10)*, with* $r(0) = 1$, $a(0) = 2$, *over the time interval* $[0, 1]$

J	h_{Γ^0}	$(\mathcal{U}_m)^h$ $\|\Gamma - \Gamma^h\|_{L^\infty}$	EOC	$(\mathcal{W}_m)^h$ $\|\Gamma - \Gamma^h\|_{L^\infty}$	EOC
32	2.1544e–01	1.8228e–01	—	4.0407e–02	—
64	1.0792e–01	4.3289e–02	2.08	1.0436e–02	1.96
128	5.3988e–02	1.0699e–02	2.02	2.6286e–03	1.99
256	2.6997e–02	2.6668e–03	2.00	6.5835e–04	2.00
512	1.3499e–02	6.6621e–04	2.00	1.6467e–04	2.00

for the schemes $(\mathcal{U}_m)^h$ and $(\mathcal{W}_m)^h$. We recall from Appendix A.1 that the circle will sink and shrink. In fact, at time $T = 1$ it holds that $r(T) = 0.645$ and $a(T) = 0.792$, so that $\sigma(T) = \frac{a(T)}{r(T)} = 1.227 < 2^{\frac{1}{2}}$; see Appendix A.1. Here we use the time-step size $\Delta t = 0.1\, h^2_{\Gamma^0}$, where h_{Γ^0} is the maximal edge length of Γ^0. The computed errors are reported in Table 6. We repeat the convergence test with the initial data $r(0) = 1$ and $a(0) = 2$, so that the circle will now rise and expand. In fact, at time $T = 1$ it holds that $r(T) = 1.677$ and $a(T) = 2.411$ so that $\sigma(T) = \frac{a(T)}{r(T)} = 1.437 > 2^{\frac{1}{2}}$; see Appendix A.1. The computed errors are reported in Table 7.

For the scheme $(\mathcal{U}_m)^h$ we show the evolution of a cigar shape in Fig. 10. The discretization parameters are $J = 128$ and $\Delta t = 10^{-4}$. Rotating the initial shape by 90° yields the evolution in Fig. 11. As expected, in both cases the curve evolves to a circle. In the first case, at time $t_m = 4$ it holds that $\sigma^m = \frac{a^m}{r^m} = 1.412 < 2^{\frac{1}{2}}$, where $a^m = \frac{1}{2}\,(\max_I \vec{X}^m \,.\, \vec{e}_2 + \min_I \vec{X}^m \,.\, \vec{e}_2)$ and $r^m = \frac{1}{2}\,(\max_I \vec{X}^m \,.\, \vec{e}_2 - \min_I \vec{X}^m \,.\, \vec{e}_2)$, and so the approximate circle is going to continue to sink and shrink. This is evidenced by the plot of a^m over time in Fig. 10, where we see that a^m eventually decreases. In the second simulation, on the other hand, we observe at time $t_m = 2$ that $\sigma_m = 1.415 > 2^{\frac{1}{2}}$, and so here the approximate circle will continue to rise and expand, which can also be seen from the plot of a^m over time in Fig. 11. The same computations for the scheme $(\mathcal{W}_m)^h$ yield almost identical results, with the main difference being the evolution of the ratio (4.3). We present the plots of this quantity for the scheme $(\mathcal{W}_m)^h$ for these two simulations in Fig. 12, where we observe that the obtained curves are far from being equidistributed, although the ratio (4.3) remains bounded, eventually settling on a value close to 4.

Finally, on recalling Remark 3.11, we repeat the simulation in Fig. 10 now for the scheme $(\mathcal{W}^{\lambda}_m)^h$ with $\lambda = 1$. As expected, the length penalization means that now the evolution reaches a steady state, as can be seen from the plots in Fig. 13.

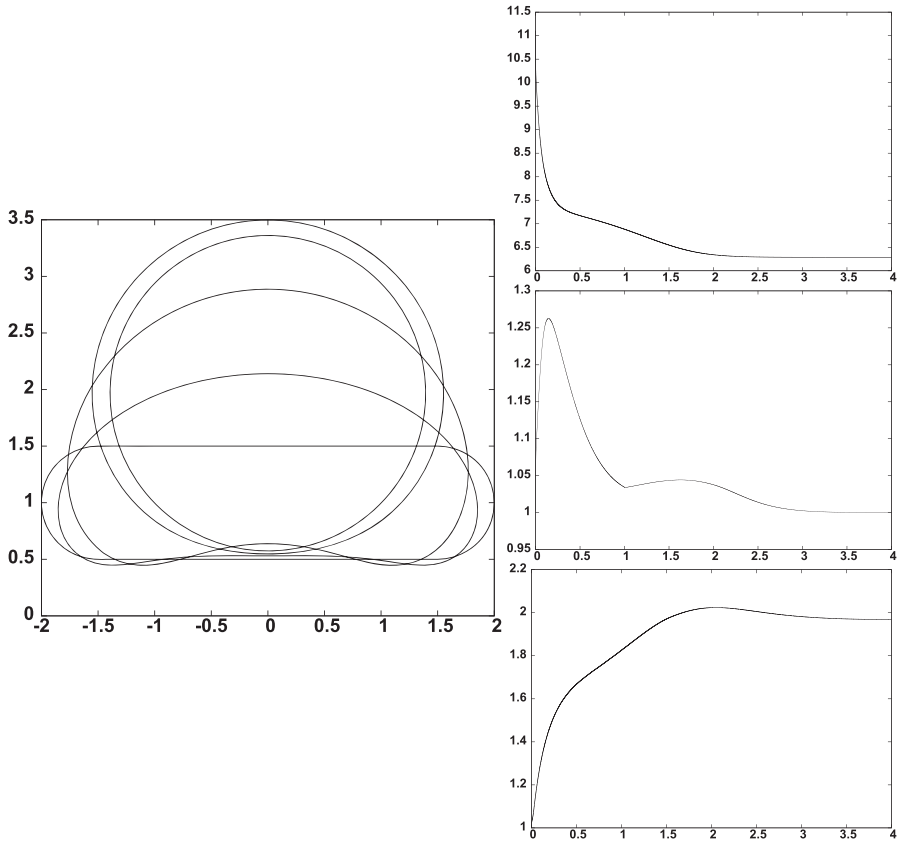

FIG. 10. $(\mathcal{U}_m)^h$: Hyperbolic elastic flow towards a sinking and shrinking circle. Solution at times $t = 0, 0.1, 0.5, 2, 4$. On the right are plots of the discrete energy (4.2), of the ratio (4.3) and of a^m.

4.2 *The elliptic plane*

All our computations in this section are for the elliptic plane, i.e. (2.72a) or, equivalently, (2.8) with $\alpha = -1$. Similarly to Fig. 4, we use the scheme $(\mathcal{A}_m^{\partial})^h$ to compute some geodesics in the elliptic plane. Here it can happen that a finite geodesic does not exist, and so the evolution of curvature flow will yield a curve that expands continuously. We visualize this effect in Fig. 14. Here the initial curve consists of two straight line segments that connect the points $(\pm 9, \mp 1)^T$ with $(9, 9)^T$ in H. As the discretization parameters we choose $J = 128$ and $\Delta t = 10^{-4}$.

4.3 *Geodesic evolution equations*

In order to demonstrate the possibility of computing geodesic evolution laws with the introduced approximations, we present a computation for geodesic curvature flow on a Clifford torus. To this end, we employ the metric induced by (2.72d) with $\mathfrak{s} = 1$, so that the torus has radii $r = 1$ and $R = 2^{\frac{1}{2}}$. As initial data we choose a circle in H with radius 4 and centre $(0, 2)^T$. For the simulation in Fig. 15 we use the scheme $(\mathcal{A}_m)^h$ with the discretization parameters $J = 256$ and $\Delta t = 10^{-3}$. In H it can be observed

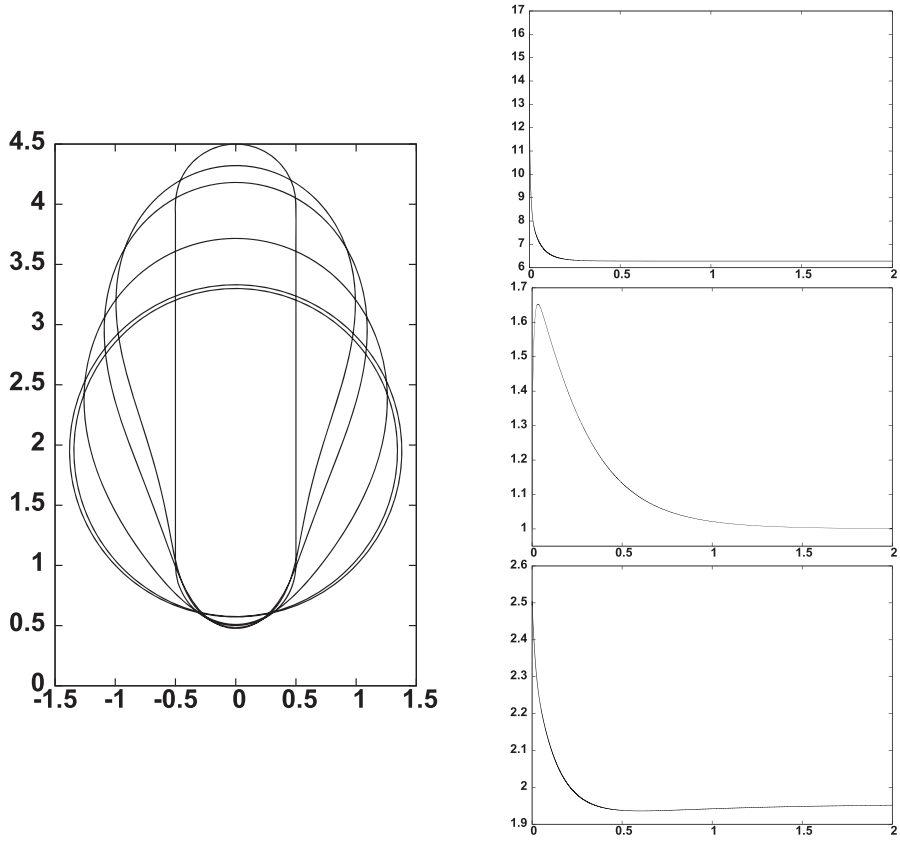

FIG. 11. $(\mathcal{U}_m)^h$: Hyperbolic elastic flow towards a rising and expanding circle. Solution at times $t = 0, 0.01, 0.02, 0.1, 0.5, 2$. On the right are plots of the discrete energy (4.2), of the ratio (4.3) and of a^m.

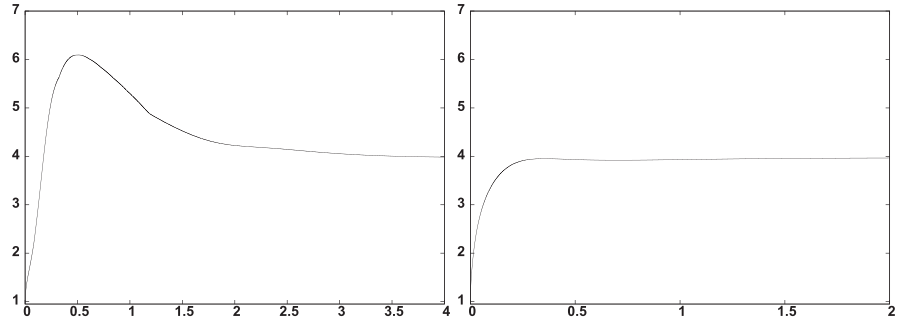

FIG. 12. $(\mathcal{W}_m)^h$: The ratio plots (4.3) for the two simulations as in Figs 10 and 11.

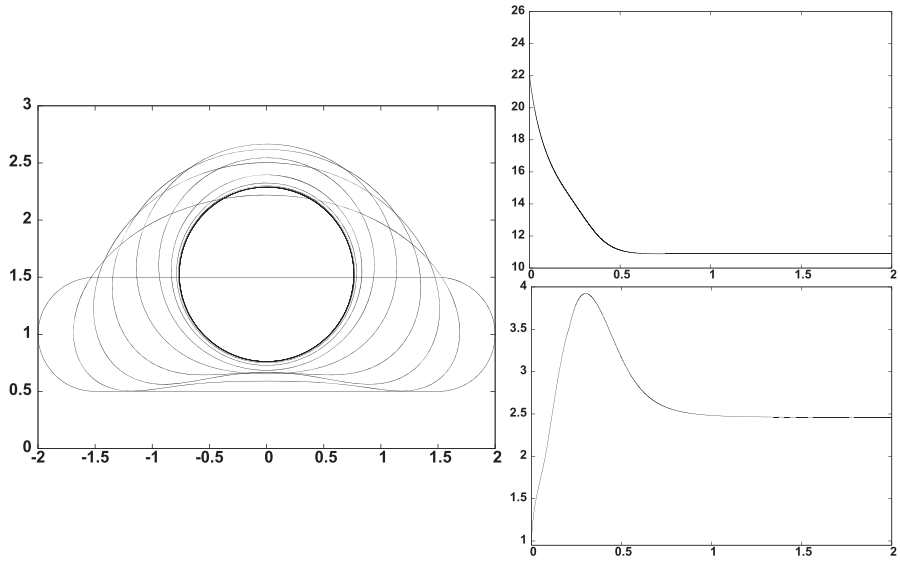

FIG. 13. $(\mathcal{W}_m^{\lambda})^h$: Generalized hyperbolic elastic flow, with $\lambda = 1$, towards a circle. Solution at times $t = 0, 0.1, \ldots, 2$. On the right are plots of the discrete energy $\widetilde{W}_g^m + \lambda L_g^h(\vec{X}^m)$, and of the ratio (4.3).

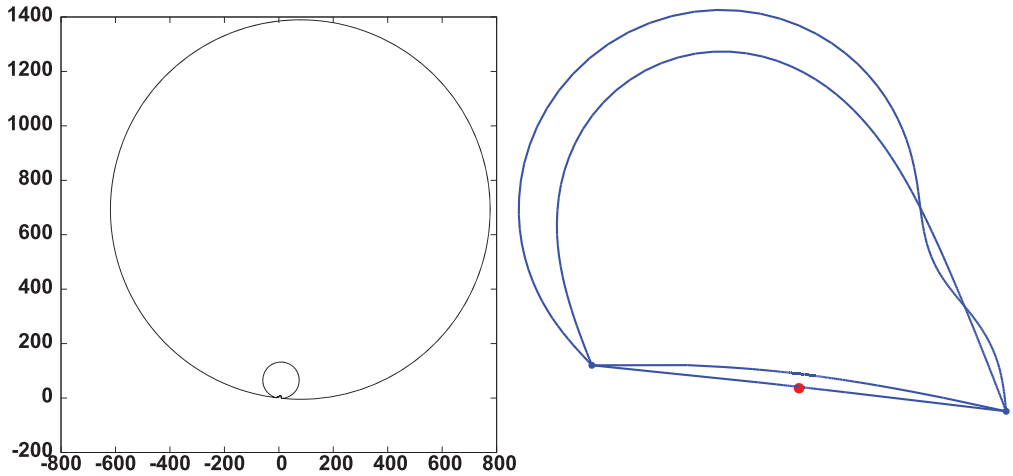

FIG. 14. $(\mathcal{A}_m^{\partial})^h$: Curvature flow towards an infinite geodesic in the elliptic plane. The solutions $\vec{X}^m$ at times $t = 10^{-3}, 10^{-2}, 0.1, 1$. On the right we visualize $\vec{\Phi}(\vec{X}^m)$ at the same times, for (2.72a), with the north pole, $\vec{e}_3$, represented by a red dot.

that the initial circle deforms and shrinks to a point. On the hypersurface $\mathcal{M} = \vec{\Phi}(H)$, the initial curve is homotopic to a point, and so unravels and then shrinks to a point.

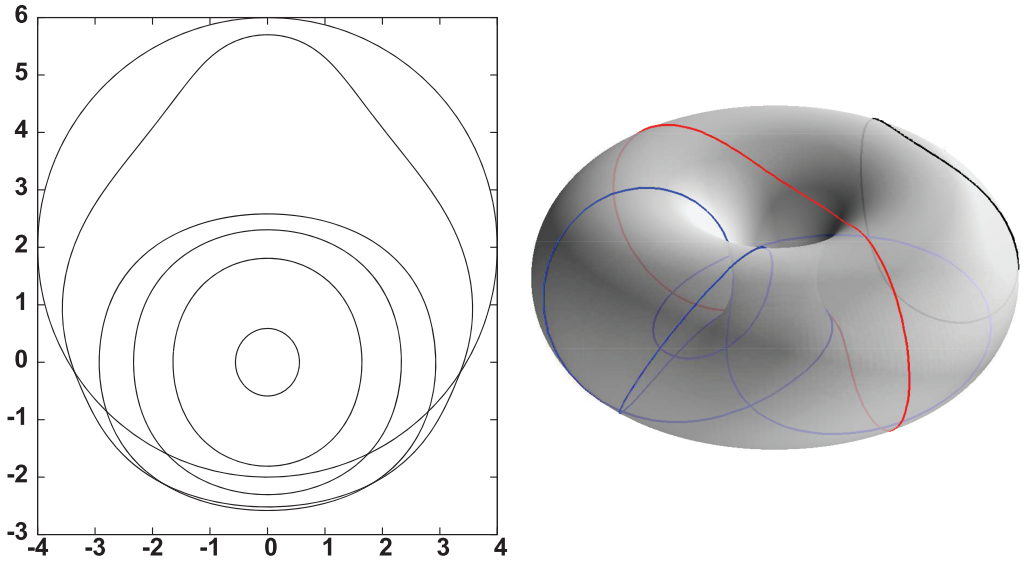

FIG. 15. $(\mathcal{A}_m)^h$: Geodesic curvature flow on a Clifford torus. The solutions $\vec{X}^m$ at times $t = 0, 1, 10, 20, 30, 39$. On the right we visualize $\vec{\Phi}(\vec{X}^m)$ at times $t = 0, 30, 39$, for (2.72d) with $\mathfrak{s} = 1$.

Conclusions

We have derived and analysed various finite element schemes for the numerical approximation of curve evolutions in two-dimensional Riemannian manifolds. The considered evolution laws include curvature flow, curve diffusion and elastic flow. The Riemannian manifolds that can be considered in our framework include the hyperbolic plane, the hyperbolic disc and the elliptic plane. More generally, any metric conformal to the two-dimensional Euclidean metric can be considered. We mention that locally this is always possible for two-dimensional Riemannian manifolds. An example of this is two-dimensional manifolds in $\mathbb{R}^d$, $d \geqslant 3$, which are conformally parameterized. Our approach also allows computations for geometric evolution equations of axisymmetric hypersurfaces in $\mathbb{R}^d$, $d \geqslant 3$.

For the standard Euclidean plane our proposed schemes collapse to variants introduced by the authors in much earlier papers; see Barrett *et al.* (2007a,b).

Acknowledgements

The authors gratefully acknowledge the support of the Regensburger Universitätsstiftung Hans Vielberth.

REFERENCES

ANDREWS, B. & CHEN, X. (2017) Curvature flow in hyperbolic spaces. *J. Reine Angew. Math.*, **729**, 29–49.

BARRETT, J. W., GARCKE, H. & NÜRNBERG, R. (2007a) A parametric finite element method for fourth order geometric evolution equations. *J. Comput. Phys.*, **222**, 441–462.

BARRETT, J. W., GARCKE, H. & NÜRNBERG, R. (2007b) On the variational approximation of combined second and fourth order geometric evolution equations. *SIAM J. Sci. Comput.*, **29**, 1006–1041.

Barrett, J. W., Garcke, H. & Nürnberg, R. (2008) Parametric approximation of Willmore flow and related geometric evolution equations. *SIAM J. Sci. Comput.*, **31**, 225–253.

Barrett, J. W., Garcke, H. & Nürnberg, R. (2010) Numerical approximation of gradient flows for closed curves in $\mathbb{R}^d$. *IMA J. Numer. Anal.*, **30**, 4–60.

Barrett, J. W., Garcke, H. & Nürnberg, R. (2011) The approximation of planar curve evolutions by stable fully implicit finite element schemes that equidistribute. *Numer. Methods Partial Differ. Equ.*, **27**, 1–30.

Barrett, J. W., Garcke, H. & Nürnberg, R. (2012) Parametric approximation of isotropic and anisotropic elastic flow for closed and open curves. *Numer. Math.*, **120**, 489–542.

Barrett, J. W., Garcke, H. & Nürnberg, R. (2017) Finite element approximation for the dynamics of fluidic two-phase biomembranes. *M2AN Math. Model. Numer. Anal.*, **51**, 2319–2366.

Barrett, J. W., Garcke, H. & Nürnberg, R. (2018) Stable discretizations of elastic flow in Riemannian manifolds. arXiv:1811.06301.

Barrett, J. W., Garcke, H. & Nürnberg, R. (2019a) Variational discretization of axisymmetric curvature flows. *Numer. Math.* , **141**, 791–837.

Barrett, J. W., Garcke, H. & Nürnberg, R. (2019b) Finite element methods for fourth order axisymmetric geometric evolution equations. *J. Comput. Phys.*, **376**, 733–766.

Benninghoff, H. & Garcke, H. (2016) Segmentation and restoration of images on surfaces by parametric active contours with topology changes. *J. Math. Imaging Vision*, **55**, 105–124.

Cabezas-Rivas, E. & Miquel, V. (2007) Volume preserving mean curvature flow in the hyperbolic space. *Indiana Univ. Math. J.*, **56**, 2061–2086.

Cheng, L.-T., Burchard, P., Merriman, B. & Osher, S. (2002) Motion of curves constrained on surfaces using a level-set approach. *J. Comput. Phys.*, **175**, 604–644.

Dall'Acqua, A., Laux, T., Lin, C.-C., Pozzi, P. & Spener, A. (2018) The elastic flow of curves on the sphere. *Geom. Flows*, **3**, 1–13.

Dall'Acqua, A. & Spener, A. (2017) The elastic flow of curves in the hyperbolic plane. arXiv:1710.09600.

Dall'Acqua, A. & Spener, A. (2018) Circular solutions to the elastic flow in hyperbolic space. *Proceedings of Analysis on Shapes of Solutions to Partial Differential Equations, (2017)*, vol. 2082. Kyoto, Japan: RIMS Kôkyûroku.

Davis, T. A. (2004) Algorithm 832: UMFPACK V4.3—an unsymmetric-pattern multifrontal method. *ACM Trans. Math Softw.*, **30**, 196–199.

Deckelnick, K., Dziuk, G. & Elliott, C. M. (2005) Computation of geometric partial differential equations and mean curvature flow. *Acta Numer.*, **14**, 139–232.

Dziuk, G. (1988) Finite elements for the Beltrami operator on arbitrary surfaces. *Partial Differential Equations and Calculus of Variations* (S. Hildebrandt & R. Leis eds). Lecture Notes in Mathematics, vol. 1357. Berlin: Springer, pp. 142–155.

Dziuk, G. (1994) Convergence of a semi-discrete scheme for the curve shortening flow. *Math. Models Methods Appl. Sci.*, **4**, 589–606.

Dziuk, G., Kuwert, E. & Schätzle, R. (2002) Evolution of elastic curves in $\mathbb{R}^n$: existence and computation *SIAM J. Math. Anal.*, **33**, 1228–1245.

Elliott, C. M. & Stuart, A. M. (1993) The global dynamics of discrete semilinear parabolic equations. *SIAM J. Numer. Anal.*, **30**, 1622–1663.

Gage, M. & Hamilton, R. S. (1986) The heat equation shrinking convex plane curves. *J. Differ. Geom.*, **23**, 69–96.

Grayson, M. A. (1987) The heat equation shrinks embedded plane curves to round points. *J. Differ. Geom.*, **26**, 285–314.

Grayson, M. A. (1989) Shortening embedded curves. *Ann. Math. (2)*, **129**, 71–111.

Hilbert, D. (1901) Ueber Flächen von constanter Gaussscher Krümmung. *Trans. Amer. Math. Soc.*, **2**, 87–99.

Jost, J. (2005) *Riemannian Geometry and Geometric Analysis*. Berlin: Springer, pp. xiv+566.

Kraus, D. & Roth, O. (2013) Conformal metrics. *Topics in Modern Function Theory*. Ramanujan Mathematical

Society Lecture Notes Series, vol. 19. Mysore, India: Ramanujan Mathematical Society, pp. 41–83. (see also http://arxiv.org/abs/0805.2235).

Kühnel, W. (2015) *Differential Geometry: Curves—Surfaces—Manifolds*. Student Mathematical Library, vol. 77. Providence, RI: American Mathematical Society, pp. xii+402.

Langer, J. & Singer, D. A. (1984) The total squared curvature of closed curves. *J. Differ. Geom.*, **20**, 1–22.

Mikula, K. & Ševčovič, D. (2006) Evolution of curves on a surface driven by the geodesic curvature and external force. *Appl. Anal.*, **85**, 345–362.

Pressley, A. (2010) *Elementary Differential Geometry*. Springer Undergraduate Mathematics Series. London: Springer, pp. xii+473.

Schippers, E. (2007) The calculus of conformal metrics. *Ann. Acad. Sci. Fenn. Math.*, **32**, 497–521.

Schmidt, A. & Siebert, K. G. (2005) *Design of Adaptive Finite Element Software: The Finite Element Toolbox ALBERTA*. Lecture Notes in Computational Science and Engineering, vol. 42. Berlin: Springer.

Spira, A. & Kimmel, R. (2007) Geometric curve flows on parametric manifolds. *J. Comput. Phys.*, **223**, 235–249.

Sullivan, J. M. (2011) Conformal tiling on a torus. *Proceedings of Bridges Coimbra 2011* (R. Sarhangi & C. H. Séquin eds). Phoenix, AZ: Tessellations Publishing, pp. 593–596.

Taylor, M. E. (2011) *Partial Differential Equations I. Basic Theory*. Applied Mathematical Sciences, vol. 115. New York: Springer, pp. xxii+654.

Appendix A. Some exact circular solutions

Here we state some exact solutions for the three geometric evolution equations we consider, i.e. (2.24), (2.38) and (2.56), for selected metrics g.

A.1 *The hyperbolic plane*

Here we consider circular solutions in the hyperbolic plane, based on the exact solution for hyperbolic elastic flow from Dall'Acqua & Spener (2018, Lemma 3.1).

In particular, we make the ansatz

$$\vec{x}(\rho,t) = a(t)\,\vec{e}_2 + r(t)\left[\cos 2\pi\rho\vec{e}_1 + \sin 2\pi\rho\vec{e}_2\right], \qquad \rho \in I, \tag{A.1}$$

for $a(t) > r(t) > 0$, for all $t \in [0,T]$. Then it follows from (2.19) for $\mu = 1$ that

$$\varkappa_g(\rho,t) = \frac{a(t)}{r(t)}, \qquad \rho \in I,\ t \in [0,T]. \tag{A.2}$$

Moreover, it holds that

$$\mathcal{V}_g = (\vec{x}\,.\,\vec{e}_2)^{-1}\,\vec{x}_t\,.\,\vec{\nu} = -\,(a(t) + r(t)\,\sin 2\pi\rho)^{-1}\,\left[a'(t)\,\sin 2\pi\rho + r'(t)\right] \qquad \text{in } I. \tag{A.3}$$

We now consider curvature flow, (2.24). With the ansatz (A.1), on noting (A.2) and (A.3), we have that (2.24) reduces to

$$a'(t)\,\sin 2\pi\rho + r'(t) = -(a(t) + r(t)\,\sin 2\pi\rho)\,\frac{a(t)}{r(t)}. \tag{A.4}$$

Differentiating (A.4) with respect to ρ yields $a'(t) = -a(t)$, and hence $a(t) = e^{-t}\,a(0)$. Combining this with (A.4) yields

$$r'(t) = -a(t)\,\frac{a(t)}{r(t)} \qquad \Rightarrow \qquad \tfrac{1}{2}\,\frac{\mathrm{d}}{\mathrm{d}t}r^2(t) = -a^2(t) = -e^{-2t}\,a^2(0).$$

Hence,

$$r^2(t) - r^2(0) = -2a^2(0) \int_0^t e^{-2u}\, \mathrm{d}u = -2a^2(0) \left[-\tfrac{1}{2} e^{-2t} + \tfrac{1}{2}\right] = a^2(0) \left[e^{-2t} - 1\right],$$

and so (A.1) with

$$a(t) = e^{-t}\, a(0)\,, \quad r(t) = \left(r^2(0) - a^2(0) \left[1 - e^{-2t}\right]\right)^{\frac{1}{2}} \tag{A.5}$$

is a solution to (2.24). We observe that circles move towards the $\vec{e}_1$-axis and shrink as they do so. The finite extinction time is $T_0 = -\frac{1}{2} \ln[1 - (\frac{r(0)}{a(0)})^2]$.

As regards (2.38), it is obvious from (A.2) that any solution of the form (A.1) satisfies $\mathcal{V}_g = 0$, and so circles are stationary solutions for curve diffusion.

Finally, for the elastic flow (2.56), we recall the exact solution for the hyperbolic elastic flow, (2.57), from Dall'Acqua & Spener (2018, Lemma 3.1).

With the ansatz (A.1), on noting (A.2) and (A.3), we have that (2.57) reduces to

$$a'(t)\, \sin 2\pi\, \rho + r'(t) = -(a(t) + r(t)\, \sin 2\pi\, \rho) \left(\frac{a(t)}{r(t)} - \frac{a^3(t)}{2r^3(t)}\right). \tag{A.6}$$

Differentiating (A.6) with respect to ρ yields

$$a'(t) = -r(t) \left(\frac{a(t)}{r(t)} - \frac{a^3(t)}{2r^3(t)}\right), \tag{A.7}$$

and combining this with (A.6) yields

$$r'(t) = -a(t) \left(\frac{a(t)}{r(t)} - \frac{a^3(t)}{2r^3(t)}\right). \tag{A.8}$$

On setting

$$\sigma(t) = \frac{a(t)}{r(t)} > 1 \qquad \Rightarrow \quad \sigma'(t) = \frac{a'(t)}{r(t)} - \frac{a(t)\, r'(t)}{r^2(t)}\,,$$

it follows from (A.7) and (A.8) that

$$\sigma'(t) = \sigma(t)\, (1 - \tfrac{1}{2}\, \sigma^2(t))\, (\sigma^2(t) - 1)\,, \tag{A.9}$$

which agrees with Dall'Acqua & Spener (2018, (3.4)) for $\lambda = 0$. If σ denotes a solution to (A.9), then it follows from (A.7) that a and r satisfy

$$\frac{\mathrm{d}}{\mathrm{d}t} \ln a(t) = \frac{a'(t)}{a(t)} = \tfrac{1}{2}\, \sigma^2(t) - 1 \quad \Rightarrow\ a(t) = a(0)\, \exp\left(-t + \tfrac{1}{2} \int_0^t \sigma^2(u)\, \mathrm{d}u\right), \tag{A.10a}$$

$$r(t) = \frac{a(t)}{\sigma(t)}\,. \tag{A.10b}$$

On recalling that $\sigma(t) > 1$, we note that $\sigma(t) = 2^{\frac{1}{2}}$ is the only steady state solution of (A.9), and hence circles with ratios $\sigma(t) = 2^{\frac{1}{2}}$ are steady state solutions of (2.57). Moreover, circles with $\sigma(t) > 2^{\frac{1}{2}}$ will rise and expand indefinitely in time, reducing the ratio $\sigma(t) > 2^{\frac{1}{2}}$ as they do so. On the other hand, circles with $\sigma(t) < 2^{\frac{1}{2}}$ will sink and shrink indefinitely in time, increasing the ratio $\sigma(t) < 2^{\frac{1}{2}}$ as they do so.

In order to compute solutions to (A.9) in practice, we let $F(y) = y^{-1}\,|1-\frac{1}{2}\,y^2|^{-\frac{1}{2}}\,(y^2-1)$, so that $F \in C^\infty((1,2^{\frac{1}{2}}) \cup (2^{\frac{1}{2}},\infty))$. Then $F'(y) = y^{-2}\,(1-\frac{1}{2}\,y^2)^{-1}\,|1-\frac{1}{2}\,y^2|^{-\frac{1}{2}}$, and hence a solution σ to (A.9) satisfies

$$\frac{\mathrm{d}}{\mathrm{d}t}\,F(\sigma(t)) = \sigma'(t)\,F'(\sigma(t)) = \frac{\sigma^2(t)-1}{\sigma(t)\,|1-\frac{1}{2}\,\sigma^2(t)|^{\frac{1}{2}}} = F(\sigma(t))\,,$$

which means that a solution σ to (A.9) satisfies the nonlinear equation

$$F(\sigma(t)) = F(\sigma(0))\,e^t\,.$$

A.2 *The hyperbolic disc and the elliptic plane*

Here we consider the metric (2.8). For $\alpha = 1$ we then obtain exact solutions for the hyperbolic disc, while $\alpha = -1$ corresponds to the elliptic plane. In the latter case these solutions can be related to the exact solutions for the corresponding geodesic flows on the sphere from Barrett *et al.* (2010); recall Section 2.4.

In particular, on making the ansatz

$$\vec{x}(\rho,t) = r(t)\left[\cos 2\pi\,\rho\,\vec{e}_1 + \sin 2\pi\,\rho\,\vec{e}_2\right], \qquad \rho \in I\,, \tag{A.11}$$

for $r(t) > 0$, for all $t \in [0,T]$, it follows from (2.20) that

$$\varkappa_g(\rho,t) = \tfrac{1}{2}\left(1+\alpha\,r^2(t)\right)[r(t)]^{-1}, \qquad \rho \in I\,,\ t \in [0,T]\,. \tag{A.12}$$

Moreover, it holds that

$$\mathcal{V}_g = g^{\frac{1}{2}}(\vec{x})\,\vec{x}_t\,.\,\vec{\nu} = -2\,(1-\alpha\,r^2(t))^{-1}\,r'(t) \qquad \text{in } I\,. \tag{A.13}$$

We now consider curvature flow, (2.24). It follows from (A.13) and (A.12) that

$$\frac{\mathrm{d}}{\mathrm{d}t}\,r^2(t) = \tfrac{1}{2}\left(\alpha^2 r^4(t) - 1\right). \tag{A.14}$$

Clearly, if $\alpha = 0$ then $r(t) = [r^2(0) - \frac{1}{2}\,t]^{\frac{1}{2}}$ is the well-known shrinking circle solution for Euclidean curvature flow. For $\alpha \neq 0$, in order to compute solutions to (A.14) in practice, we let

$$G(y) = \left|(1+\alpha\,y^2)^{-1}\,(1-\alpha\,y^2)\right|^{\frac{1}{\alpha}},$$

so that $G \in C^\infty((0,|\alpha|^{-\frac{1}{2}}) \cup (|\alpha|^{-\frac{1}{2}},\infty))$; recall also (2.8). Then $G'(y) = 4\,y\,(\alpha^2\,y^4-1)^{-1}\,G(y)$ and hence a solution to (A.14) satisfies

$$\frac{\mathrm{d}}{\mathrm{d}t}\,G(r(t)) = r'(t)\,G'(r(t)) = G(r(t)),$$

means that a solution to (A.14) satisfies the nonlinear equation

$$G(r(t)) = G(r(0))\,e^t\,, \tag{A.15}$$

which can be inverted explicitly. In the case $\alpha = -1$, we recall from (2.72a) that the circle (A.11) of radius $r(t)$ in the elliptic plane corresponds to a circle of radius $R(t) = 2\,(1+r^2(t))^{-1}\,r(t)$, and at height

$(r^2(t)+1)^{-1}\,(r^2(t)-1)$, on the unit sphere in $\mathbb{R}^3$. It can be easily shown that if $r(t)$ satisfies (A.15) for $\alpha=-1$, then

$$R(t)=\left[1-(1-R^2(0))\,e^{2t}\right]^{\frac{1}{2}}\,,$$

which is the solution of geodesic curvature flow on the unit sphere, given by Barrett *et al.* (2010, (5.6)). Observe that for $R(0)\in(0,1)$, the finite extinction time is $T_0=\frac{1}{2}\,\ln\frac{1}{1-R^2(0)}$.

As regards (2.38), it is obvious from (A.12) that any solution of the form (A.11) satisfies $\mathcal{V}_g=0$, and so circles centred at the origin are stationary solutions to curve diffusion for (2.8).

Finally, we consider the elastic flow (2.56). With the ansatz (A.11), on noting (A.12), (A.13) and (2.11), we have that (2.56) reduces to

$$-2\,(1-\alpha\,r^2(t))^{-1}\,r'(t)=-\tfrac{1}{16}\,(1+\alpha\,r^2(t))^3 r^{-3}(t)+\tfrac{1}{2}\,\alpha\,(1+\alpha\,r^2(t))\,r^{-1}(t)\,.$$

This implies the ordinary differential equation

$$\frac{\mathrm{d}}{\mathrm{d}t}\,r^4(t)=\tfrac{1}{8}\,(1-\alpha^2r^4(t))\,(1-6\,\alpha\,r^2(t)+\alpha^2r^4(t))\,. \tag{A.16}$$

In the case $\alpha=-1$, we recall from (2.72a) that the circle (A.11) of radius $r(t)$ in the elliptic plane corresponds to a circle of radius $R(t)=2\,(1+r^2(t))^{-1}\,r(t)$, and at height $(r^2(t)+1)^{-1}\,(r^2(t)-1)$, on the unit sphere in $\mathbb{R}^3$. It can be easily shown that if $r(t)$ satisfies (A.16) for $\alpha=-1$, then $R(t)$ satisfies $\frac{\mathrm{d}}{\mathrm{d}t}\,R^4(t)=2\,(1-R^4(t))$, i.e.

$$R(t)=[1-(1-R^4(0))\,e^{-2t}]^{\frac{1}{4}},$$

which is the solution for geodesic elastic flow on the unit sphere given by Barrett *et al.* (2010, (5.7)). Hence, in the case $\alpha=-1$ we can obtain $r(t)$ from

$$r(t)=R^{-1}(t)\begin{cases}(1+[1-R^2(t)]^{\frac{1}{2}}), & r(0)\geqslant 1\,,\\ (1-[1-R^2(t)]^{\frac{1}{2}}), & r(0)<1\,,\end{cases}\quad\text{where}\quad R(t)=[1-(1-R^4(0))\,e^{-2t}]^{\frac{1}{4}}\,, \tag{A.17}$$

with $R(0)=2\,(1+r^2(0))^{-1}\,r(0)$.

Finally, for the case $\alpha=1$, it follows from (A.16) that

$$\frac{\mathrm{d}}{\mathrm{d}t}\,r^4(t)=\tfrac{1}{8}\,(1-r^4(t))\,(1-6r^2(t)+r^4(t))\,. \tag{A.18}$$

We note, on recalling (2.8), that $r(t)=2^{\frac{1}{2}}-1$ is a stable stationary solution to (A.18). Hence, circles with larger radii will shrink, and circles with smaller radii will expand. In order to solve (A.18) in practice, we define $Q(y)=(1+y^2)^{-1}\,|1-6\,y^2+y^4|^{-\frac{1}{2}}\,(1-y^2)^2$, so that $Q\in C^\infty((0,2^{\frac{1}{2}}-1)\cup(2^{\frac{1}{2}}-1,1))$ with $Q'(y)=32\,(1-y^4)^{-1}\,(1-6\,y^2+y^4)^{-1}\,y^3\,Q(y)$. Hence, $\frac{\mathrm{d}}{\mathrm{d}t}\,Q(r(t))=Q(r(t))$, and so a solution to (A.18) satisfies the nonlinear equation

$$Q(r(t))=Q(r(0))\,e^t\,. \tag{A.19}$$

We remark that an alternative to (A.17) for the case $\alpha=-1$ is to solve, similarly to (A.19), the nonlinear equation $Q_-(r(t))=Q_-(r(0))\,e^t$, where $Q_-(y)=(1-y^2)^{-1}\,(1+6\,y^2+y^4)^{-\frac{1}{2}}\,(1+y^2)^2$.

Appendix B. Geodesic curve evolution equations

Let $\vec{\Phi} : H \to \mathbb{R}^d$ be a conformal parameterization of an embedded two-dimensional Riemannian manifold $\mathcal{M} \subset \mathbb{R}^d$, i.e. $\mathcal{M} = \vec{\Phi}(H)$ and $|\partial_{\vec{e}_1} \vec{\Phi}(\vec{z})|^2 = |\partial_{\vec{e}_2} \vec{\Phi}(\vec{z})|^2$ and $\partial_{\vec{e}_1} \vec{\Phi}(\vec{z}) \,.\, \partial_{\vec{e}_2} \vec{\Phi}(\vec{z}) = 0$ for all $\vec{z} \in H$. Given the parameterization $\vec{x} : I \to H$ of the closed curve $\Gamma \subset H$, we let $\vec{y} = \vec{\Phi} \circ \vec{x}$ be a parameterization of $\mathcal{G} \subset \mathcal{M}$. We now show that geodesic curvature flow, geodesic curve diffusion and geodesic elastic flow for $\mathcal{G} = \vec{y}(I)$ on $\mathcal{M}$ reduce to (2.24), (2.38) and (2.56) for the metric g defined by

$$g(\vec{z}) = |\partial_{\vec{e}_1} \vec{\Phi}(\vec{z})|^2 = |\partial_{\vec{e}_2} \vec{\Phi}(\vec{z})|^2, \qquad \vec{z} \in H\,.$$

For later use we observe that

$$D\vec{\Phi}(\vec{z})\,\vec{v}\,.\,D\vec{\Phi}(\vec{z})\,\vec{w} = g(\vec{z})\,\vec{v}\,.\,\vec{w} \quad \forall\, z \in H\,,\ \vec{v},\vec{w} \in \mathbb{R}^2\,, \tag{B.1}$$

where $D\vec{\Phi}(\vec{z}) = [\partial_{\vec{e}_1} \vec{\Phi}(\vec{z})\ \partial_{\vec{e}_2} \vec{\Phi}(\vec{z})] \in \mathbb{R}^{d\times 2}$ for $\vec{z} \in H$. A simple computation, on noting (B.1) and (2.1), yields

$$\vec{y}_\rho = D\vec{\Phi}(\vec{x})\,\vec{x}_\rho \quad \Rightarrow \quad |\vec{y}_\rho| = g^{\frac{1}{2}}(\vec{x})\,\vec{x}_\rho = |\vec{x}_\rho|_g \qquad \text{in } I\,. \tag{B.2}$$

Hence, it follows from (2.13) that

$$\partial_{s_y} = |\vec{y}_\rho|^{-1}\,\partial_\rho = |\vec{x}_\rho|_g^{-1}\,\partial_\rho = \partial_{s_g} \qquad \text{in } I\,, \tag{B.3}$$

and so the unit tangent to the curve $\vec{y}(I)$ is given by

$$\vec{\tau}_{\mathcal{M}} = \vec{y}_{s_y} = D\vec{\Phi}(\vec{x})\,\vec{x}_{s_g} = D\vec{\Phi}(\vec{x})\,\vec{\tau}_g \qquad \text{in } I\,, \tag{B.4}$$

on recalling (2.14). Similarly, we define the normal $\vec{\nu}_{\mathcal{M}}$ as the unit normal to $\vec{y}(I)$ that is perpendicular to $\vec{\tau}_{\mathcal{M}}$ and that lies in the tangent space to $\mathcal{M}$, i.e.

$$\vec{\nu}_{\mathcal{M}} = (\vec{x}_{s_g}\,.\,\vec{e}_1)\,\partial_{\vec{e}_2} \vec{\Phi}(\vec{x}) - (\vec{x}_{s_g}\,.\,\vec{e}_2)\,\partial_{\vec{e}_1} \vec{\Phi}(\vec{x}) = D\vec{\Phi}(\vec{x})\,[-\vec{x}_{s_g}^{\,\perp}] = D\vec{\Phi}(\vec{x})\,\vec{\nu}_g \qquad \text{in } I\,, \tag{B.5}$$

where we have recalled (2.14). Note that (B.5), in the case $d = 3$, agrees with the definition of $\vec{\nu}_{\mathcal{M}}$ in Barrett *et al.* (2010, p. 10). We further note from (B.4) that $\vec{y}_{s_y s_y}$ is perpendicular to $\vec{\tau}_{\mathcal{M}}$, and hence

$$\vec{y}_{s_y s_y} = \varkappa_{\mathcal{M}}\,\vec{\nu}_{\mathcal{M}} + \vec{\varkappa}_F \qquad \text{in } I\,, \tag{B.6}$$

where $\vec{\varkappa}_F$ is normal to $\mathcal{M}$, and where $\varkappa_{\mathcal{M}}$ denotes the geodesic curvature of $\vec{y}(I)$.

Clearly, it follows from (B.2) that the length of $\vec{y}(I)$ is given by

$$L_{\mathcal{M}}(\vec{y}) = \int_I |\vec{y}_\rho|\,\mathrm{d}\rho = \int_I |\vec{x}_\rho|_g\,\mathrm{d}\rho = L_g(\vec{x})\,. \tag{B.7}$$

We compute, on noting (B.7), (B.3), (B.6), (B.5), (B.1), (2.15) and (2.14), that

$$\begin{aligned}
\frac{\mathrm{d}}{\mathrm{d}t} L_{\mathcal{M}}(\vec{y}) &= \int_I \frac{\vec{y}_\rho}{|\vec{y}_\rho|}\,.\,(\vec{y}_\rho)_t\,\mathrm{d}\rho = -\int_I \left(\frac{\vec{y}_\rho}{|\vec{y}_\rho|}\right)_\rho .\,\vec{y}_t\,\mathrm{d}\rho = -\int_I \vec{y}_{s_y s_y}\,.\,\vec{y}_t\,|\vec{y}_\rho|\,\mathrm{d}\rho \\
&= -\int_I \varkappa_{\mathcal{M}}\,\vec{\nu}_{\mathcal{M}}\,.\,\vec{y}_t\,|\vec{y}_\rho|\,\mathrm{d}\rho = -\int_I \varkappa_{\mathcal{M}}\,D\vec{\Phi}(\vec{x})\,\vec{\nu}_g\,.\,D\vec{\Phi}(\vec{x})\,\vec{x}_t\,|\vec{x}_\rho|_g\,\mathrm{d}\rho \\
&= -\int_I \varkappa_{\mathcal{M}}\,g(\vec{x})\,\vec{\nu}_g\,.\,\vec{x}_t\,|\vec{x}_\rho|_g\,\mathrm{d}\rho = -\int_I \varkappa_{\mathcal{M}}\,\mathcal{V}_g\,|\vec{x}_\rho|_g\,\mathrm{d}\rho\,.
\end{aligned} \tag{B.8}$$

It follows from (B.8), (2.17) and (B.7) that

$$\varkappa_g = \varkappa_{\mathcal{M}} \qquad \text{in } I\,. \tag{B.9}$$

In addition we have from (B.5), (B.1), (2.14) and (2.15) that

$$\mathcal{V}_{\mathcal{M}} = \vec{y}_t \,.\, \vec{\nu}_{\mathcal{M}} = D\,\vec{\Phi}(\vec{x})\,\vec{x}_t \,.\, D\,\vec{\Phi}(\vec{x})\,\vec{\nu}_g = \mathcal{V}_g \qquad \text{in } I\,. \tag{B.10}$$

Hence, the flow (2.24) for $\vec{x}(I)$ in H is equivalent to the flow

$$\mathcal{V}_{\mathcal{M}} = \varkappa_{\mathcal{M}} \qquad \text{in } I$$

for $\vec{y}(I)$ on $\mathcal{M}$, which is the so-called geodesic curvature flow; see also Barrett *et al.* (2010, (2.19)) for the case $d = 3$.

Similarly, it follows from (B.10), (B.9) and (B.3) that the flow (2.38) for $\vec{x}(I)$ in H is equivalent to the geodesic curve diffusion flow

$$\mathcal{V}_{\mathcal{M}} = -(\varkappa_{\mathcal{M}})_{s_g s_g} \qquad \text{in } I;$$

see also Barrett *et al.* (2010, (2.20)) for the case $d = 3$. Finally, in order to relate (2.56) for $d = 3$ to geodesic elastic flow, i.e. the L^2-gradient flow of

$$\tfrac{1}{2}\int_I \varkappa_{\mathcal{M}}^2\,|\vec{y}_\rho|\,\mathrm{d}\rho = \tfrac{1}{2}\int_I \varkappa_g^2\,|\vec{x}_\rho|_g\,\mathrm{d}\rho = W_g(\vec{x})\,,$$

recall (B.9), (B.2) and (2.45), we note from from Barrett *et al.* (2010, (2.32)) that geodesic elastic flow for $\vec{y}(I)$ on $\mathcal{M}$ is given by

$$\mathcal{V}_{\mathcal{M}} = -(\varkappa_{\mathcal{M}})_{s_y s_y} - \tfrac{1}{2}\,\varkappa_{\mathcal{M}}^3 - \mathcal{K}(\vec{y})\,\varkappa_{\mathcal{M}} \qquad \text{in } I\,, \tag{B.11}$$

where $\mathcal{K}(\vec{z})$ denotes the Gaussian curvature of $\mathcal{M}$ at $\vec{z} \in \mathcal{M}$. It follows from (B.10), (B.9), (B.3) and (2.71) that (B.11) and (2.56) are equivalent.